ORNL-2318
Reactors - General Cy. 4
TID-4500 (13th ed., Rev.)

REACTOR SAFETY SYSTEM RESPONSE

OAK RIDGE NATIONAL LABORATORY
OPERATED BY
UNION CARBIDE NUCLEAR COMPANY
Division of Union Carbide Corporation
UCC
POST OFFICE BOX X · OAK RIDGE, TENNESSEE

Printed in USA. Price $2.75 cents. Available from the
Office of Technical Services
U. S. Department of Commerce
Washington 25, D. C.

UNCLASSIFIED

ORNL-2318

Contract No. W-7405-eng-26

Instrumentation and Controls Division

REACTOR SAFETY SYSTEM RESPONSE*

Edited by F. P. Green

DATE ISSUED

JAN 31 1958

*A collection of papers presented at the Third Annual Meeting of the American Nuclear Society, June 10, 1957, by the Reactor Controls Department. Pittsburg, Pa.

OAK RIDGE NATIONAL LABORATORY
Operated by
UNION CARBIDE NUCLEAR COMPANY
Division of Union Carbide Corporation
Post Office Box X
Oak Ridge, Tennessee

UNCLASSIFIED

INTERNAL DISTRIBUTION

1. C. E. Center
2. Biology Library
3. Health Physics Library
4-5. Central Research Library
6. Reactor Experimental Engineering Library
7-11. Laboratory Records Department
12. Laboratory Records, ORNL, R.C.
13. A. M. Weinberg
14. L. B. Emlet (K-25)
15. J. P. Murray (Y-12)
16. J. A. Swartout
17. E. H. Taylor
18. E. D. Shipley
19. C. S. Harrill
20. C. P. Keim
21. J. H. Frye, Jr.
22. R. S. Livingston
23. W. H. Jordan
24. S. C. Lind
25. F. L. Culler
26. A. H. Snell
27. A. Hollaender
28. M. T. Kelley
29. K. Z. Morgan
30. T. A. Lincoln
31. A. S. Householder
32. C. E. Winters
33. D. W. Cardwell
34. J. A. Lane
35. D. Phillips
36. M. J. Skinner
37. C. J. Borkowski
38. R. R. Dickison
39. P. M. Reyling
40. C. W. Angel
41. E. P. Blizard
42. C. Brashear
43. E. S. Bettis
44. R. B. Briggs
45. C. D. Cagle
46. W. R. Casto
47. R. A. Charpie
48. C. E. Clifford
49. T. E. Cole
50. J. A. Cox
51-96. E. P. Epler
97. J. P. Gill
98-143. F. P. Green
144. K. M. Henry
145. S. H. Hanauer
146. L. B. Holland
147. E. B. Johnson
148. J. Lewin
149. F. C. Maienschein
150. E. R. Mann
151. W. F. Mruk
152. L. C. Oakes
153. W. Ragen, Jr.
154. M. E. Ramsey
155. E. Silver
156. T. C. Weeks
157. ORNL - Y-12 Technical Library, Document Reference Section

EXTERNAL DISTRIBUTION

158. R. F. Bacher, California Institute of Technology
159. Division of Research and Development, AEC, ORO
160-694. Given distribution as shown in TID-4500 (13th ed., Rev.) under Reactors - General category (75 copies OTS)

CONTENTS

A PROGRAM TO EVALUATE THE PERFORMANCE OF A SAFETY SYSTEM

E. P. Epler and S. H. Hanauer

ABSTRACT

Reactor accidents are discussed which might be caused by failure of the control system and which might be eliminated by better controls design. A second group of accidents, not caused by controls, and which therefore cannot be eliminated by better controls design, can be mitigated by a fast safety system. Factors are enumerated which govern the realization of a fast safety system. The swimming pool reactor is used as an example.

A Program to Evaluate the Performance of a Safety System

E. P. Epler and S. H. Hanauer

Reactors have now been built and operated for 15 years, yet there are still no clear-cut criteria establishing the performance requirements for a reactor safety system. It is easily understood that for the earliest reactors the maximum of performance was desirable. However, the years of operation have yielded very few accidents on which to build a case for high-performance systems, and the recent trend toward complete containment of reactors has mitigated the consequences of a serious reactor accident. In addition, the requirement for operating continuity, as in power reactors, has made designers reluctant to apply a multiplicity of fast-acting safety devices. Recently, the Borax[2] and SPERT[3,4] experiments have been conducted at the National Reactor Testing Station for the purpose of determining the self-limiting properties of the water-moderated solid-fuel reactor. The reactors under test were able to withstand without damage excursions involving periods as short as 5 milliseconds. In the light of these facts, it is easy for the designer to satisfy his conscience by providing a safety system which is no more than perfunctory.

The Startup Accident

In reactors such as the MTR, it is necessary to withdraw rods containing massive amounts of reactivity in a reasonably short time. The rods must have a high worth because of the large loaded excess k of these reactors; the startup must take place promptly if the increasing xenon poisoning is to be overridden after a shutdown. During the design of the MTR, Newson[1] undertook an inquiry into the hazards of such a procedure. He postulated that failure of instruments or mis-operation by the console operator would cause all control rods to be withdrawn simultaneously at their maximum rate set by motor speeds and gear ratios. This is defined as the startup accident. Safety devices set to operate just above normal operating power of the reactor would release the control rods, and they would be accelerated in the direction to decrease the reactivity. The safety-system response time and rod acceleration must be such that the reactor would not be damaged by the power excursion. Thus, accidents involving only rods moving at their rated speeds cannot harm the reactor. Therefore, the consequence of mis-operation by the console operator or malfunction of an instrument can be tolerated, since at worst this is a startup accident. This statement is true, however, only if the safety system approaches absolute reliability, and if the limitation on rod withdrawal speed is equally reliable.

The smaller reactors, such as the swimming-pool type reactors, point up a different problem in specifying safety system response. In this instance, the amount of reactivity to be added through rod withdrawal during startup is not large; 5 to 10% in $\Delta k/k$ is typical whereas in the MTR it is 40%. Furthermore, there is seldom as much compulsion to start the reactor quickly, since xenon poison buildup after shutdown is not usually a problem. Finally, the permissible peak power is much higher with respect to the normal operating power, and therefore with respect to the trip level of the safety devices. Where the overload which can be withstood without damage is a factor of 10 in the MTR, it may be as high as a factor of 10^4 or even 10^6, if the reactor can be depended on to perform in the manner of the Borax and SPERT experimental reactors. Figure 1 illustrates, from the SPERT-1 experiment, the response of a water-moderated reactor to a startup-accident situation with no safety devices in operation. The control rods were withdrawn continuously at the average speeds shown, and the withdrawal continued until after the first power burst was finished. The speeds, in $\Delta k/k$, of .1 %/sec and .01 %/sec, represent reasonable upper and lower bounds, respectively, on startup rod withdrawal speed. An intermediate speed of .05%/sec will give, for a typical swimming-pool reactor, a rod withdrawal time of 100 to 200 sec., which should be sufficiently fast, and is well within the range of these experiments. Since these accidents are not particularly frightening even if the safety system fails to work, it may be concluded that for this reactor the response requirements for the safety system may be stated in terms of seconds rather than milliseconds. Thus, the startup accident alone is not a useful criterion for specifying safety system response.

Other Accidents Induced by Control Elements

Much attention has been given to the subject of reactor runaway during startup and it has been shown that fast safety system response is not required providing one has assurance that the control rods cannot be withdrawn at a rate greater than the designed speed and that there is no other possible accident which can be greater than the startup accident. On looking more closely, however, one discovers that there may indeed be sources of accidents of much greater severity than the start up accident and that these accidents can be generated by the control system on which the operator is depending. Again the swimming pool reactor is used as an example to illustrate some of the possibilities.

(1) The rod-withdrawal mechanisms of several reactors consist of motor-driven cable drums, with the control rod suspended from the cable, or from a magnet supported by the cable. The motors and drums are located in easily accessible positions, in the interest of arrangement flexibility in the active lattice. Thus, it is possible for the rods to be withdrawn entirely independently of the drive motors and interlocks. It remains a matter of chance by what agency (e.g. the crane hook) and at what speed the rods might be withdrawn. The severity of an accident involving such unprogrammed withdrawal might well exceed that of the startup accident. More recent designs for rod-actuating mechanisms[5] eliminate the flexible and exposed elements, and move the rods positively with rigid actuators. At ORNL, rod-drive mechanisms of the earlier design have been or are being replaced with the more recent type.

(2) For a given speed in Δk/sec, the reactor may be started by withdrawing all n rods simultaneously, or by withdrawing them one at a time, each at a rate n times greater than the rate for simultaneous withdrawal. If the latter method is used, a failure in the interlocking device can cause all rods to move simultaneously, yielding an unplanned withdrawal speed n times greater than expected.

(3) If the rod-drive mechanism is mounted on a platform of some kind, any binding between the control element and other parts of the reactor could result in the other parts' being withdrawn with the control rod, perhaps to be dropped when the rod nears the top of its stroke. In particular, the device which locks down a fuel element may be neglected or defective and the fuel element adjacent

UNCLASSIFIED
ORNL-LR-DWG 21817

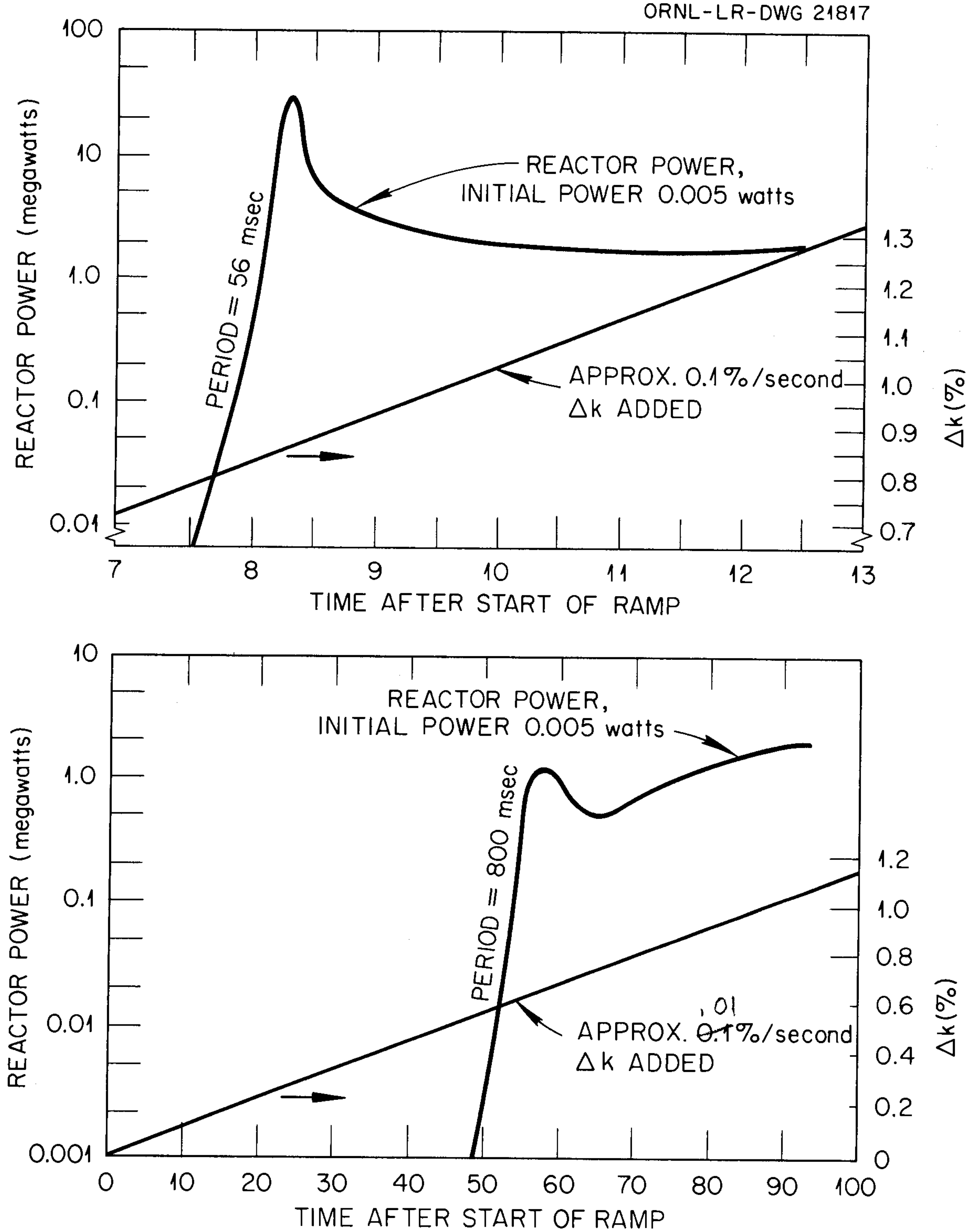

Fig. 1. Startup Accident.

to or surrounding the control rod may be withdrawn with it and then dropped. Rod-drives now in use in the ORNL Swimming-Pool Reactor are supported directly from the fuel element within which the control rod moves, so this type of accident is rendered much less likely. The principle is illustrated in Figure 2.

(4) It is often proposed that the automatic flux or power controller (the servo system) be so arranged that when the automatically-controlled rod reaches the upper limit of its travel, additional control rods will automatically be withdrawn as needed. This could be a convenience in compensating for fuel burn-up, growth of xenon poison concentration, and the effect on reactivity of temperature increases. Each of these constitutes a loss of reactivity which does indeed call for rod withdrawal. The danger in this arrangement lies in automatic compensation for unpredicted losses of reactivity whose cause is unknown, followed by the sudden return of the lost reactivity. Examples of such cases are an unintentional fuel withdrawal which precedes the dropping of the fuel back into the lattice or gas-bubble formation within the core of a water-moderated reactor and the subsequent sweeping out of the bubble.

(5) A still more deadly accident on which to speculate is one in which a control element worth several percent in Δk is inserted from above with an acceleration of several g's - and drops completely through the bottom of the reactor. This may not be as unlikely as it appears. Elements of this accident were discovered in one reactor after construction had actually started; changes had to be made in the reactor hardware so the rods would strike stops when their thin supports broke, rather than fall out the bottom.

Weaknesses similar to those in the above examples can be found in many reactors; often they can be identified only after an accident or a near accident. Only after such weaknesses have been eliminated can one operate a reactor with the assurance that the prompt action of the safety system will protect the reactor from any mistake on the part of the human operator or from any failure on the part of the devices on which he must depend.

Other Sources of Accidents

Reactor accidents external to the control and safety system may be postulated which do not involve failure of the instruments, the console operator or the control elements. The occurrence of these accidents may require the fastest possible safety system response. Some examples are listed below:

(1) Any mechanism which might alter the position of fuel is a potential hazard. Since the central fuel element of many reactors may be worth as much as 5% in Δk, any small vertical motion of this element might produce a large accident.

(2) When water is used as a moderator, substantial reactivity changes can result from voids. For example, a leaking gas line associated with an experiment can reduce the reactivity. When the leaking gas is shut off or the void collapses the reactivity is suddenly increased.

UNCLASSIFIED
ORNL–LR–DWG 21815

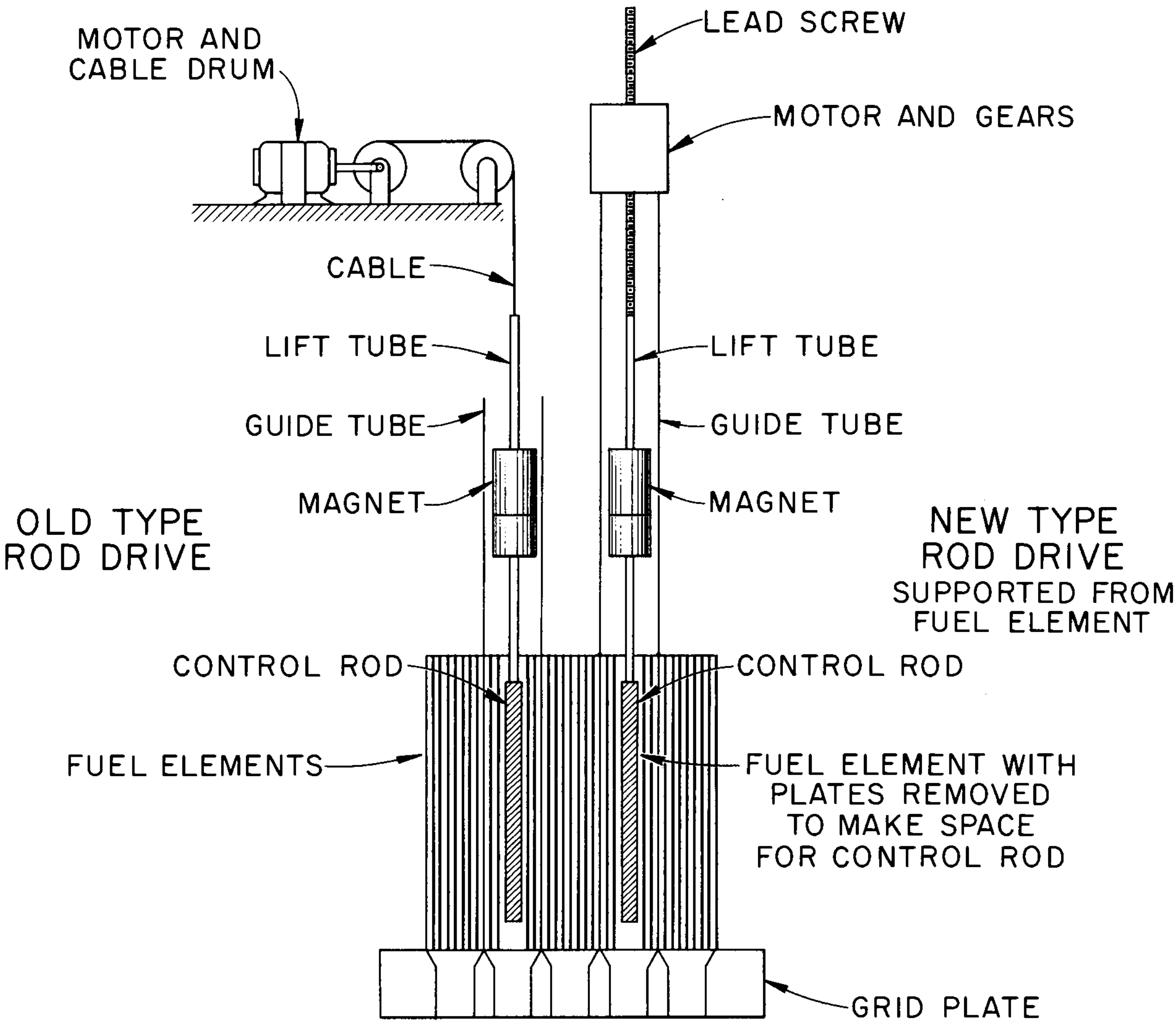

Fig. 2. Typical Swimming-Pool Rod Drives.

(3) The very accessibility of research reactors increases the possibility for unscheduled changes in reactivity.

In spite of experimental evidence that some reactor types have successfully withstood test excursions with reactor periods approaching one or two milliseconds, one remains unwilling to subject an operating reactor to periods shorter than 10 milliseconds, if this can be avoided. It is also true that very few practical reactors will behave as well as the Borax and SPERT reactors. It is proposed, therefore, that the safety system should be the fastest available, consistent with the type of reactor to which it is to be applied, and consistent with any necessary limitations on speed imposed by the thermal properties of the reactor.

Factors Limiting Safety System Response

A program is under way at ORNL to measure the practical limits of safety-system response under various conditions, and to develop suitable hardware.

In reviewing the factors which influence safety system response, it is observed that existing methods are not fully exploited.

(1) Sensing Delays

Equipment now available has a fast response to danger signals. The level safety amplifiers and chambers[6] now in use may be arranged to have a very short delay - much less than 1 millisecond. Preliminary evidence seems to show that the presently-used period instruments also have satisfactory response for handling fast accidents. For periods short compared to one second and for all currents within the range of the instrument, the reactor power increases less than a factor of *e* before the period safety instrumentation initiates a scram.

(2) Short and Consistent Release Time[7,8]

The need for short magnet release time is obvious when one is discussing periods in the 10-millisecond range. Consistency of release time is necessary in view of the wide variation possible in such factors as alignment and water-flow forces.

(3) Position of the Rods When They Are Released

Careful attention must be given to deciding where to position the limit switches which determine the upper limit of rod travel. If the rods are released from the fully-withdrawn position, their motion during the first increments of time will be through a region where they have low sensitivity (Δk/inch). Some time must elapse while the rods move to a more sensitive position where their motion can cause an appreciable reduction of reactivity. If the rods are actually withdrawn beyond the point of zero sensitivity, the price in delay time is tremendous. For the typical case of a rod moving in water with an acceleration of 0.75 g[7], starting the rod insertion from a point only 1-1/2 inches above the point of zero sensitivity will result in an added delay of 100 milliseconds.

Very significant gains in response may be realized by withdrawing the rods simultaneously during startup as opposed to withdrawing them singly or in small groups. If they are withdrawn together, they will be in the position of best possible overall sensitivity if at any time they must be released. This principle is illustrated in Figure 3. These considerations reinforce the argument given in an earlier paragraph in support of simultaneous rod withdrawal.

(4) Rod Acceleration After Release[9]

Even very bad accidents do not require the rods to reach the bottom of their travel in order to cope with the power excursion. The important decrease in reactivity is accomplished in the first few inches of rod insertion; in fact the rise of the power excursion is temporarily halted when the reactivity is reduced to prompt critical[4,10]. In reactors with short neutron lifetime, short-period accidents will involve reactivities not very much above prompt critical. Thus for these reactors which are most susceptible to short periods, a very small rod motion is needed to limit the excursion. In considering rod insertion speeds, therefore, the important parameter is the acceleration of the rod over the initial portion of its downward travel.

As a result of recent tests reported elsewhere,[7,8,9,10] there has been constructed at ORNL, and is now under test, a safety mechanism having a total delay time of 3 milliseconds with an initial rod acceleration of 8 g. While this development has been undertaken for a particular class of reactors, the writers feel that the principles underlying a specification of this type have general application. For each reactor type there is surely a comparable frontier of safety system response, taking into account the neutron lifetime, thermal characteristics, and so forth. It is planned to continue this work in order to improve understanding of the phenomena involved, both in Swimming-Pool reactors and in other types.

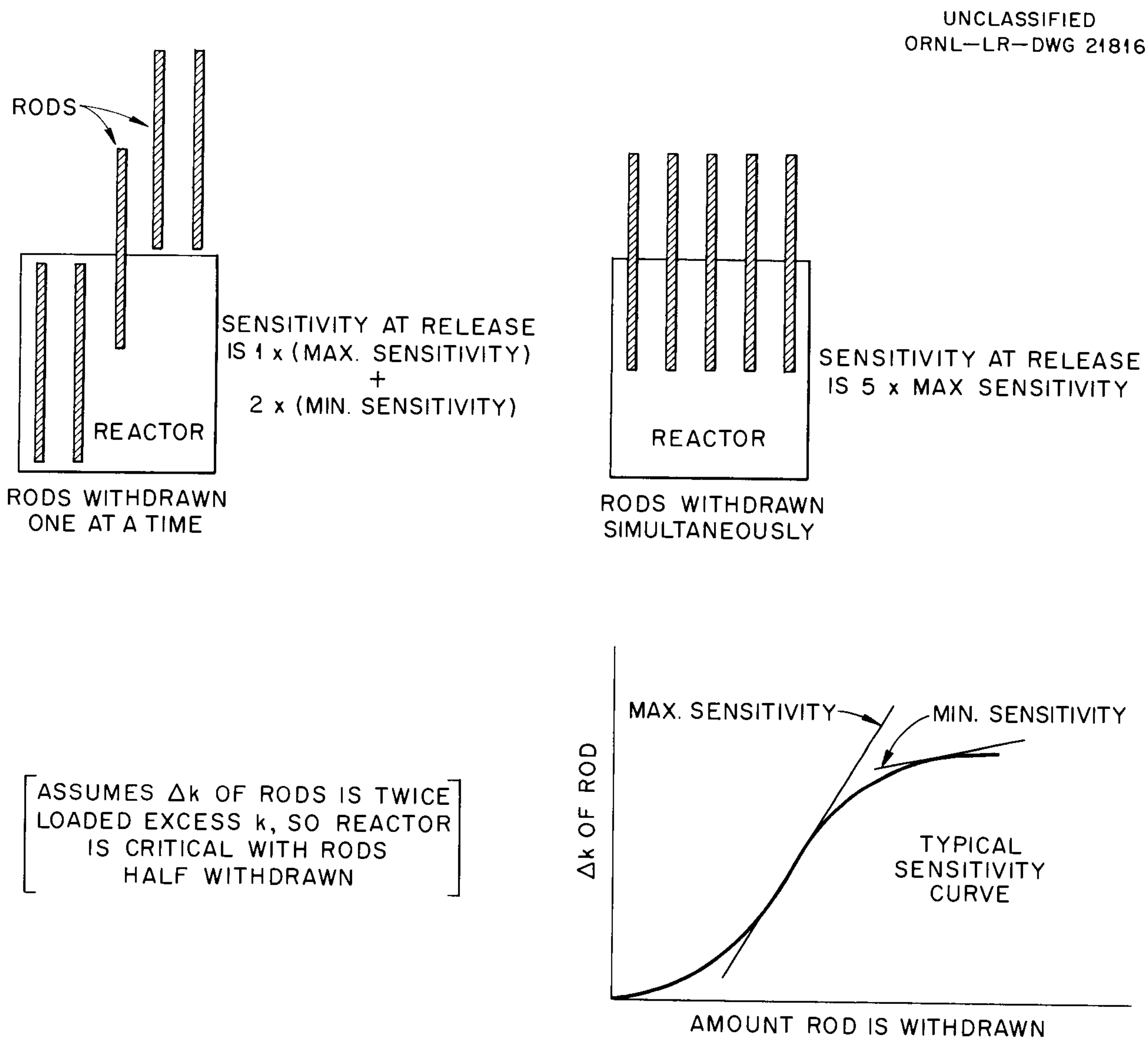

Fig. 3. Effect of Withdrawal Pattern on Sensitivity.

References

1. H. W. Newson, "The Control Problem in Piles Capable of Very Short Periods", AEC Document ORNL-1857, April 21, 1947.

2. J. R. Dietrich, Geneva Conference Paper No. 481, (1955).

3. W. E. Nyer, et. al., "Experimental Investigations of Reactor Transients", AEC Document IDO-16285, April 20, 1956.

4. F. Schroeder, et. al.,"Experimental Study of Transient Behavior in a Subcooled, Water-Moderated Reactor", Nucl. Sci. and Engr. 2, 96 (Feb. 1957)

5. R. J. Fox and L. C. Oakes (O.R.N.L.), private communication.

6. T. E. Cole, et. al., "The M.T.R. Safety System and its Components", AEC Document ORNL-1139, April 4, 1952.

7. C. Michelson, accompanying paper.

8. L. C. Oakes, accompanying paper.

9. A. A. Sorensen, accompanying paper.

10. E. R. Mann and F. P. Green, accompanying paper.

A DEVICE FOR DETERMINING SHIM ROD MAGNET RELEASE TIMES

L. C. Oakes

ABSTRACT

There are several methods by which the release time of shim safety rod electromagnets may be obtained in the laboratory. However, these methods are not generally applicable to magnets in operation.

This paper describes a pulse method for determining magnet release time in a field installation. The method also gives consistent and accurate measurements of release time in laboratory tests.

A Device for Determining Shim Rod Magnet Release Times

L. C. Oakes

In the control of reactors it is of interest to know as much as possible about the dynamics of the shim rods from the instant an emergency scram is initiated until the flux is reduced to a safe level. The work described in this paper is applicable to reactors which have shim rods supported by d.c. electromagnets supplied with current from the ORNL Safety System.

Initiation of the shim rod motion depends on the time required for the sensor to determine that such motion is needed and the time required for magnet release. Determining the release time under both laboratory and field conditions presents something of a problem. For accurately determining the magnet release time in the laboratory and in the field as well, a pulse release technique was developed.

This technique allows one to determine the release time of installed magnets. The method has also contributed to the establishment of specifications for an optimum magnet design.

Several methods have been used from time to time at ORNL to check release times of a given magnet in the laboratory. They almost always employ an electrical continuity measurement between magnet face and armature. An impulse is applied to interrupt the source of power to the magnet and simultaneously set a timer in motion to record the time interval between the initiation of the impulse and the separation of the magnet and armature. The timing system usually consists of a recording oscillograph or an audio oscillator and an oscilloscope with photographic attachment. See Figure 1.

This system has several inherent weaknesses which adversely affect the accuracy of the data; namely,

1. The armature does not move squarely away from the magnet. Thus one edge of the armature may maintain electrical contact long after the rod is in motion. This effect may be minimized by precise alignment of the vertical axis of the magnet and armature and by rigidly attaching the armature to the shim rod. However the latter is contrary to normal practice where a universal joint is frequently incorporated between the armature and the rod to provide better mating between the armature and the magnet to improve the reproducibility of the drop out current. Thus, the rigid coupling which improves the cocked armature effect may introduce still larger errors by altering the initial holding force. An experimental variation between similar drops is shown in Figure 2.

2. Frequently, the gap between the armature and magnet may be made in whole or part by a thin membrane of stainless steel, aluminum, or other low permeability metal which serves as a seal in potted magnets. This membrane may be stressed in manufacture so that it behaves like an oil can bottom. It may be held against the magnet by the armature while the current is on and upon release will follow the armature for a few thousandths of an inch, introducing

UNCLASSIFIED
ORNL-LR-DWG 21402

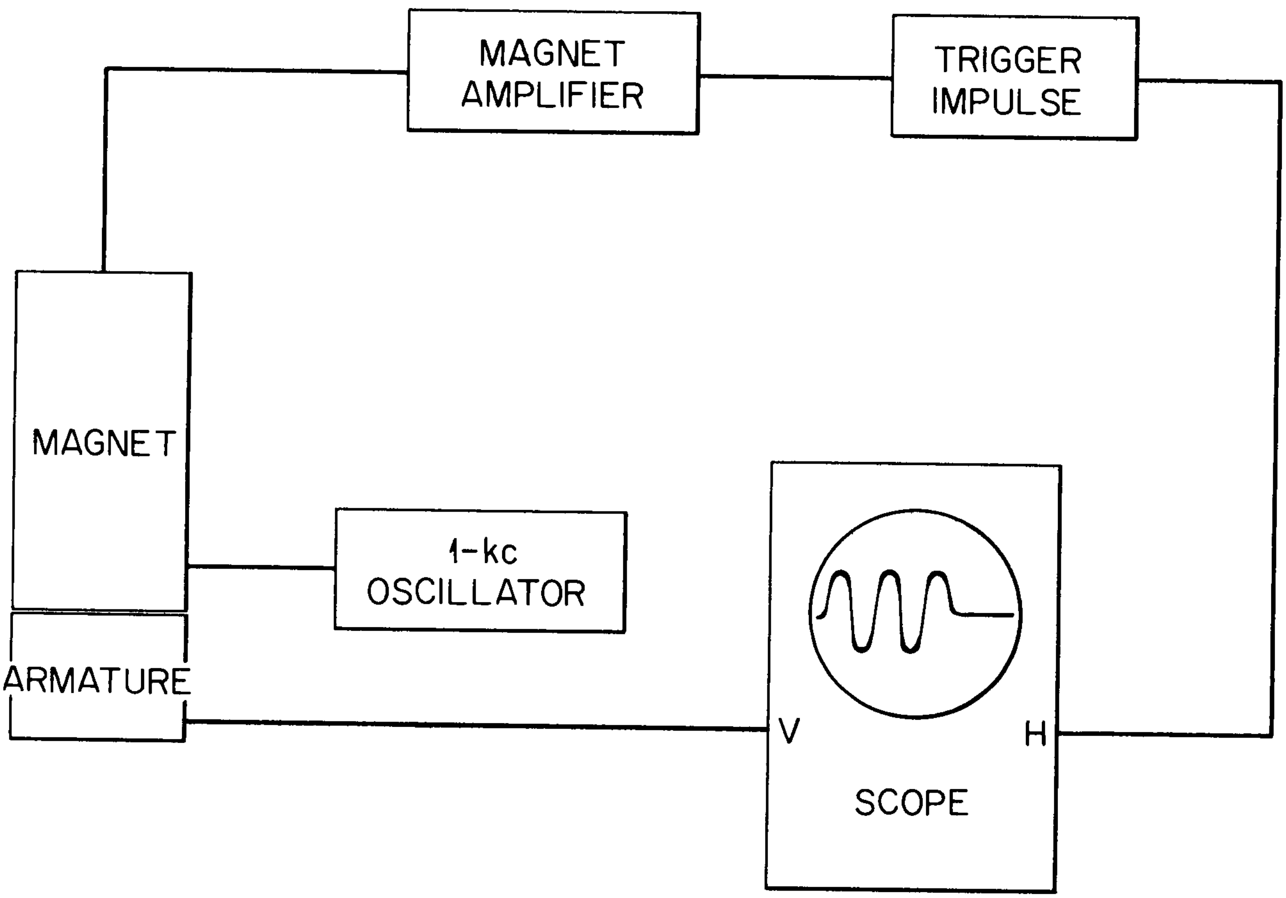

Fig. 1. Block Diagram of the Timing System.

UNCLASSIFIED
ORNL-LR-DWG 21278

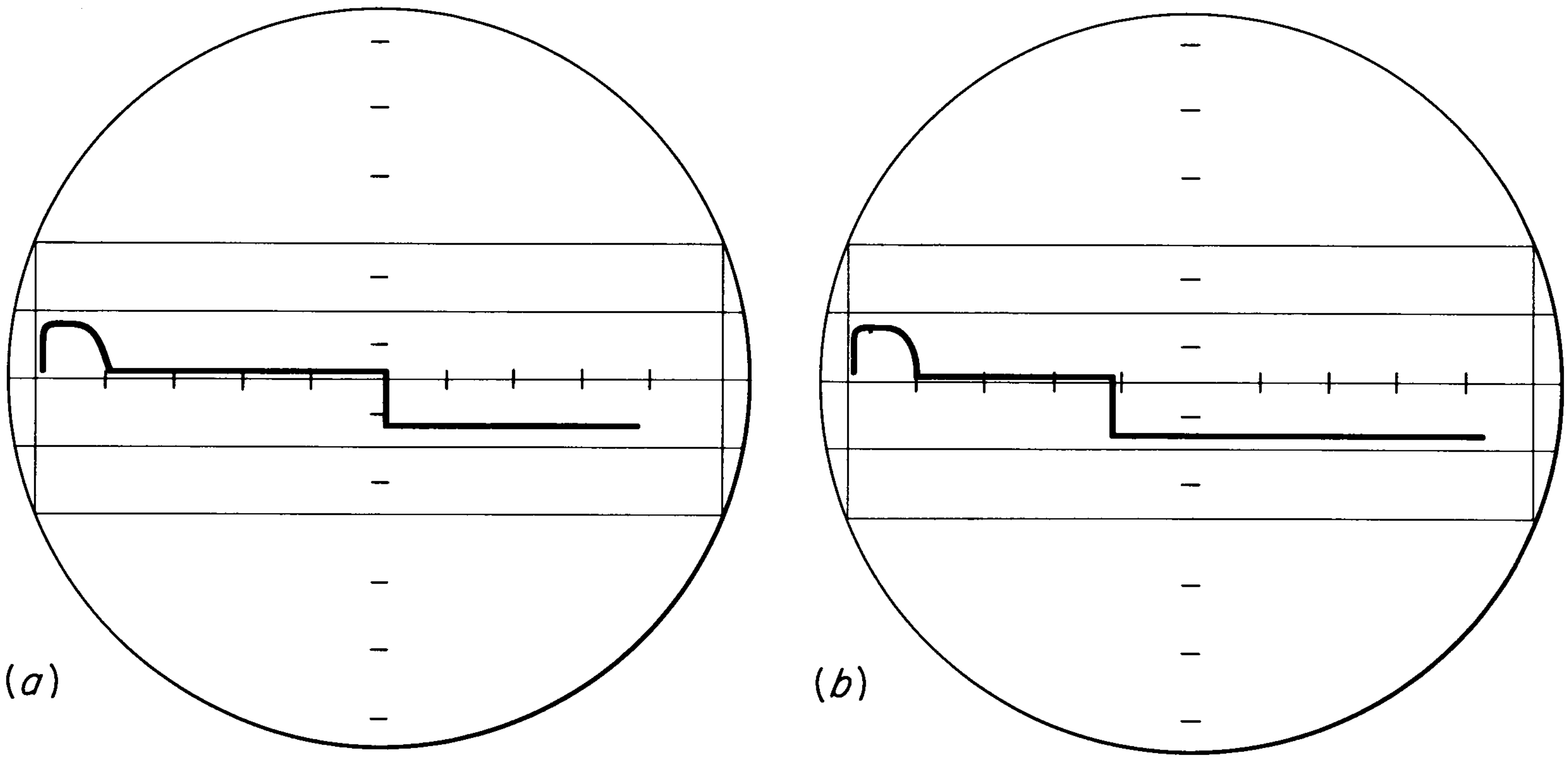

Fig. 2. Experimental Variation Between Similar Drops Obtained by System Shown in Fig. 1.

considerable error in a system with one g acceleration. The error is 2.3 milliseconds for the first 1/1000 of an inch follow, 3.2 milliseconds for a 2/1000 of an inch follow, etc. for a one g system.

3. There is some difficulty involved in synchronizing the start of the timing device and the interruption of the magnet current.

Most of these difficulties can be resolved sufficiently to gather useful data in the laboratory; however, the system is very nearly useless for checking installed units.

In order to discuss the operation of the pulse release method, a knowledge of the ORNL Safety System is needed for reference[1,2]. The fundamental circuits are shown connected in Figure 3.

The voltage shown at points "A" and "B" are the voltages one would measure with the reactor at zero power, 100% power and 150% power, respectively. These points show the most suitable places to which one can apply the output of the pulser.

If a potential of 22 volts is applied at point "A" the magnet current should read maximum. If the voltage at point "A" is increased until 37 volts is reached, the magnet current will have reduced to the point at which the weight of the shim rod can no longer be supported. This requires the amplifiers to be adjusted properly. Likewise, if the voltage at point "B" is varied from 37 to 43-1/2, the magnet current will vary from maximum to the release value. These variables dictate the design of the pulsing instrument. The output must have a quiescent level which may be set to either 22 volts to match the steady state of zero power level of point "A" or 37 volts to match point "B". The amplitude of the pulse must be sufficiently large to drive point "A" from 22 volts to a value somewhat larger than 37 volts to guarantee release of the rod. This maximum value is approximately 40 volts, requiring that the pulse have a peak value of at least 18 volts. The pulse amplitude needed to accomplish the same thing at point "B" is only approximately 8 volts. The instrument should have a pulse width variable from zero to the longest release time anticipated.

The ORNL pulser is shown by the block diagram in Figure 4. The circuit is timed by a free running blocking oscillator whose recurrence frequency may be adjusted from 1/2 cycle/second to 3 cycles/second. The output is fed through a buffer stage to trigger a one-shot multivibrator which has a variable pulse width. The multivibrator drives a cathode follower stage whose output may be adjusted to give the desired static level. The amount of drive from the multivibrator is controlled to give any desired output pulse amplitude from zero to 50 volts as read on the output voltmeter. The circuit diagram is shown in Figure 5.

Operation of the unit is relatively simple and consists of applying the output to either point "A" or to point "B" in the safety system and adjusting the steady state level accordingly. The pulse width should be zero and the blocking oscillator should be turned off. Depressing push button "P" forces the multivibrator to remain triggered and permits the drive to the cathode follower to be adjusted to reduce the magnet current to zero (or at least to the release value). The rod is then re-cocked, the blocking oscillator is turned on and the pulse

UNCLASSIFIED
ORNL-LR-DWG 21275

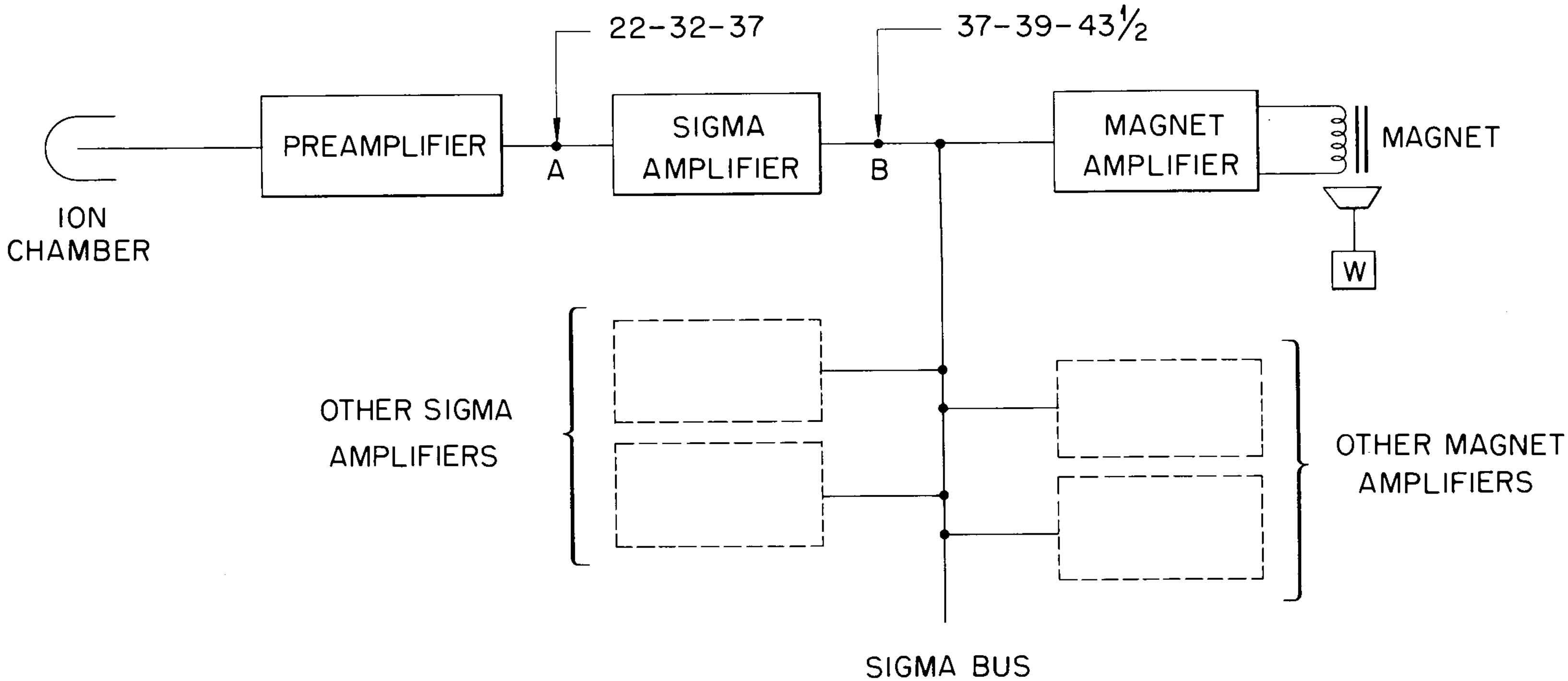

Fig. 3. Typical Safety Channel.

UNCLASSIFIED
ORNL-LR-DWG 21276

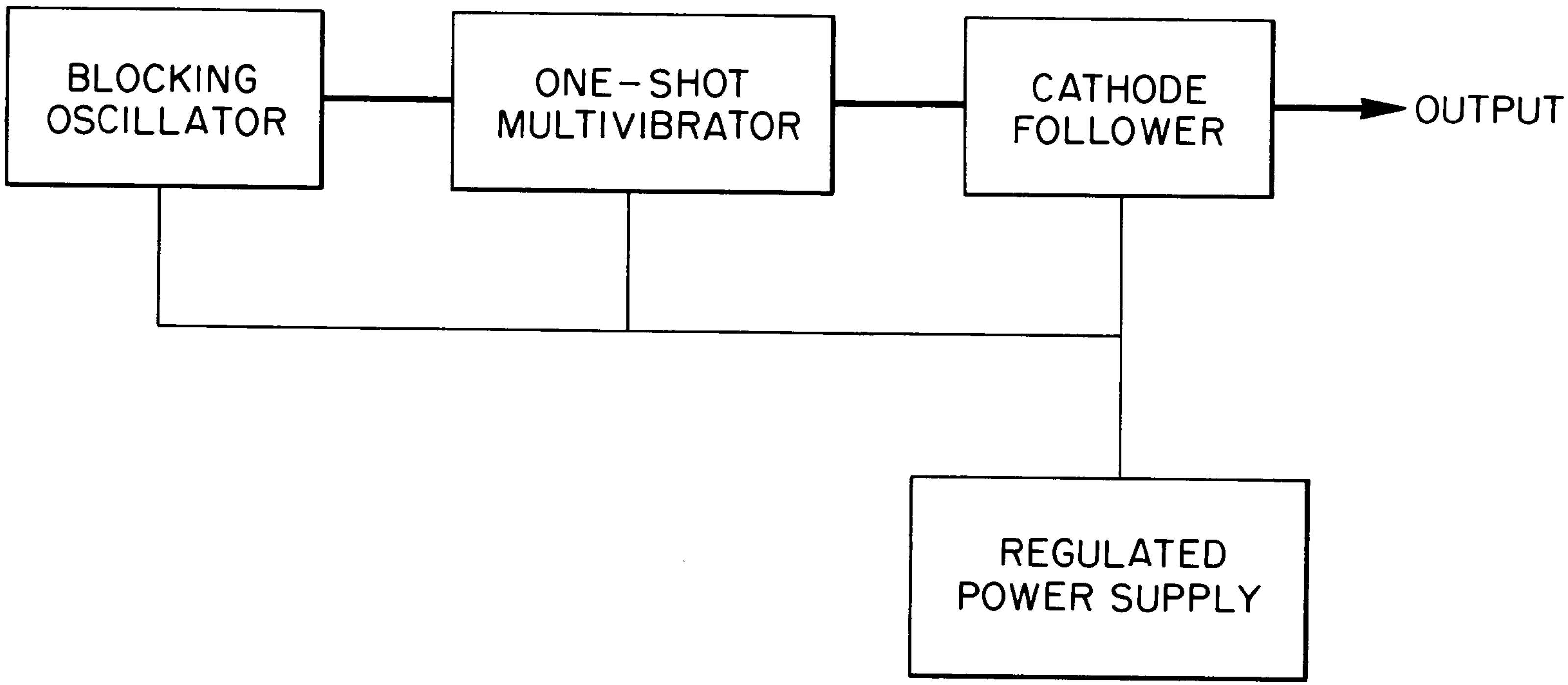

Fig. 4. Pulser Block Diagram.

width is slowly increased until the magnet releases the rod. The release time may then be read directly in milliseconds from the calibrated pulse width dial.

The accuracy of the indicated release time has proven to be very good. If one defines the actual release time as the elapsed time between the initiation of a scram impulse and the first movement of the armature, it is obvious that the indicated release time is greater than the actual release time since the magnet is capable of retrieving the armature when the current is re-established even though they have separated some small distance. The amount of error introduced by this effect does not lend itself easily to a mathematical analysis because it is influenced by many factors such as excess holding force exerted by the magnet, and the medium in which the system is operating. Therefore, an experiment was set up to establish trends and limits to the error in some practical cases. The assembly for this experiment is shown in Figure 6. It consists of a 100 turn test coil embedded in the armature in such a way as to link the same flux lines which are producing the holding force on the armature. The output voltage is proportional to the rate of change of flux linking the test coil. A typical pattern is shown in Figure 7, and represents a single pulse approximately 78 milliseconds long which did not release the weight. Figure 8 shows a series of pulses, each successive one longer than the preceding one and each showing the flux decaying to a lower value. Figure 9 shows the armature beginning to fall away just before the flux is re-established and Figure 10 shows the final break away. The time between the inflection point on the curve in Figure 10 and the final break away is the error in milliseconds. In the example in Figure 10, the error is 8 milliseconds which is a percentage error of 9%.

The results of some tests on the LITR are shown in Figure 11.

In conclusion it may be said that:

1. The pulser may be readily applied in the field without additional equipment and without the necessity of altering the safety system.

2. The release data are more consistent and do not have the widespread variation inherent in other release time measuring devices.

3. The pulser will measure release time with an accuracy of approximately 10%.

4. The pulse width is always larger than the time interval between the initiation of an impulse and the first movement of the armature; consequently, the actual release time is less than the pulse width.

UNCLASSIFIED
ORNL-LR-DWG 21277

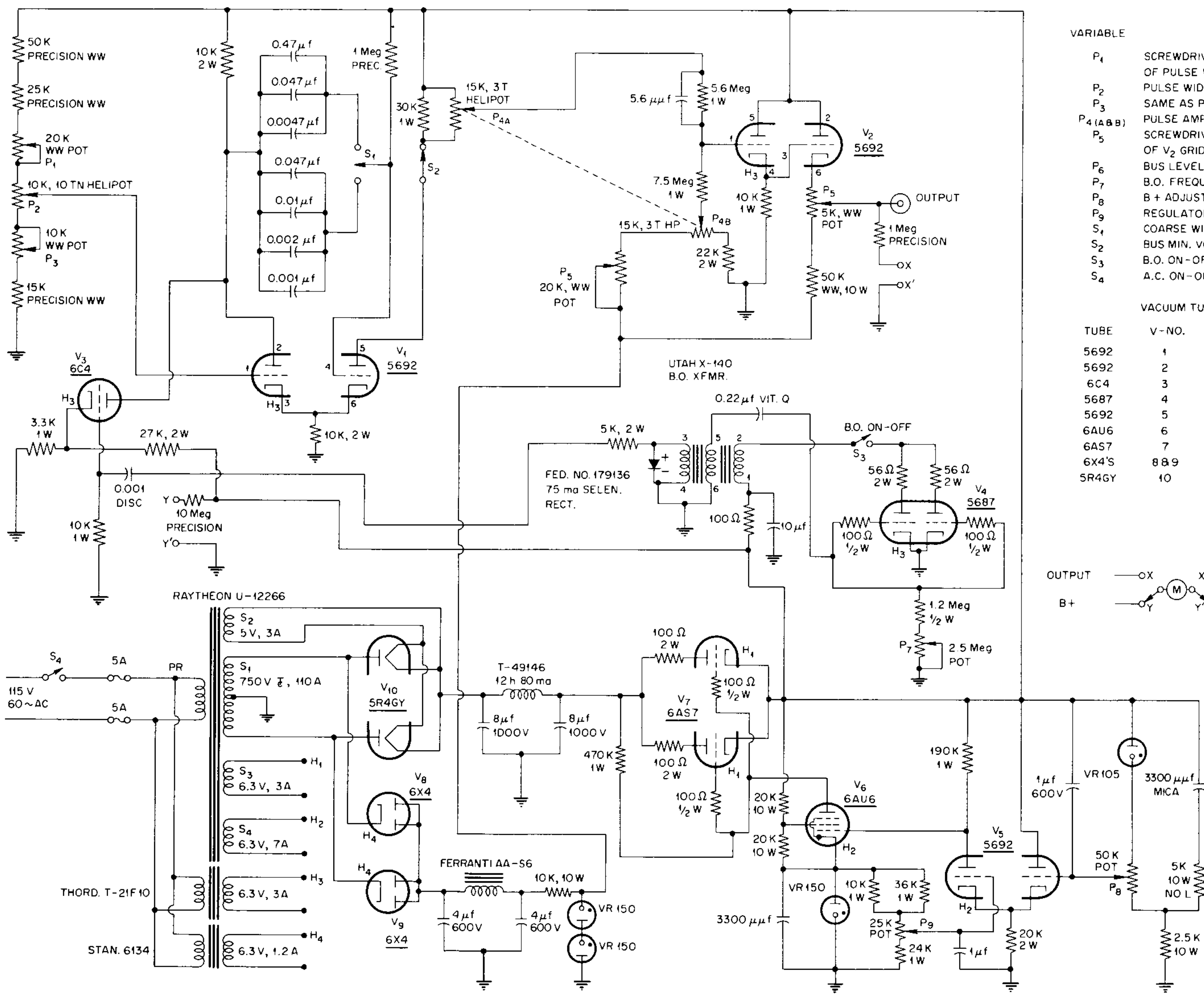

VARIABLE	CIRCUIT FUNCTION
P_1	SCREWDRIVER ADJUST POT FOR SETTING LIMITS OF PULSE WIDTH CONTROL.
P_2	PULSE WIDTH CONTROL.
P_3	SAME AS P_1.
$P_{4(A\&B)}$	PULSE AMPLITUDE CONTROL.
P_5	SCREWDRIVER ADJUST POT FOR SETTING LEVEL OF V_2 GRID NO. 1.
P_6	BUS LEVEL ADJUST POT.
P_7	B.O. FREQUENCY ADJUST.
P_8	B + ADJUST.
P_9	REGULATOR BIAS ADJUST.
S_1	COARSE WIDTH CONTROL.
S_2	BUS MIN. VOLTAGE ADJUST.
S_3	B.O. ON-OFF SWITCH.
S_4	A.C. ON-OFF SWITCH.

VACUUM TUBE COMPLEMENTS

TUBE	V-NO.	CIRCUIT FUNCTION
5692	1	MULTIVIBRATOR.
5692	2	C.F. LEVEL SET.
6C4	3	MULTIVIBRATOR TRIGGER.
5687	4	BLOCKING OSCILLATOR.
5692	5	REGULATOR AMP.
6AU6	6	REGULATOR AMP.
6AS7	7	SERIES REGULATOR.
6X4'S	8 & 9	NEG. RECTIFIER.
5R4GY	10	B + RECTIFIER.

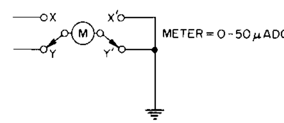

Fig. 5. Pulse Generator for Magnet Release Test Measurements.

UNCLASSIFIED
PHOTO 40563

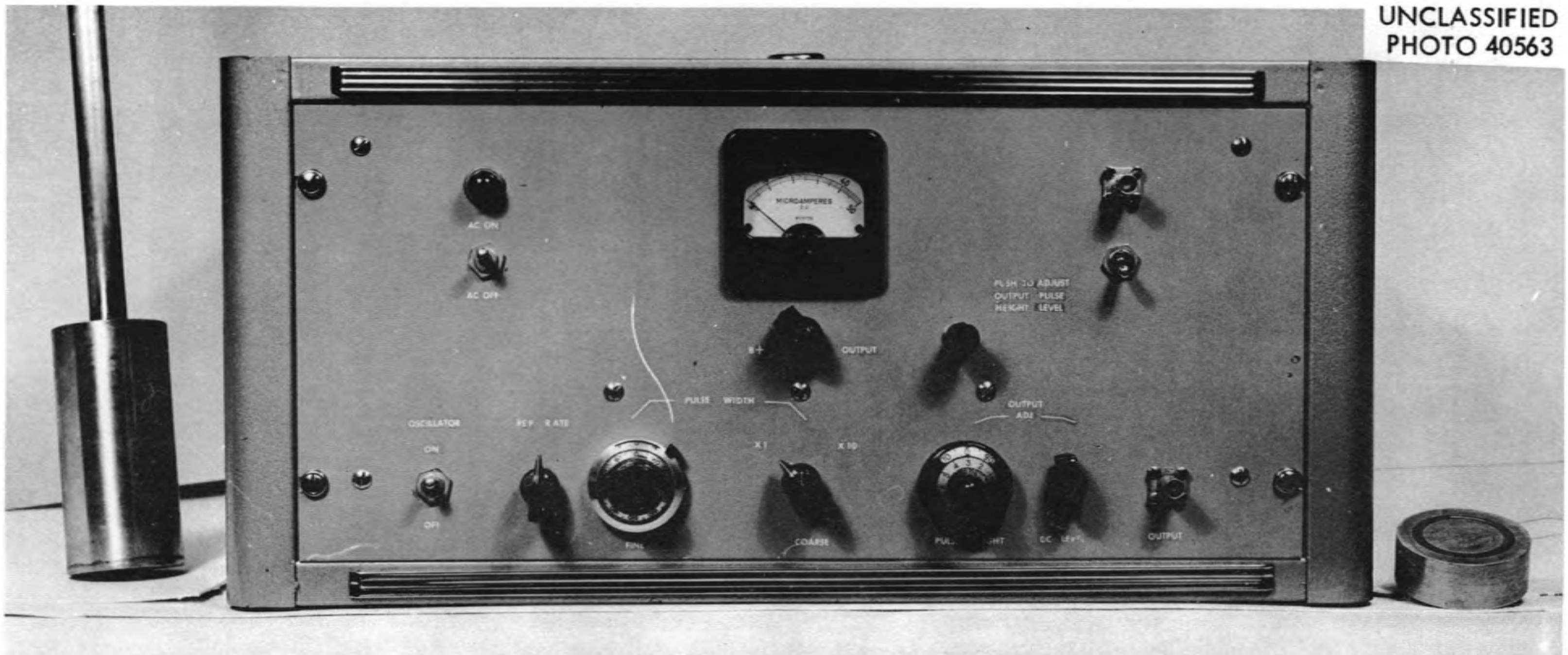

Fig. 6. Instrument Shown Schematically in Fig. 1 with Magnet and Armature.

UNCLASSIFIED
ORNL-LR-DWG. 21419

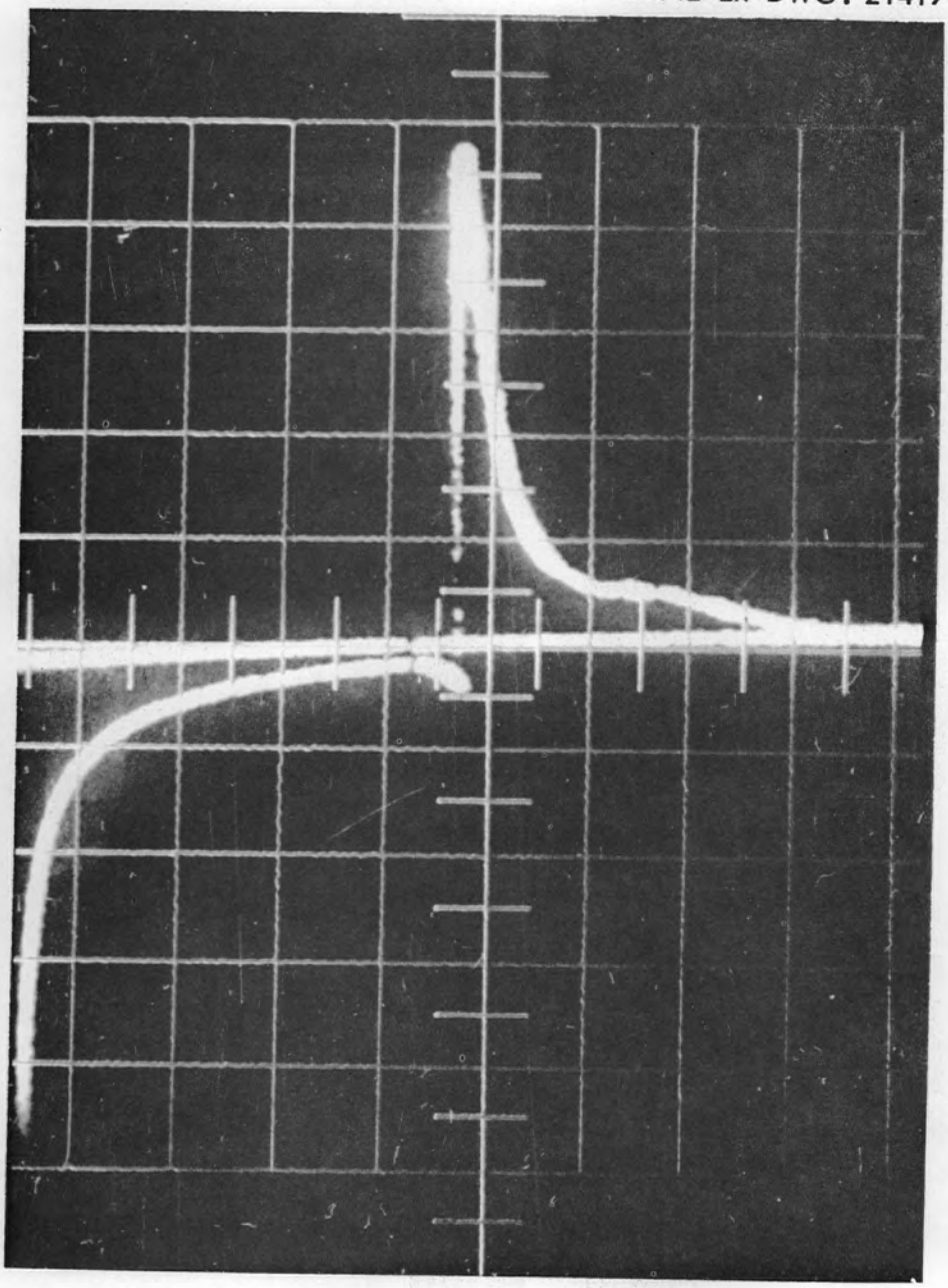

MAGNET: BSF
AIR GAP: 6 mils
CURRENT: 100 ma

ROD WEIGHT: 12 lb
PULSE WIDTH: 78 msec

Fig. 7. Oscilloscope Trace.

UNCLASSIFIED
ORNL-LR-DWG. 21420

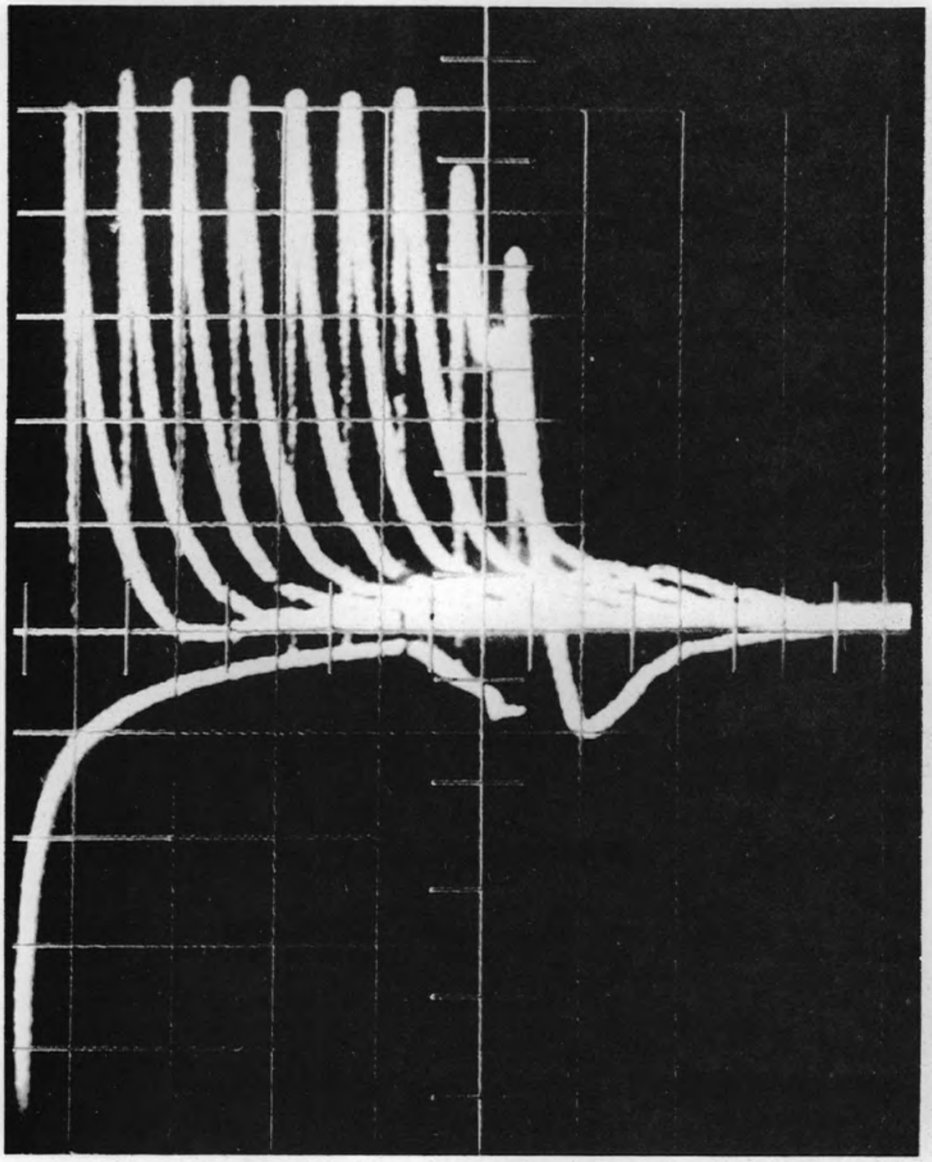

MAGNET: BSF
AIR GAP: 6 mils
CURRENT: 100 ma
ROD WEIGHT: 12 lb
PULSE WIDTHS: 10, 20--90 msec

Fig. 8. Oscilloscope Trace.

UNCLASSIFIED
ORNL-LR-DWG. 21418

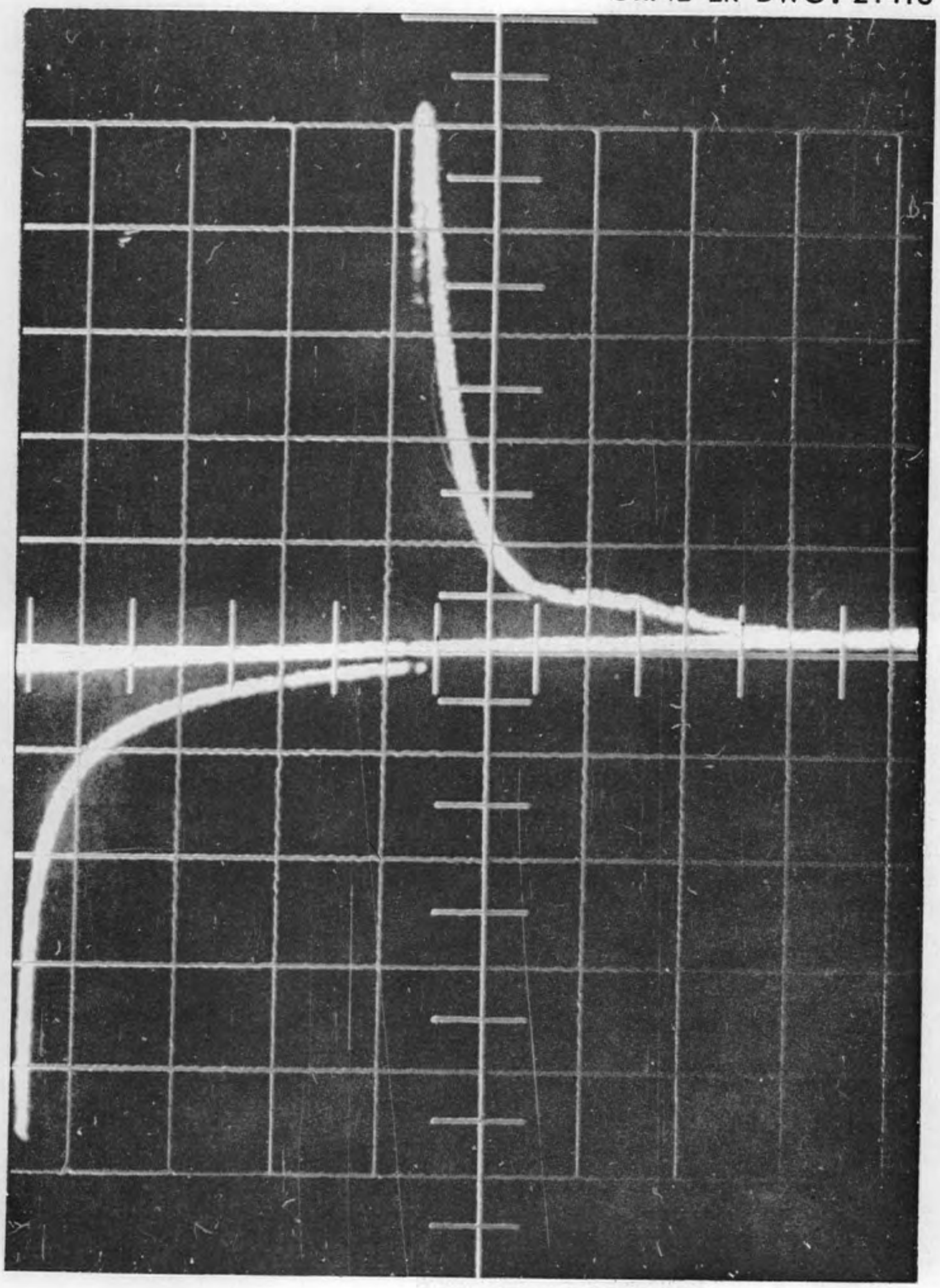

MAGNET: BSF
AIR GAP: 6 mils
CURRENT: 100 ma
ROD WEIGHT: 12 lb
PULSE WIDTH: 78 msec

Fig. 9. Oscilloscope Trace.

UNCLASSIFIED
ORNL-LR-DWG. 21416

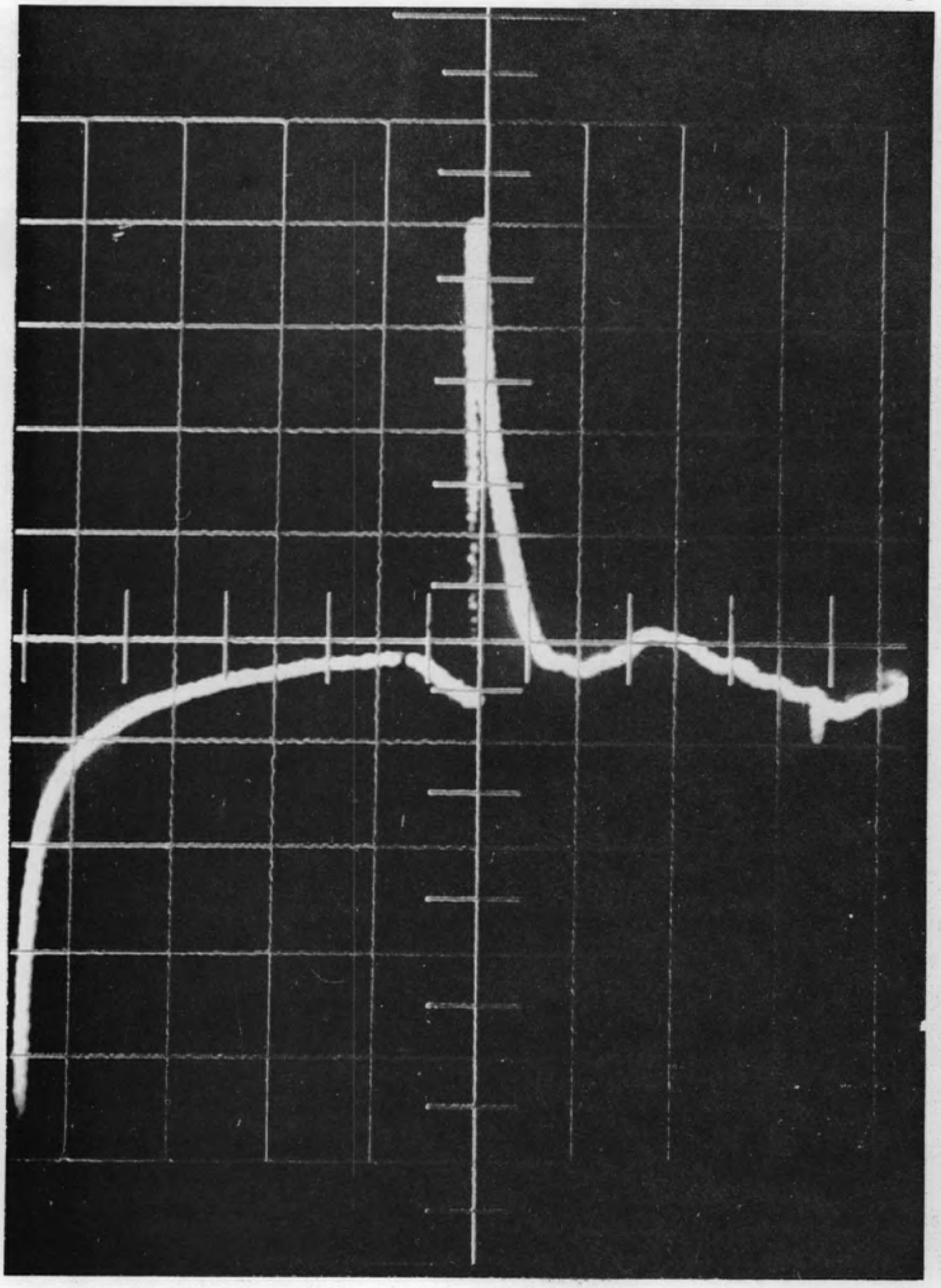

MAGNET: BSF
AIR GAP: 6 mils
CURRENT: 100 ma
ROD WEIGHT: 12 lb
PULSE WIDTH: 82 msec

Fig. 10. Oscilloscope Trace.

UNCLASSIFIED
ORNL—LR—DWG 21485

ROD NO.	WITHDRAWN 3 INCHES	WITHDRAWN 15 INCHES
1	26 ms	32 ms
2	11.5 ms	11 ms
3	21 ms	21.2 ms

Fig. 11. Data from LITR.

References

1. H. E. Banta, S. H. Hanauer, Procedure for Testing Magnet Amplifiers, ORNL CF-56-5-30.

2. C. Michelson, accompanying paper.

EXPERIMENTAL EVALUATION OF ELECTROMAGNETS FOR RESEARCH REACTORS

C. Michelson

On loan from Tennessee Valley Authority

ABSTRACT

This report reviews the basic principles of electromagnet design, with special emphasis on the factors which affect release time, and presents an experimental evaluation of the performance of solid and slotted pole electromagnets used in research type reactors. The potential hazards of improper magnetic circuit arrangements are pointed out, and the problem of performance specification and evaluation is reviewed.

Experimental Evaluation of Electromagnets for Research Reactors

C. Michelson

I. INTRODUCTION

Many research type reactors built to date use electromagnets in their safety systems to hold scram rods in cocked position during normal operation. These magnets may be of the direct lifting type which support the entire rod weight, or they may be of the type designed to hold accelerating springs or latch mechanisms. Regardless of the method of transmitting support, however, these magnets have one common requirement. They must release quickly in the event of a scram situation. Acceptable magnet release times range from about five to fifty milliseconds, as determined by the nuclear, thermal, and physical characteristics of the particular reactor and the response time of the associated safety system components.

If a high degree of safety confidence is placed in a fast release electromagnet, it is important that the release behavior of the device be well understood and established by careful laboratory calibration. There must be no chance for manufacturing error, equipment adjustment error, or aging or radiation effects to appreciably increase the release time. It is the purpose of this report to review the basic principles of electromagnet design, with special emphasis on the factors which affect release time, and to establish basic design criteria and methods of experimental evaluation which will assure fast release for all operating situations.

Type of Magnet Studied

The scope of this report is limited to flat-faced cylindrical electromagnets such as used in the swimming pool type research reactor. Figure 1 is a pictorial representation of this magnet type. The magnet is shaped as a right circular cylinder. Its inside and outside poles, and yoke and armature are made of ingot iron. The poles may be tapered. The magnet coil is wound on a linen Bakelite bobbin and held in place by a metal retaining ring. The magnet coil wire is triple-layer enameled copper. The coil is vacuum impregnated with an epoxy resin. The coil leads are Teflon insulated. In the swimming pool type reactor this magnet is supported at the end of a 17-foot lift tube which extends from the pool surface to the reactor lattice. The lift tube is welded to the magnet support. The magnet support is bolted to the yoke. The entire magnet assembly is encased in a stainless steel can which is seal welded to the magnet support. This provides a water-tight conduit for the coil leads. The magnet can is usually provided with a nickel face because it must be sufficiently thick to maintain good structural integrity, and yet have low reluctance. In the pool type research reactor, the safety (scram) rod is attached to the magnet armature. The magnet supports the entire weight of the safety rod and shock absorber assembly, plus the armature. This weight ranges from twelve to eighteen pounds.

UNCLASSIFIED
ORNL-LR-DWG 21257

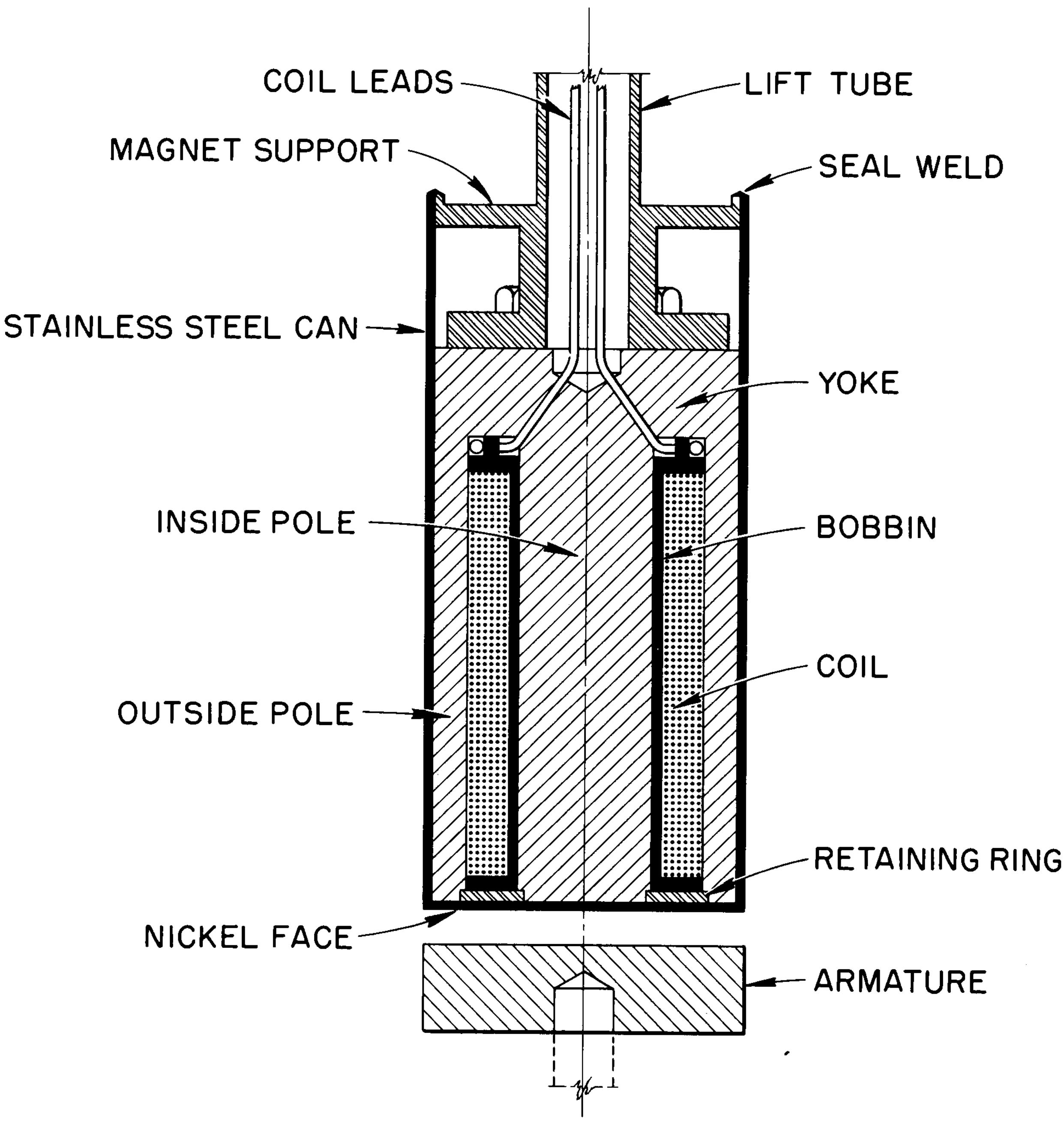

Fig. 1. BSF-Type Magnet.

An important point to bring out in regard to this magnet is the requirement that it must operate like a precision relay, and yet be held at the end of a 17-foot tube under water with varying amounts of dirt on the contact surfaces, and with a wide range of possible misalignment conditions due to a bent lift tube or axial displacement. It must be large forcewise, and yet small in diameter, and it must operate on a very small magnet current. Its excess holding force must be sufficient to prevent accidental scram due to jars or vibrations, but its release time must still be very short.

The shape of the magnet shown in Figure 1 is not ideal, magnetically speaking. An optimum design would be shorter and larger in diameter, but space restrictions force the design to small diameters and proportionally greater lengths.

Magnet Power Supply

In order to obtain fast release, it is necessary to break the magnet's electrical circuit through a very high impedance. This is accomplished by supplying magnet current through the plate circuit of a pentode tube which can be biased highly negative. It is not feasible to break the electrical circuit through relay contacts because the contact arc forms a very low resistance path which may persist for a long period of time. The magnets included in this study are designed for use with a single vacuum tube power supply (magnet amplifier) delivering 100 ma. maximum. This instrument is described in detail in the literature[1].

The operating characteristics of the magnet amplifier, shown in Figure 2, are controlled by the voltage from a safety amplifier. This voltage, termed the sigma bus voltage, indirectly controls the bias on a pentode tube supplying the magnet current. When the power level of the reactor is zero, the sigma bus voltage is 37 V. As the reactor increases to full power the sigma bus voltage increases to 39 V. At 150% full power the sigma bus voltage is 43.5 V. The magnet amplifier is designed to reduce the magnet current about 15 ma. between zero power and full power, and another 27 ma. between full power and 150% full power. At 150% full power the magnet current equals the drop current for the given magnet. As the sigma bus voltage continues to increase, the magnet current quickly goes to zero. For slow periods or power rises, magnet release will occur at 43.5 V. on the sigma bus. For fast periods or power rises, the time required to increase the sigma bus voltage from 37 V. to current cut-off voltage is small compared to the magnet release time.

Behavior of Elementary Model

One method of interpreting experimental measurements of magnet parameters is to create a simplified model of the device and study its behavior from idealized basic equations. Such a model is shown in Figure 3. This model is constructed from annealed ingot iron. For this idealized case, all flux which does not pass perpendicularly through the air gap is assumed to be leaking or fringing. This leakage and fringing flux is nonuniformly distributed along the inside and outside poles and armature, but it is assumed its effect can be fully evaluated by averaging the flux along an average path length (L_1). The average flux in the iron (ϕ_1) is equal to the total perpendicular flux in

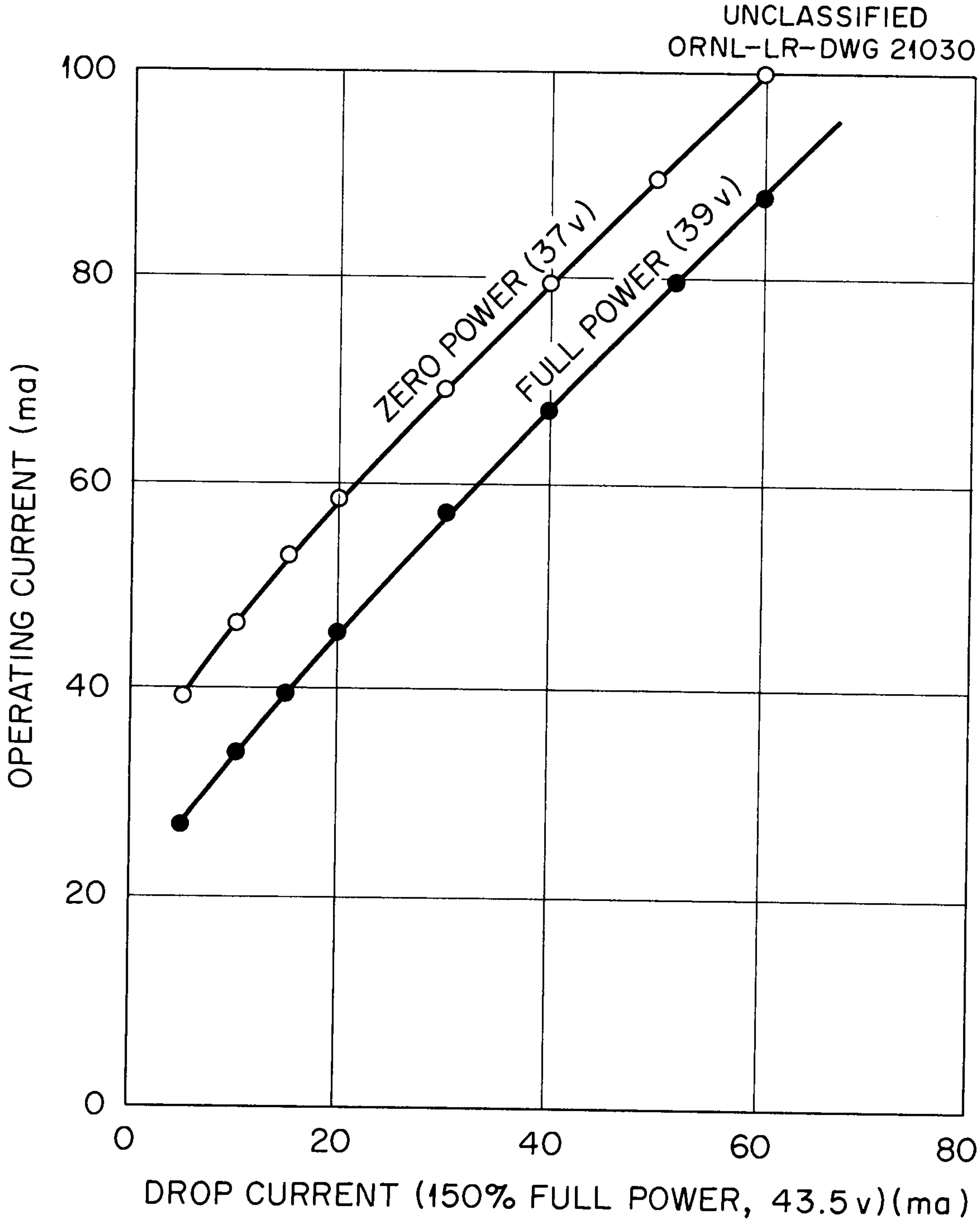

Fig. 2. Magnet Amplifier Characteristics.

UNCLASSIFIED
ORNL-LR-DWG 21256

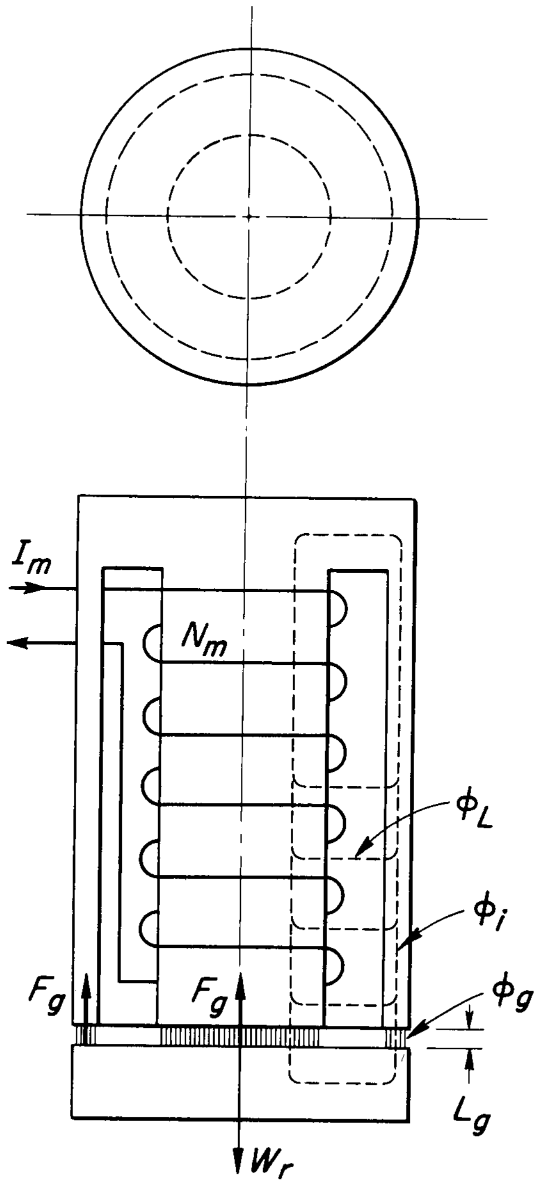

MATERIAL: ANNEALED INGOT IRON

$\phi_i = \phi_g + K\,\phi_L = 1.3\,\phi_g$

$L_i = 8$ in.

$A_i = A_g = 0.6$ in.^{2}

$N_m = 5000$ TURNS

I_m – VARIABLE

L_g – VARIABLE

Fig. 3. Magnet Model.

the air gap (ϕ_g), plus a K portion of the total leakage and fringing flux (ϕ_L). The resulting average flux in the iron is assumed to be a constant percentage of the air gap flux. For this model it is 1.3 ϕ_g. The cross-section iron area (A_i) at all points along the average flux path is equal to the cross-sectional area of the air gap (A_g). The holding force produced by the perpendicular flux in the air gap is F_g. Since there are two effective air gaps in parallel, the magnet produces a total holding force (F_m) equal to $2F_g$, acting along the magnet axis. The magnet coil contains 5000 turns of wire. The magnet current (I_m) and air gap (L_g) are variable.

The basic equations which influence the model behavior are given in Figure 4. The general magnet equation is for the summation of magnetomotive forces around a closed loop. This loop follows the average path length in the iron and includes two air gaps. The driving force required for the iron is a function of flux density in the iron. The value of this function is obtained from magnetization curves and hysteresis loops for the material. The driving force required for the air gaps varies as the first power of flux density in the air gaps. The holding force varies as the square of this flux density.

From the data given for the magnet model, and the basic equations, it is possible to construct model operating characteristics as a function of magnet current and air gap. Figure 5 shows a set for L_g = 0.005-in. The hysteresis loop for iron is obtained from Roters[2] for the case, $B_i = 1.3\ B_g$. The ingot iron curve indicates the magnet current required to establish a given flux density in the air gap, assuming the magnetic reluctance drop across the air gap to be zero. The air gap curve indicates the current required to establish a given flux density in the air gap, assuming the magnetic reluctance drop in the iron to be zero. The total current required to establish a given flux density in the air gap is the sum of these two currents. The force produced is proportional to the square of the established flux density.

The hysteresis of iron results in negative values of current being required to establish low flux densities in the iron after it is first raised to high flux values. This negative current is subtracted from the current required for the air gaps. The resulting flux density curve and holding force curve follow a hysteresis type path over a given operating cycle.

In evaluating an electromagnet, the information most easily obtained in the laboratory is a set of holding force curves. Figure 6 shows the holding force curves which would be observed for this idealized magnet. From these curves it can be seen that even small air gaps have a pronounced effect on the overall magnet characteristics. The rapid loss of holding force with increasing air gap is a characteristic of this magnet type.

The energy storage and release which occurs in this model during a complete magnetic cycle is shown in Figure 7b, for a constant 0.005-in. air gap. As the magnet current (I_m) is increased from zero, the flux density in the air gap (B_g) increases along the path 0-A to point A (a long tail on the curve is omitted to conserve space). The energy (E_m) stored in the magnet during the flux rise is:

$$E_m = K \int I_m \, dB_g \qquad (1)$$

UNCLASSIFIED
ORNL-LR-DWG 21255

MAGNET (m)

$$I_m N_m = MMF_i + 2\,MMF_g$$

$$F_m = 2\,F_g$$

IRON (i)

$$MMF_i = H_i L_i$$

$$H_i = f(B_i)$$

AIR GAP (g)

$$MMF_g = \frac{B_g L_g}{3.2}$$

$$F_g = \frac{B_g^{\,2} A_g}{72 \times 10^6}$$

MMF = MAGNETOMOTIVE FORCE (amp – turns)
F = HOLDING FORCE (lb)
B = FLUX DENSITY (lines/in.^{2})
H = MAGNETIC INTENSITY (amp – turns/in.)
A = AREA (in.^{2})
L = LENGTH (in.)
I = CURRENT (amp)
N = TURNS

Fig. 4. Basic Equations.

UNCLASSIFIED
ORNL-LR-DWG 20927R

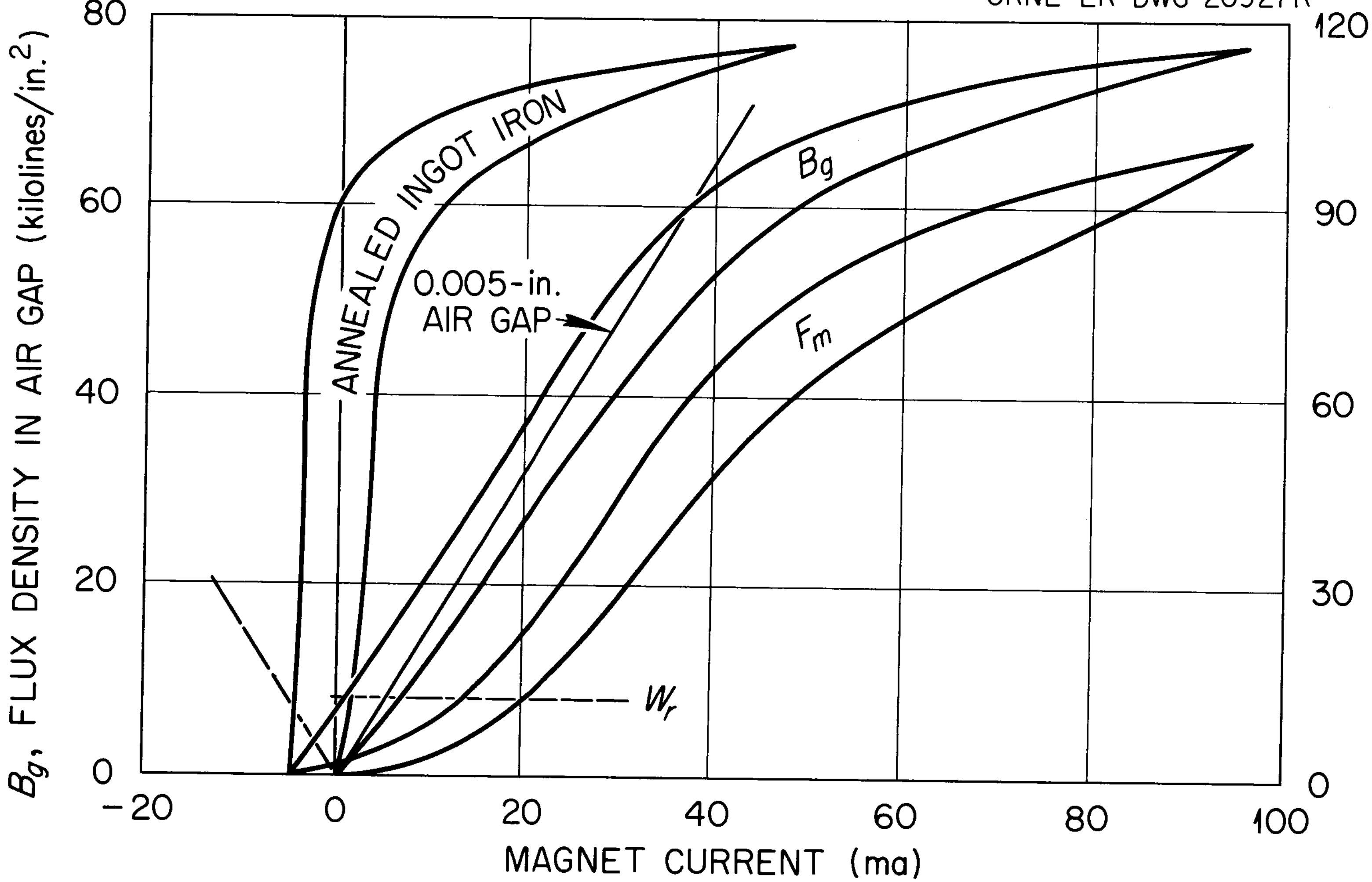

Fig. 5. Operating Characteristics of Magnet Model.

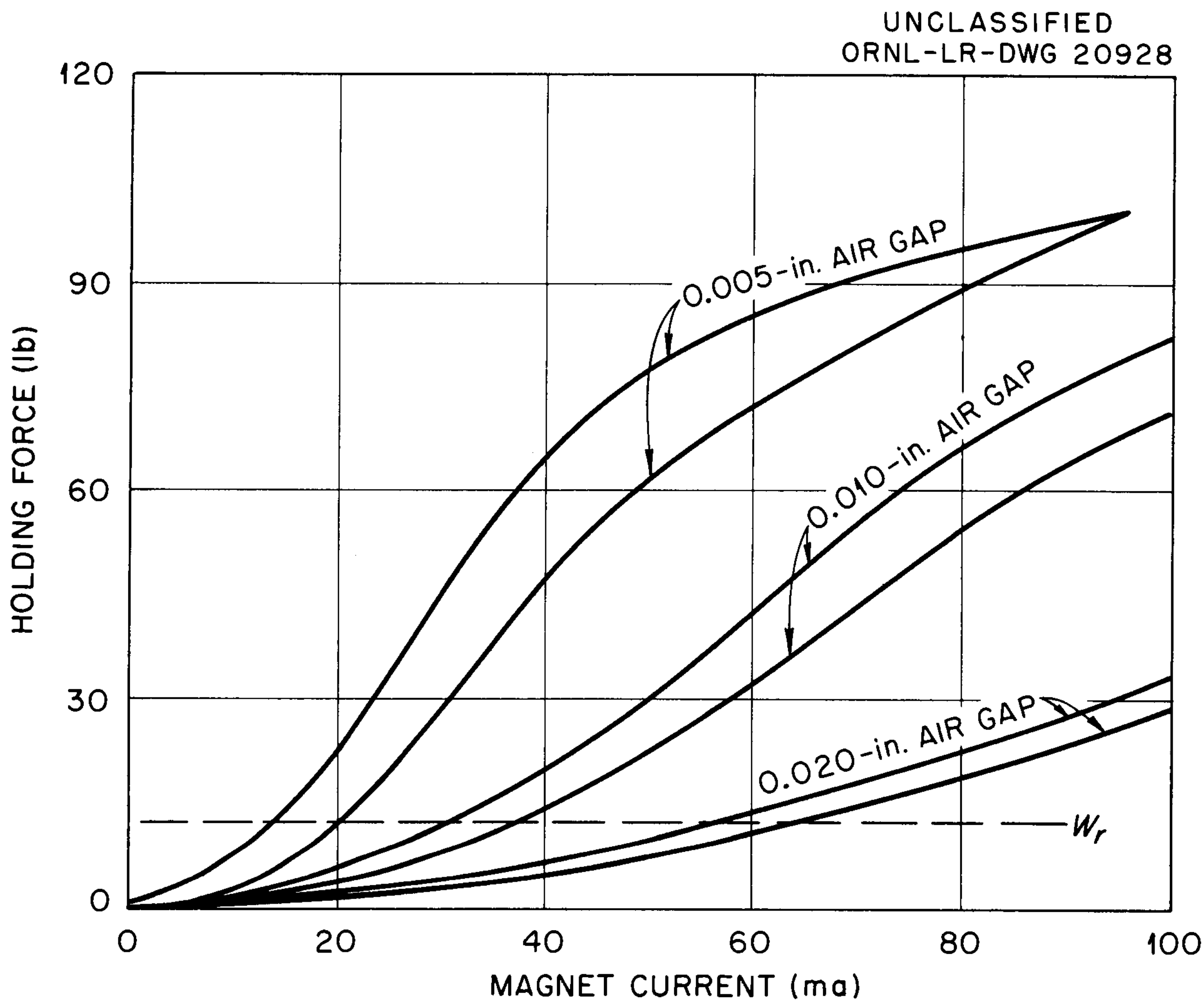

Fig. 6. Holdging Force Characteristics of Magnetic Model.

UNCLASSIFIED
ORNL-LR-DWG 20926A

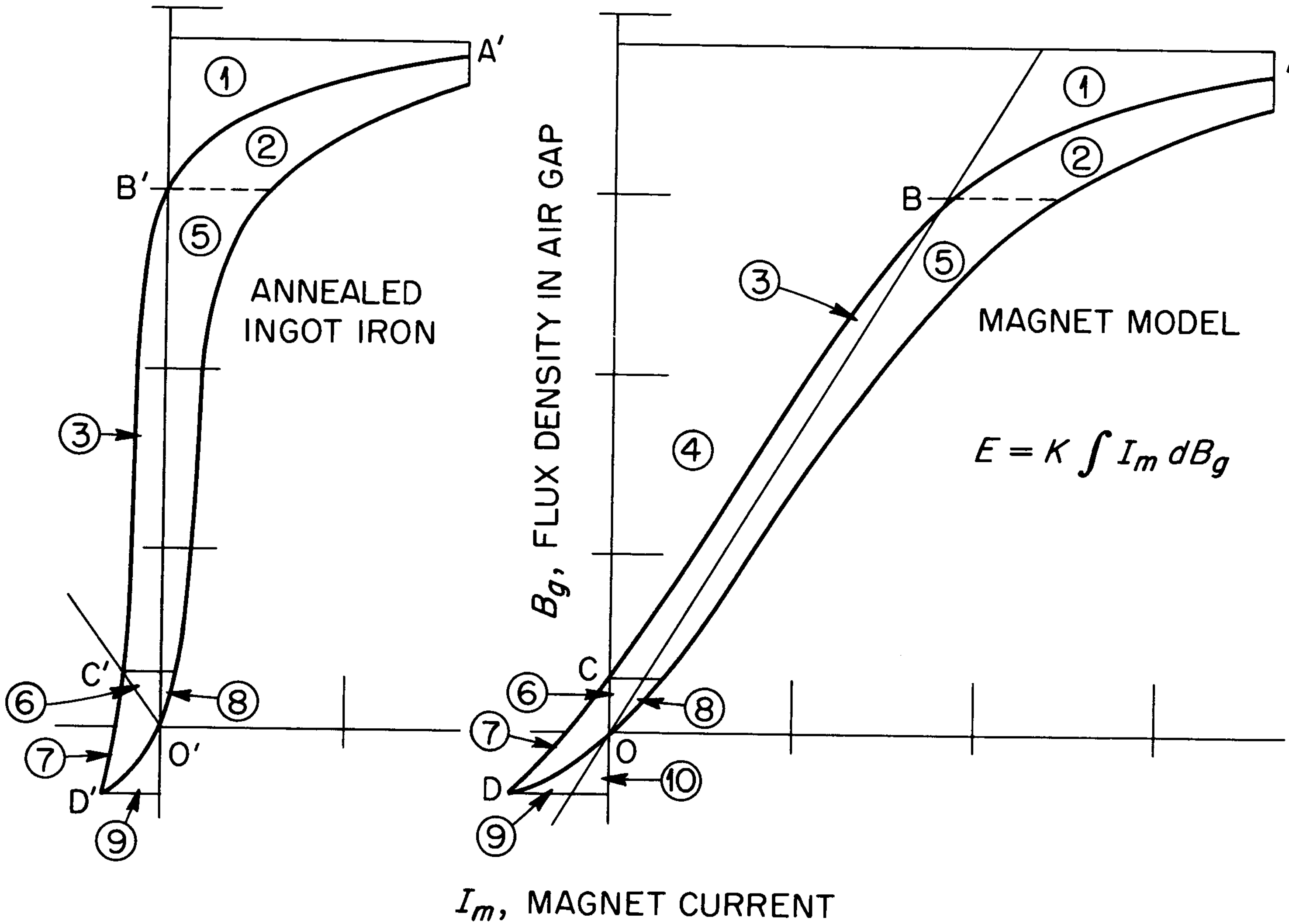

Fig. 7. Energy Storage and Release in Magnet Model.

This total stored energy is the sum of areas 1, 2, 3, 4, 5, 6, and 8. Of this total, areas 1, 2, 5, and 8 represent energy stored in the iron. The remaining energy is stored in the air gap (area 5 is below the dashed line to the right of B; area 2 is above this line).

To continue the cycle, the magnet current is decreased along path A-B to point B. During this time energy stored in the iron (area 1 and area 4 above the dashed line) is returned to the electrical circuit. The energy of area 2 is absorbed by the iron in the form of hysteresis heating. The flux density at point B is termed the residual flux density in the iron. In order to remove this residual, it is necessary to supply energy from an outside source. In the case of a solid piece of iron, this energy is supplied by reversing the magnetizing current to a value D' and then reducing the current to zero, as shown in Figure 7a. In the case of an iron circuit with a finite air gap, most of this energy is obtained from energy stored in the air gap. As the magnet current is reduced from point B to zero, the flux density in the air gap follows the curve B-C to point C. During this decay the energy required to demagnetize the iron (area 3) is supplied by the air gap and is absorbed in the iron as hysteresis heating. The remaining energy in the air gap (area 4 below the dashed line) is returned to the electrical system. The remaining energy stored in the iron (area 5) is consumed by hysteresis heating. The flux remaining in the air gap at point C is due to a small amount of residual magnetism still present in the iron after the demagnetizing force of the air gap has been expended. The general equation given in Figure 4 indicates that for $I_m = 0$:

$$2MMF_g = - MMF_i \qquad (2)$$

This equality is satisfied when the air gap curve intersects the iron hysteresis curve at point C' in Figure 7a, which corresponds to point C in Figure 7b. To remove this final residual magnetism it is necessary to reverse the magnetizing current to a value D in Figure 7b, and then reduce the current to zero. During this process the energy of area 6 which goes to hysteresis heating of the iron is supplied by the small remaining stored energy in the air gap. The energy of area 7 is stored in the iron. The small amount of stored energy which remains in the iron at point C (area 8) is consumed in hysteresis heating. During the current reversing process energy is again stored in the iron (area 9) and air gap (area 10), but is returned to the electrical circuit as the current is reduced to zero. The energy of area 6 plus 7 appears as further hysteresis heating. The final residual magnetism may also be removed by supplying the energy of area 7 in the form of external work applied to the armature (force x distance). This external work appears as a drag force on the armature as it leaves the magnet face.

During the demagnetization cycle, a condition of special interest occurs if the armature weight is not sufficient to initiate armature motion and thereby complete the cycle. Figure 8 shows how this condition can arise. This figure is an enlargement of the area near the origin in Figure 7a. The residual flux density remaining in the air gap, after the demagnetizing effect of the air gap has been fully expended, is indicated by the intersection of the air gap and iron hysteresis curves (Eq. 2). The holding force which this flux produces is termed the coercive holding force. This terminology is applied because it is the coercive intensity of the iron as well as the air gap length which determines the magnitude of this force. For very small air gaps the model

UNCLASSIFIED
ORNL-LR-DWG 20929

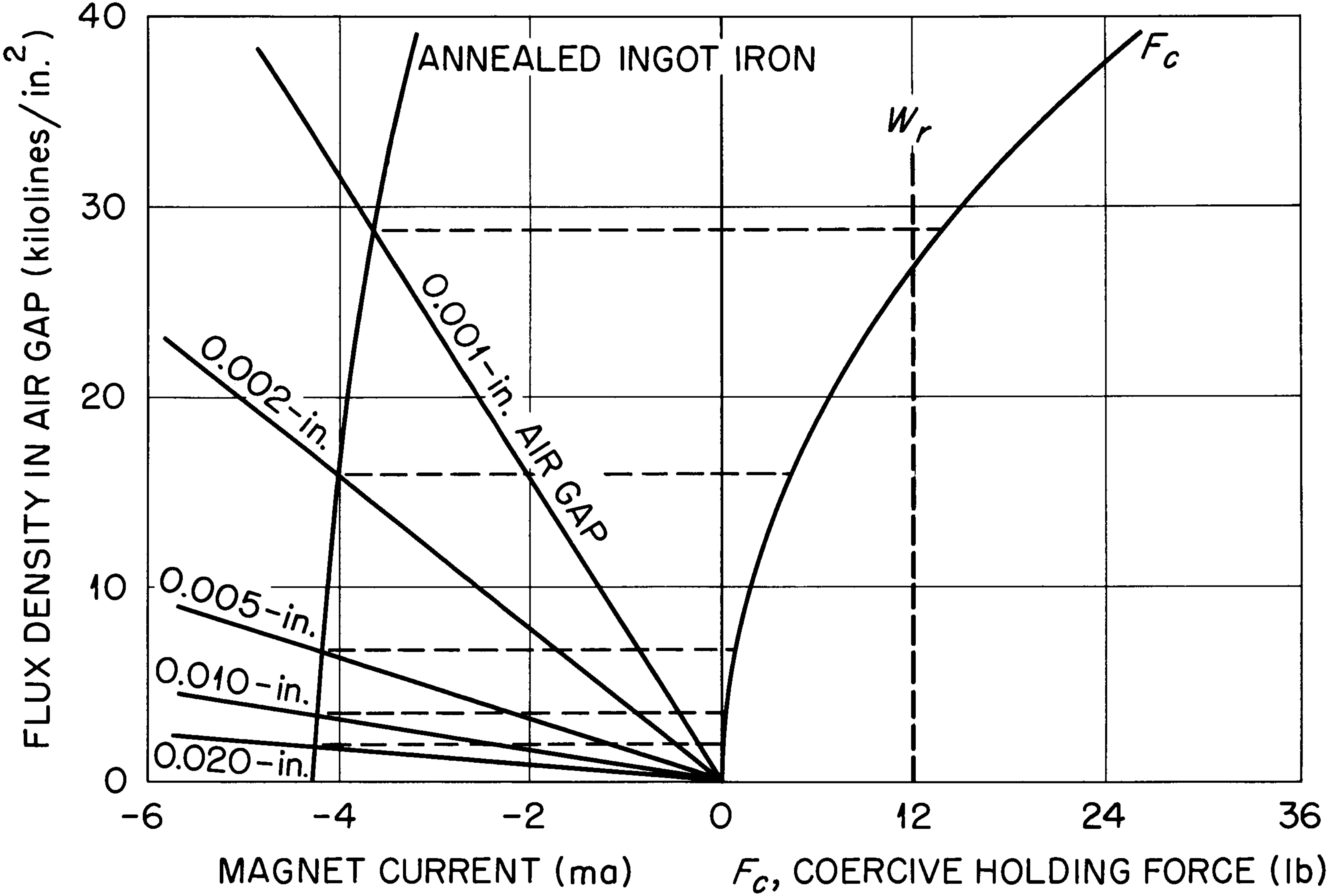

Fig. 8. Coercive Holding Force of Magnetic Model.

quickly reaches the point where it is unable to drop a given rod weight (W_r). For very small air gaps it is also apparent that very small changes in the iron characteristics may quickly increase the coercive force. Any change in the rod weight attached to the magnet armature is also an important consideration since armature release will occur only if the rod weight exceeds the coercive holding force. Referring to Figure 7, it is seen that a large area 7 will occur when the air gap is small. This energy appears as drag on the armature as it leaves the magnet face. If the rod weight is just sufficient to initiate armature motion, a slow release will still result due to the large drag force.

Another point to recognize in regard to Figure 8 is that the annealed ingot iron curve is a function of the maximum magnet current. As the magnet current increases, the curve shifts to the left until iron saturation is reached. When a magnet designed for small air gaps and low maximum flux densities is surged to high flux densities, this shift of the iron curve may be sufficient to prevent armature release.

The problem of large coercive forces may be overcome by using magnetic materials with low coercive intensities. The ferronickel alloys offer the best combination of low residual flux density, low coercive intensity, and good magnetization and saturation characteristics. Figure 9 shows the characteristics of 47% ferronickel compared to annealed ingot iron. Note the coercive intensity is practically zero. Very little air gap in the magnetic circuit is thus required to demagnetize the pole material.

II. HOLDING FORCE AND RELEASE TIME CHARACTERISTICS

The behavior of the magnet model discussed in the preceding section indicates that considerable variations in magnet holding force can be expected for small air gap changes. The air gap changes are easily attributed to dirty contact faces, or misalignment conditions. The holding force variations are not objectionable providing the magnet is able to lift and hold the rod weight with sufficient force to stabilize it against shock or vibration. The real question of concern is the possible variation of magnet release time for this wide range of holding forces.

Measurement of Holding Force and Release Time

Holding force was measured in the laboratory by dead weight loading with lead bricks. The bricks were held in a tray suspended from the magnet armature by a 1/16-in. steel rope. The magnet was held in a support plate firmly clamped to a laboratory table top. Care was taken to maintain near perfect alignment to obtain consistent results. The magnet holding force, for a given current, is the maximum weight which the magnet can support when the armature is lifted and carefully engaged to the magnet face. The magnet is considered to hold its maximum weight if a current reduction of less than 0.5 ma. is required to drop the weight again.

No special demagnetization procedure was followed after each measurement other than removal of the armature. The large air gap thus introduced demagnetized most of the iron. For measurements with small air gaps this procedure is not acceptable, but for large air gaps it yields sufficiently accurate results.

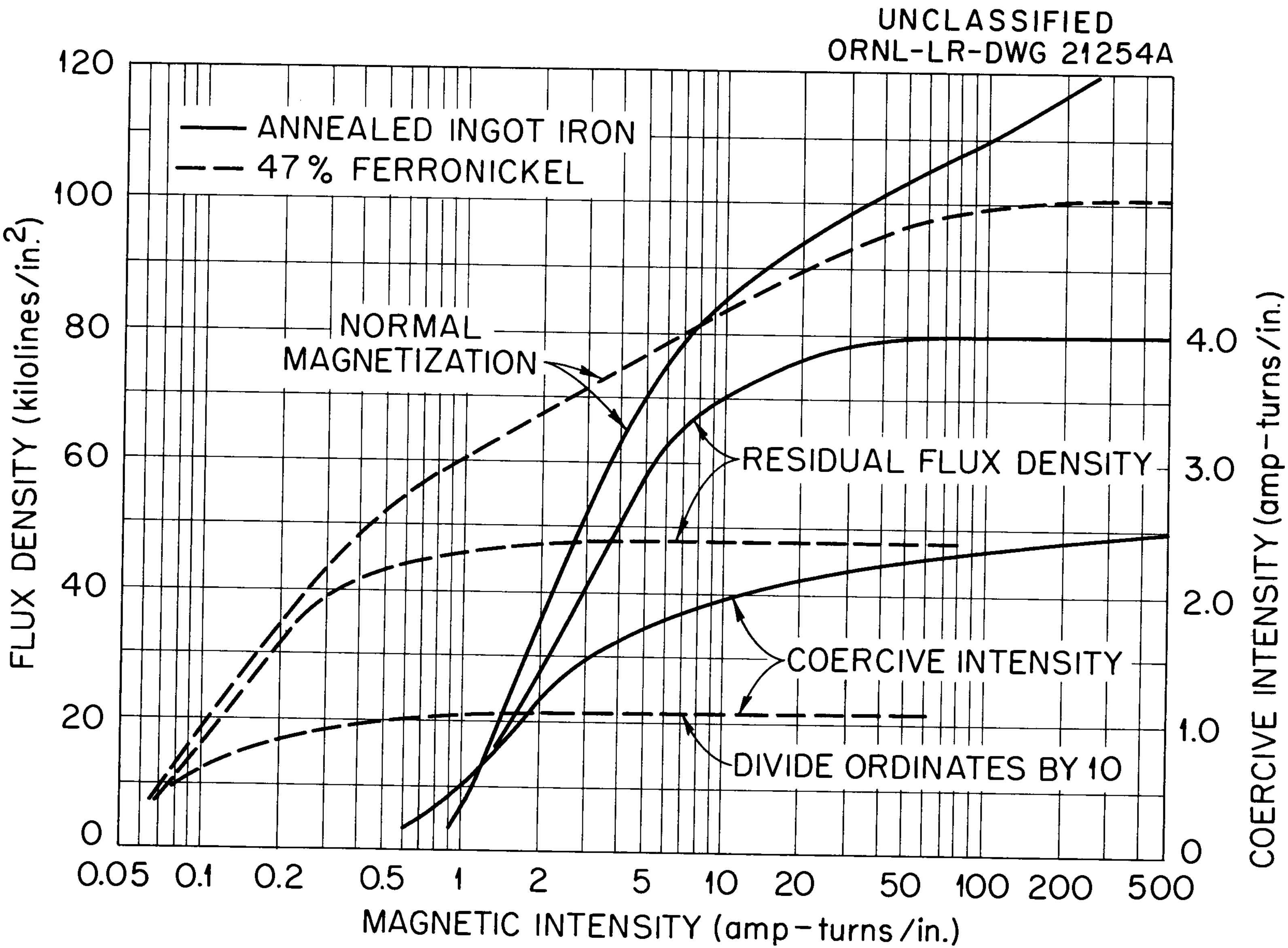

Fig. 9. Magnetic Characteristics of Ferronickel and Ingot Iron.

Aluminum foils were used when known air gaps 0.005-in. and larger were required between the magnet face and armature. Copper foils were used for smaller gaps. The foils were glued to the magnet armature with a thin layer of Pliobond adhesive. All magnet characteristics were measured with the magnet can off. A nickel foil of the same thickness as the magnet can face was glued to the armature to simulate the can.

Magnet release times less than 0.1 second were measured by the pulsed current technique reported in a companion document[3]. Times greater than 0.1 second were measured by timing the break of electrical continuity between magnet face and armature.

Reduction of Peak Voltage

Since the current obtainable from a vacuum tube power supply is very small, it is necessary to use a large number of turns in the magnet coil to obtain a given holding force. It is further required that the magnet be fast releasing which necessitates a rapid rate of flux change. This rapid flux change coupled with the large number of turns results in a very high peak voltage appearing across the coil leads during a flux transient. Precautions must be taken to prevent this peak voltage from puncturing the enameled insulation on the magnet wire, or the Teflon insulated leads. Thyrite resistors have been adopted for this application. In effect, these resistors clip the high voltage peaks, but appear as near infinite resistances during the remaining voltage surge. Peak voltage clipping prolongs the measured release time, but if the clipping is confined to the high voltage peak occurring during the first millisecond, the effect can, in most cases, be neglected. Low voltage clipping results in a prohibitive delay time. All measurements made for this report are based on limiting the peak voltage to 1600 V. by using Thyrite resistors (G. E. - 8355083G1 - three in series - 880,000 ohms each). The results of each experiment can thus be evaluated without regard to possible differences in insulation requirements.

Pole Tapering

Many BSF-Type magnets have been built with tapered poles, but unless otherwise noted, all measurements in the following section of this report are for flat poles.

BSF-Type Magnet with Large Air Gaps

Release time and holding force measurements made on a BSF-Type magnet with large air gaps are shown in Figure 10. The interesting feature of this data is the wide range of release times obtained, depending on the value of air gap, rod weight, and holding force selected. For this particular magnet and range of air gaps, the release time for a given rod weight was experimentally found to be directly proportional to the holding force exerted. Since holding force is proportional to flux squared, for a given area, the release time follows a flux squared relationship. Another point of interest is the observation that release time does not vary appreciably with stored energy in the system. Points over the entire range of air gaps are grouped together at the same release time for the same holding force. For an idealized case, the same holding force infers the same flux level in the air gap. For this

UNCLASSIFIED
ORNL-LR-DWG 21041

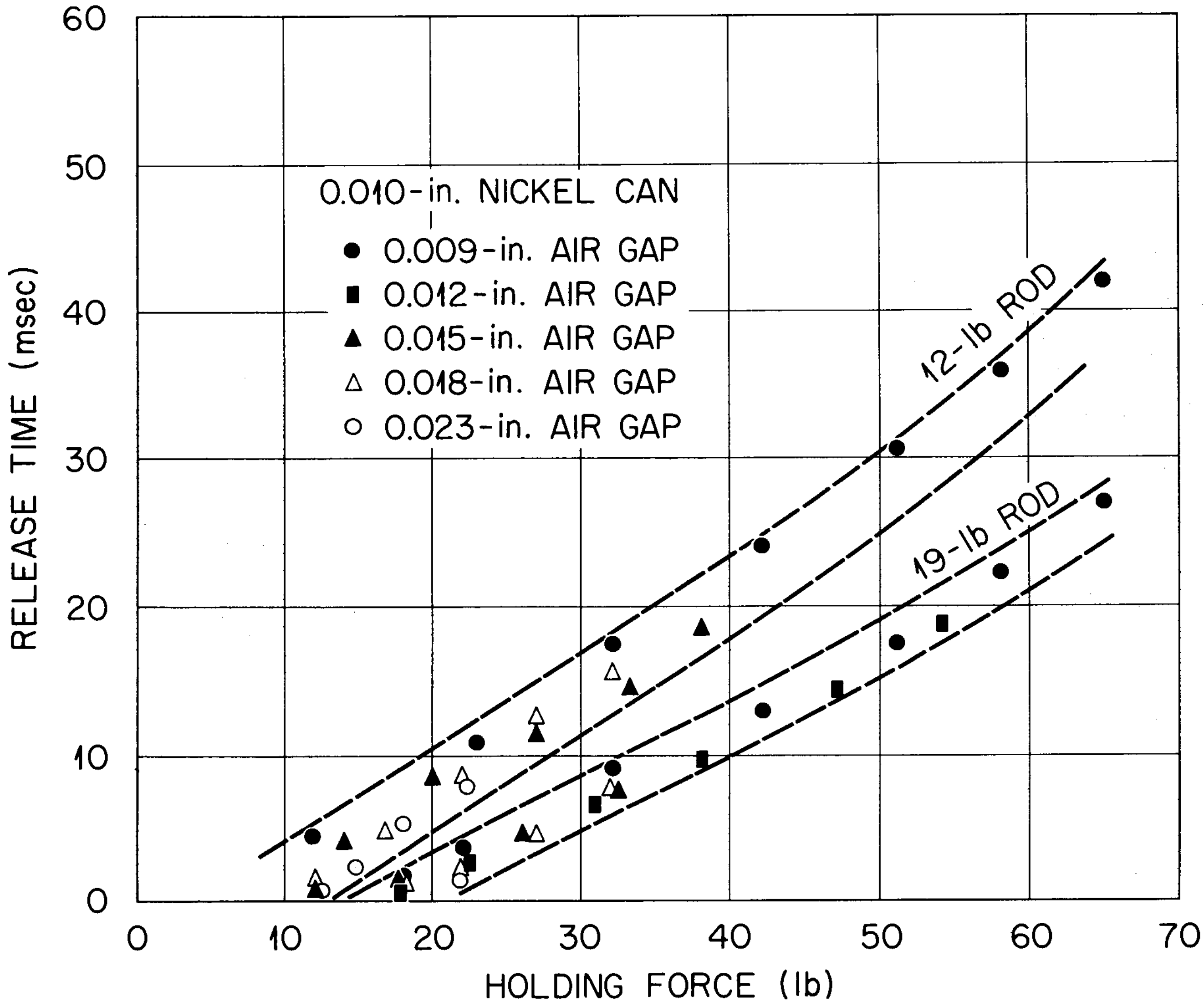

Fig. 10. Release Time of BSF-Type Magnet.

condition the stored energy in the air gap varies directly as its length.

From the data in Figure 10, it is concluded that magnet performance must be judged by the time required to release a given weight when exerting a given holding force on that weight. To state that a magnet has a certain release time is, by itself, not sufficient. It is necessary to have additional information concerning conditions existing during the measurement. For instance, the magnet in Figure 10 has a release time anywhere from one to forty milliseconds, as determined by the conditions of rod weight and holding force selected.

Delays Due to Eddy Currents

The effect of eddy currents in delaying the release of an electromagnet is not easy to treat analytically. However, an appreciation for the important parameters leading to the effect may help to indicate methods for reducing it.

The iron used for the magnet poles, yoke, and armature, shown in Figure 1, is a fairly good electrical conductor (conductivity 1/6 that of copper). Since this iron may be linked by part or all of the magnetic flux lines, eddy currents normal to the flux lines will be induced whenever the flux linkage changes. As an example, the center pole of a cylindrical magnet will be examined for circulating currents during a flux transient (Fig. 11)[4]. An original uniform flux (ϕ_o) is assumed to exist in a solid pole of radius (r_1) and total length (L). A given cylindrical shell of radius (r) and thickness (dr) within the pole is treated as a cylindrical conductor linked by all flux lines within (r). Any changes of this linkage flux (ϕ_L) within (r) will induce a voltage (e_r) normal to the flux lines and establish a circulating current in the cylindrical section about (r). This current in turn creates a magnetic field tending to oppose the original linkage flux change. These circulating currents retard the build-up or decay of the flux field. The flux field is assumed to be uniformly distributed at all times. The magnitude of the circulating current established is determined, in part, by the resistance (R_r) of the cylindrical shell about (r), and its inductance. For this study the inductive effects are assumed negligible in comparison with the resistance. This simplifying assumption is necessary because the non-linearity of the iron is difficult to treat mathematically.

The basic equations for this model are given in Figure 11. The condition of interest occurs when the linkage flux undergoes a change which is a known function f(t) of time:

$$\phi_L\,(t) = \left[\phi_L\right]\ f(t) \qquad (3)$$

The infinitesimal current (dI) induced in the cylindrical shell during the flux change is found by substituting the flux change into the basic equations for the model:

$$dI = \frac{\phi_o\, L}{2\pi\,\rho\, r_1^2}\ r\,dr\ \frac{d\,f(t)}{dt} \qquad (4)$$

UNCLASSIFIED
ORNL—LR—DWG 22232

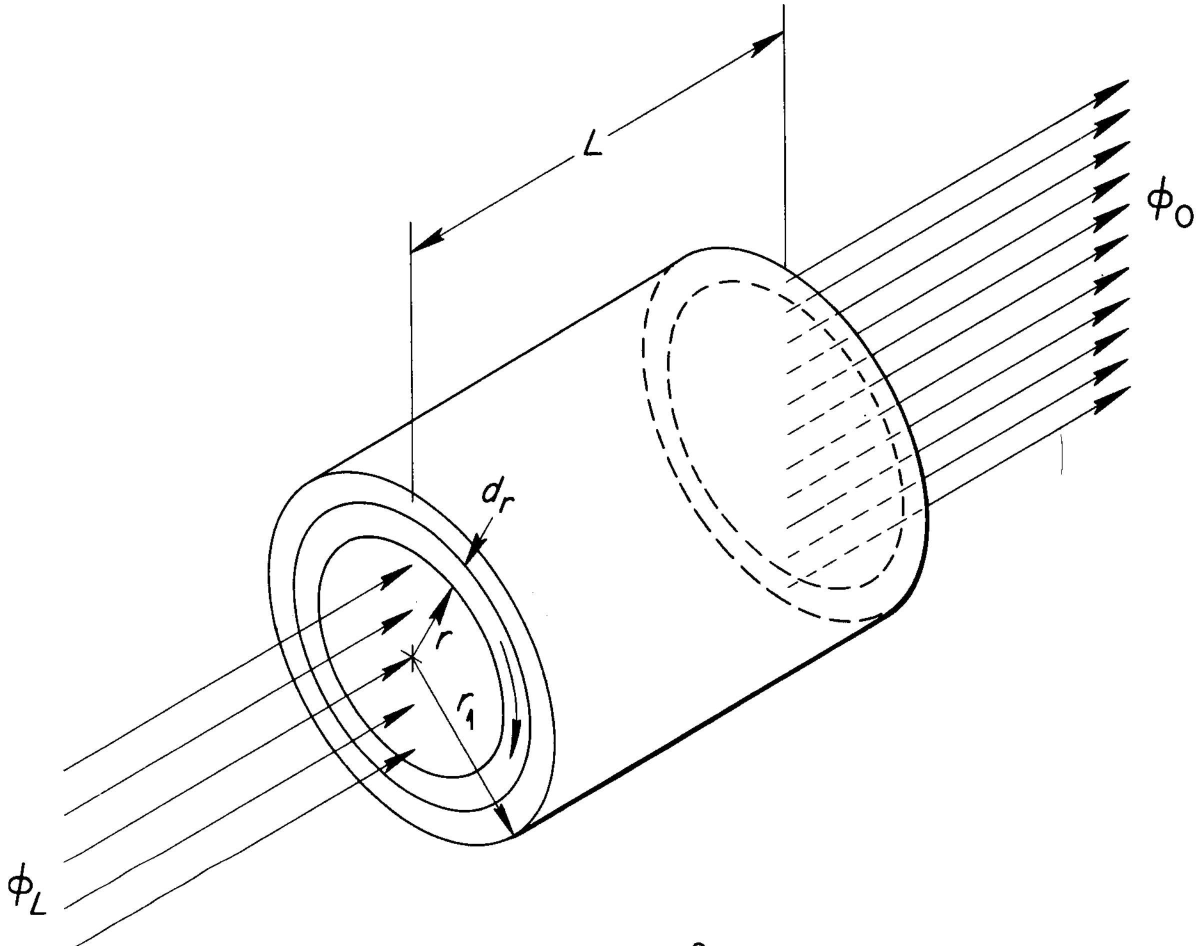

$$\phi_L = \phi_0 \frac{r^2}{r_1^2}$$

$$e_r = \frac{d\phi_L}{dt} \qquad dI = \frac{e_r}{R_r}$$

$$R_r = \frac{2\pi r \rho}{L dr} \qquad dP = \frac{e_r^2}{R_r}$$

Fig. 11. Eddy Current Model.

The total circulating current (I_e) in the model is the sum of the infinitesimal currents established in the individual shells:

$$I_e = \int_0^{r_1} dI = \frac{\phi_o L}{4\pi \rho} \frac{d\,f(t)}{dt} \qquad (5)$$

This current is established in the pole by the initiation of a primary flux change. It in turn establishes a magnetic field which tends to oppose the initiating field. As a result, the net flux through the pole changes at a somewhat slower rate as determined by the mutual interaction.

The infinitesimal power (dP) required to establish the infinitesimal circulating current in the cylindrical shell about (r), due to the primary flux change, is:

$$dP = \frac{\phi_o^2 L}{2\pi \rho r_1^4} r^3 \, dr \left(\frac{d\,f(t)}{dt}\right)^2 \qquad (6)$$

The total power (P_e) required by the sum of the infinitesimal currents is:

$$P_e = \int_0^{r_1} dP = \frac{\phi_o^2 L}{8\pi \rho} \left(\frac{d\,f(t)}{dt}\right)^2 \qquad (7)$$

The resulting power density (P_{de}) in the iron is:

$$P_{de} = \frac{B_o^2 r_1^2}{8 \rho} \left(\frac{d\,f(t)}{dt}\right)^2 \qquad (8)$$

where

$$B_o = \frac{\phi_o}{\pi r_1^2}$$

For rapid flux decays this power density becomes very large due to the squared time rate of change. Integration over the first increment of time yields a very high energy value if the initial decay function remains unaltered. A system absorbing no power during a change will follow the change instantaneously. Such is the case of air where the resistivity is infinite. For systems with finite resistivity, the energy consumed by the circulating currents appears as resistive heating, and must be added to the loop representing hysteresis heating in Figure 7. The resulting flux density curve follows a somewhat higher path as determined by the amount of eddy current energy consumed.

Examination of equation 7 shows that, for a given flux and decay pattern, the eddy current power can be reduced by increasing the resistivity of the pole material. A practical way of increasing the resistivity is to use ferronickel alloys or silicon steels as shown below[2]:

	Resistivity (micro-ohm-inches)
Ingot Iron	4.2
Medium Silicon Steel (2-1/2%)	16.0
Ferronickel (47%)	18.0
High Silicon Steel (4-1/4%)	23.0

Equation 8 indicates that a possible method for reducing eddy current power density, for a given flux density and resistivity, is to cut the pole into several segments. For example, the original eddy current model shown in Figure 11 may be replaced by a segmented model containing eight small cylinders of radius $r_1 / \sqrt{8}$, instead of the one large cylinder. The same total cross-sectional area and flux density is retained, but the eddy current power density in the iron is one-eighth of its value for the single pole case. Examination of equation 8 shows that by segmenting the pole a power density reduction of 1/N can be accomplished, where N is the number of segments into which the pole is cut.

Equation 8 shows the eddy current power density to be a function of flux density squared. Note the release times shown in Figure 10 are proportional to holding force and therefore flux density squared, for a fixed cross-sectional area.

Slotting BSF-Type Magnet

An experiment was conducted on a BSF-Type magnet to verify the desirability of pole slotting for reducing eddy current power density in the iron and thereby reducing release time. The results of this experiment are shown in Figure 12. Only the outside pole was slotted (1/16-in. milling cutter). The brass ring indicated was a retaining ring used to hold the magnet coil in place. On this particular magnet the retaining ring was rather large. The circulating currents set up in this ring of low resistivity contributed measurably to the total release time. A material of higher resistivity such as 347 stainless steel would reduce this.

The results of this experiment verify that pole slotting can be a useful tool for obtaining faster release from this type of solid pole magnet.

BSF-Type Magnet with Small Air Gaps

As indicated in Part I, the drag forces exerted on the armature to complete iron demagnetization are very small for large air gaps. Therefore, they do not appreciably influence the release times shown in Figure 10. For small air gaps, however, the situation is somewhat different. The drag energy indicated by area 7, Figure 7, appears as a sharp increase in magnet release time as shown in Figure 13. The high permeability of the nickel face at low flux densities[5] makes it appear as an extension of the pole iron instead of an air gap; so, for the case of no added shims, the magnetic air gap is

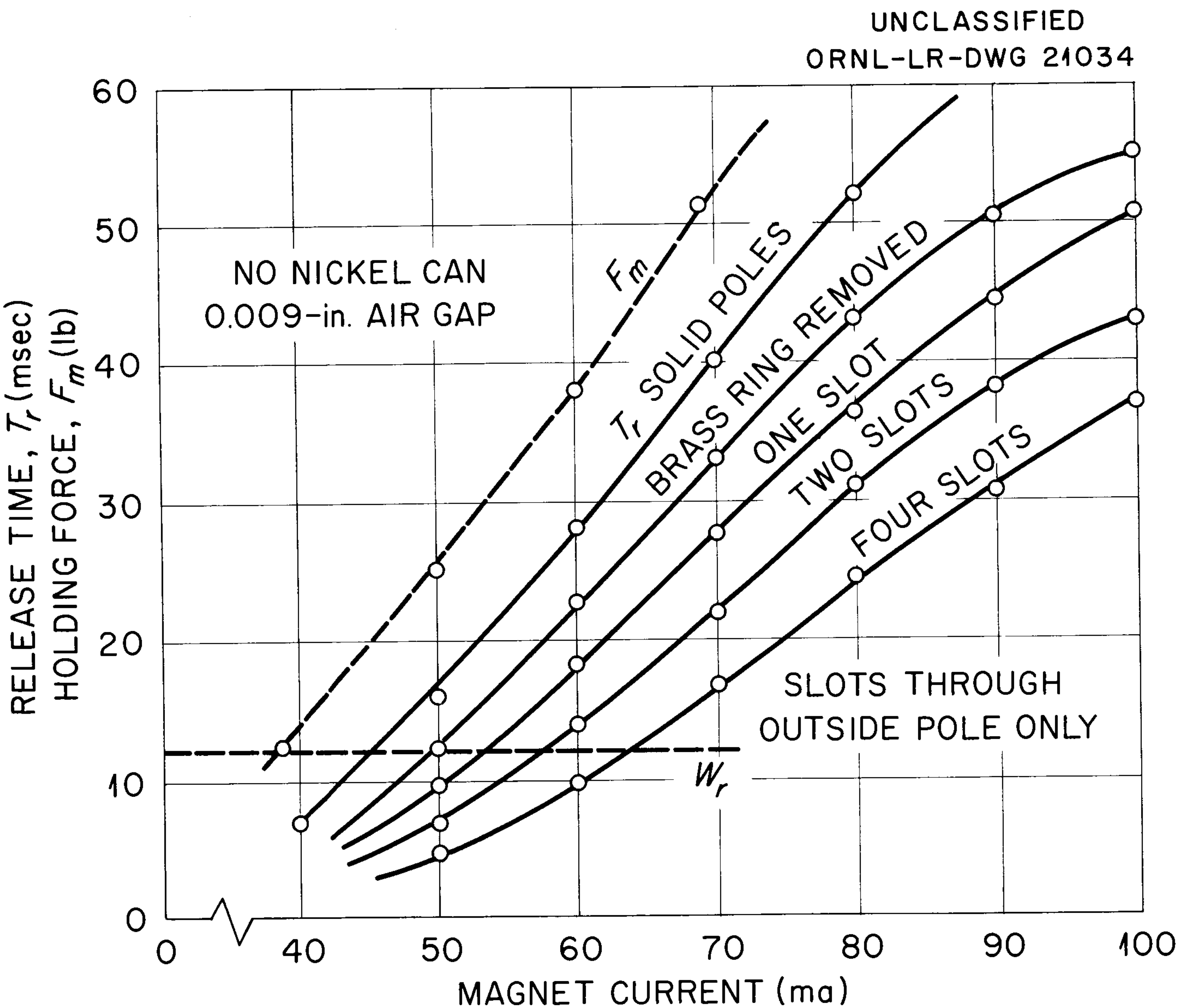

Fig. 12. BSF-Type Magnet with Slotted Pole.

UNCLASSIFIED
ORNL-LR-DWG 21033

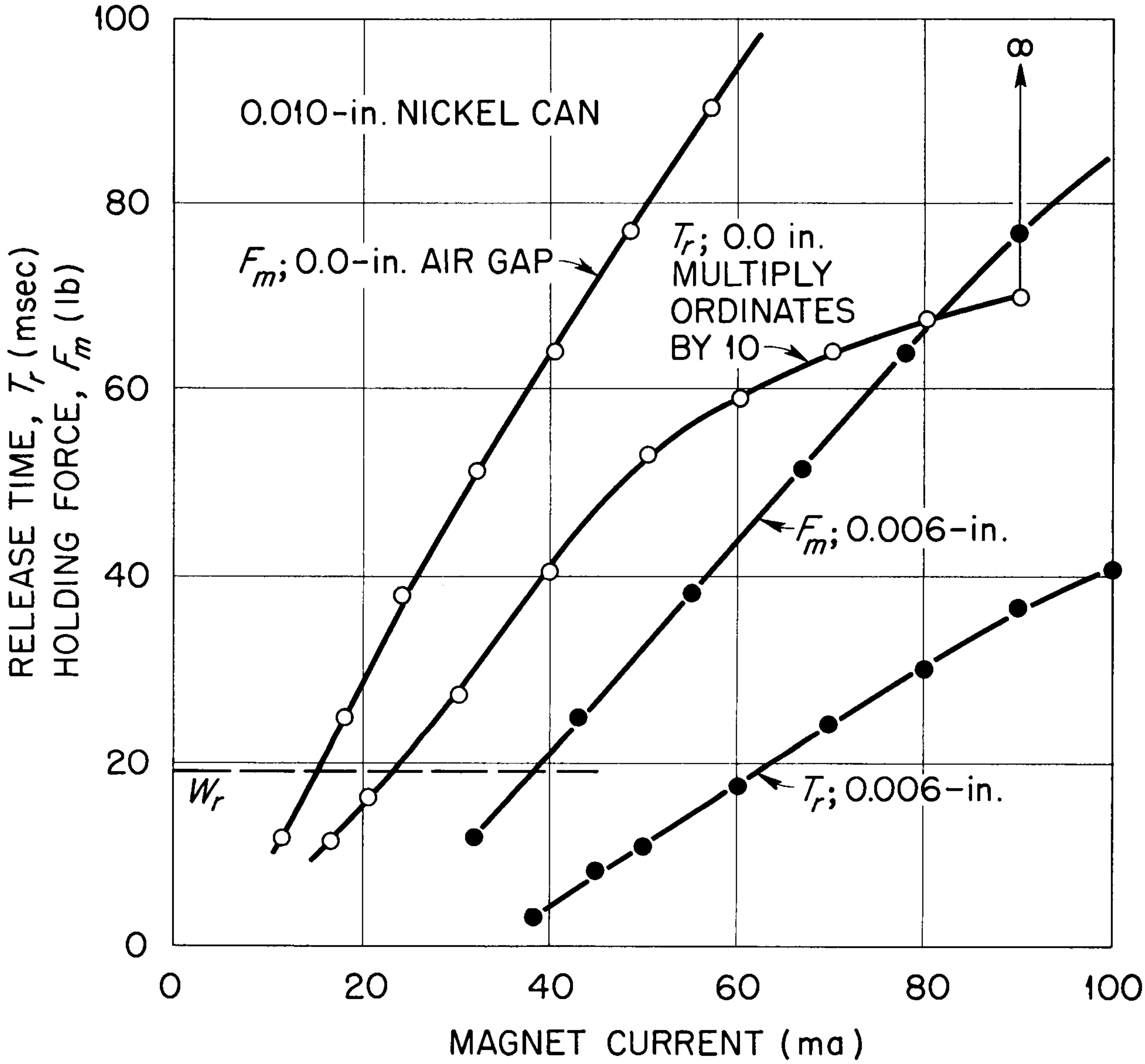

Fig. 13. BSF-Type Magnet with Small Air Gaps.

extremely small. The only true gap is that due to contact surface irregularities between the magnet face and nickel, and between the nickel and armature. This may total less than 0.001-in. The stored energy in this small air gap is the only energy available to demagnetize the iron. The remaining energy must be supplied by work applied to the armature. This work appears as a retarding force to armature movement. From Figure 13 it is seen that, for no added air gap, the release time increases toward infinity as the magnet current is increased.

Figure 8 predicts large coercive forces will exist for small air gaps. Figure 14 shows the coercive force of a BSF-Type magnet for small air gaps, and no nickel can. As predicted, these forces are indeed large for small air gaps, but taper off rapidly as the air gap exceeds 0.005-in. They are, of course, a function of the maximum current to which the magnet is surged.

The approach to very long release times can be predicted by observing the drop current. Figure 15 shows that as the magnet drop current becomes less than 20 ma., for the particular magnet and rod under test, the release time approaches the dangerous region beyond 100 milliseconds in Figure 13. If the characteristics of the magnet are known from previous laboratory calibration, the approach to a long release time can be predicted by this technique. If a continuous log on a given magnet shows a slowly decreasing drop current over a period of time, this condition may be attributed to changes in the magnet iron or can fit. The approach of very low magnet drop currents must be considered a warning for immediate magnet replacement.

Removal of Temporary Air Gaps

A problem of particular concern occurs when a temporary air gap is removed without readjustment of the magnet amplifier. For instance, if a 0.006-in. temporary air gap is present, the magnet drop current is 38 ma. (neglecting hysteresis) (Fig. 13). This fixes the zero power magnet amplifier current at 78 ma. (Fig. 2) and the magnet release time at 30 milliseconds for zero power scram. If the temporary air gap is removed without readjustment of the magnet amplifier, the zero power scram release time increases to 650 milliseconds, as indicated by the 0.0-in. air gap curve. This situation exists whenever an air gap change is made, but the magnitude of the change is largest for small final air gaps. Another point to note is the change in drop current which occurs when the temporary air gap is removed. With 0.0-in. air gap the drop current is 16 ma. instead of 38 ma. (neglecting hysteresis). If the magnet amplifier is not readjusted after removal of the air gap, magnet release due to level-induced scram will occur at well over 150% full power, or on a period shorter than one second. Figure 16 indicates the change in release time which will occur with the same magnet, but a 12-lb. control rod, when a 0.015-in. temporary air gap is reduced to 0.009-in. without readjustment of the magnet amplifier. In this case, the release time still increases more than a factor of two.

Introduction of Permanent Air Gaps

Delays due to small air gaps must be avoided by the introduction of a small permanent air gap. Whenever possible, this permanent air gap should be located inside the magnet can where it is least subject to change by reactor

UNCLASSIFIED
ORNL-LR-DWG 21040

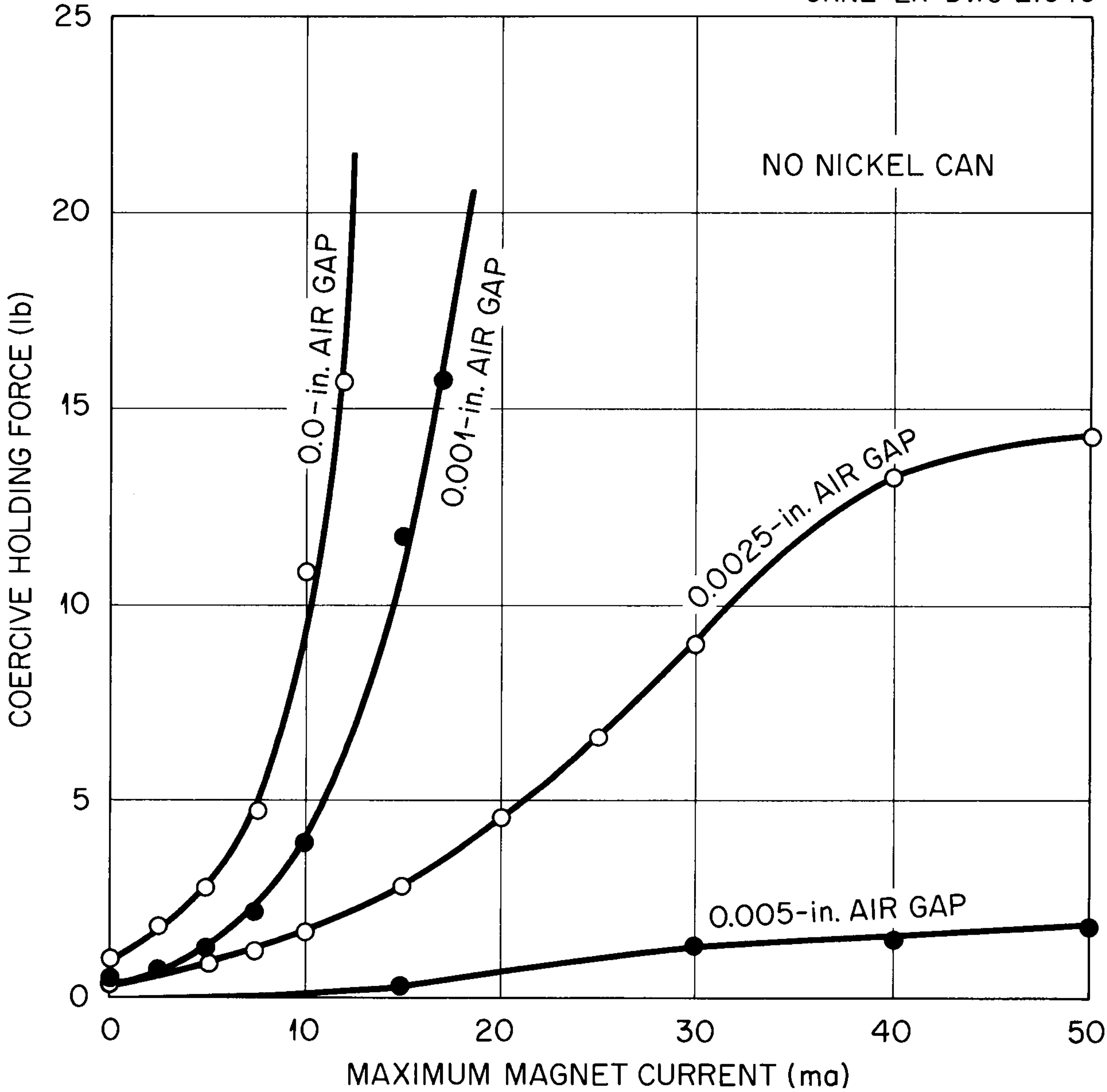

Fig. 14. Coercive Force of BSF-Type Magnet.

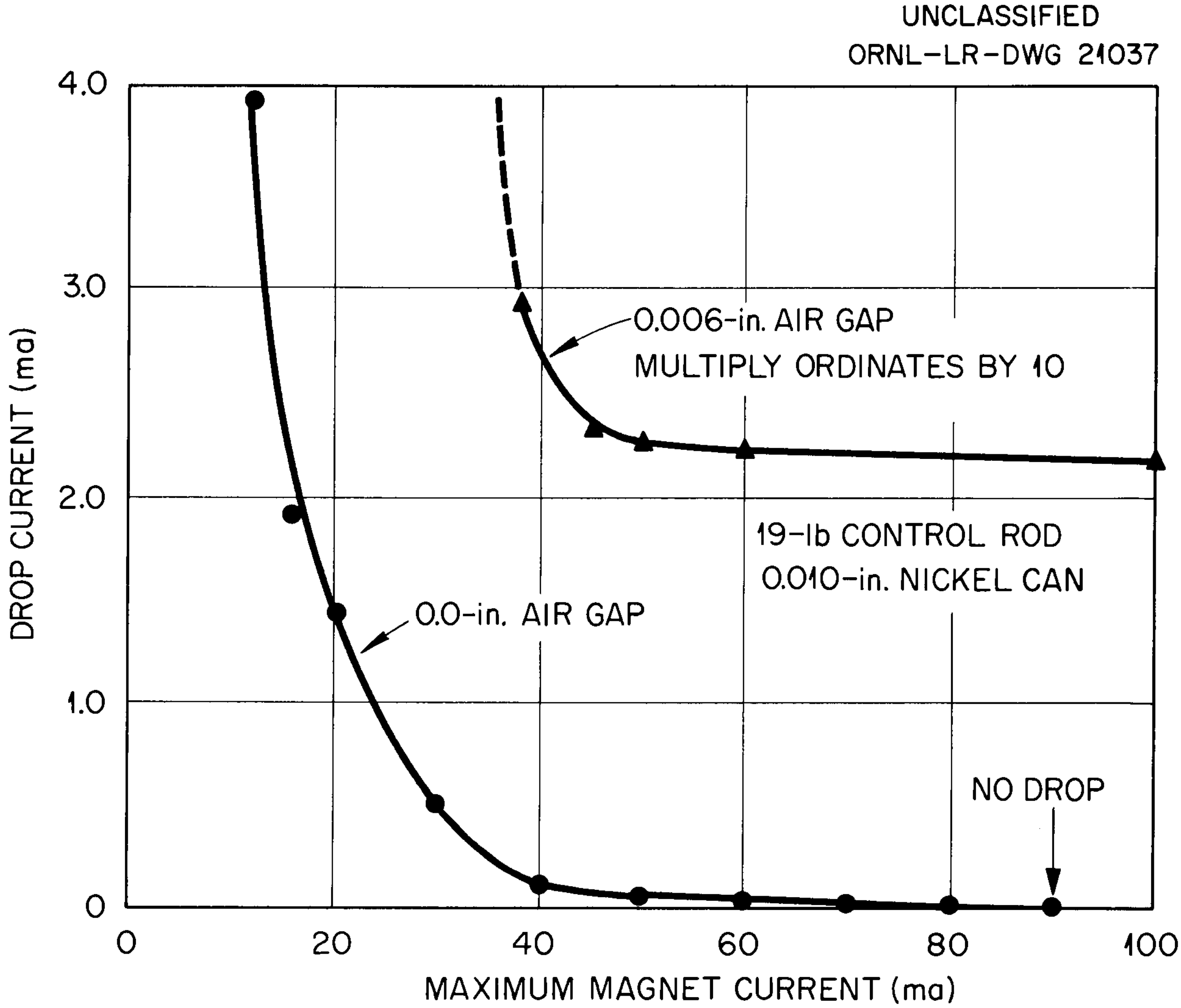

Fig. 15. Drop Current for BSF-Type Magnet.

UNCLASSIFIED
ORNL-LR-DWG 22234

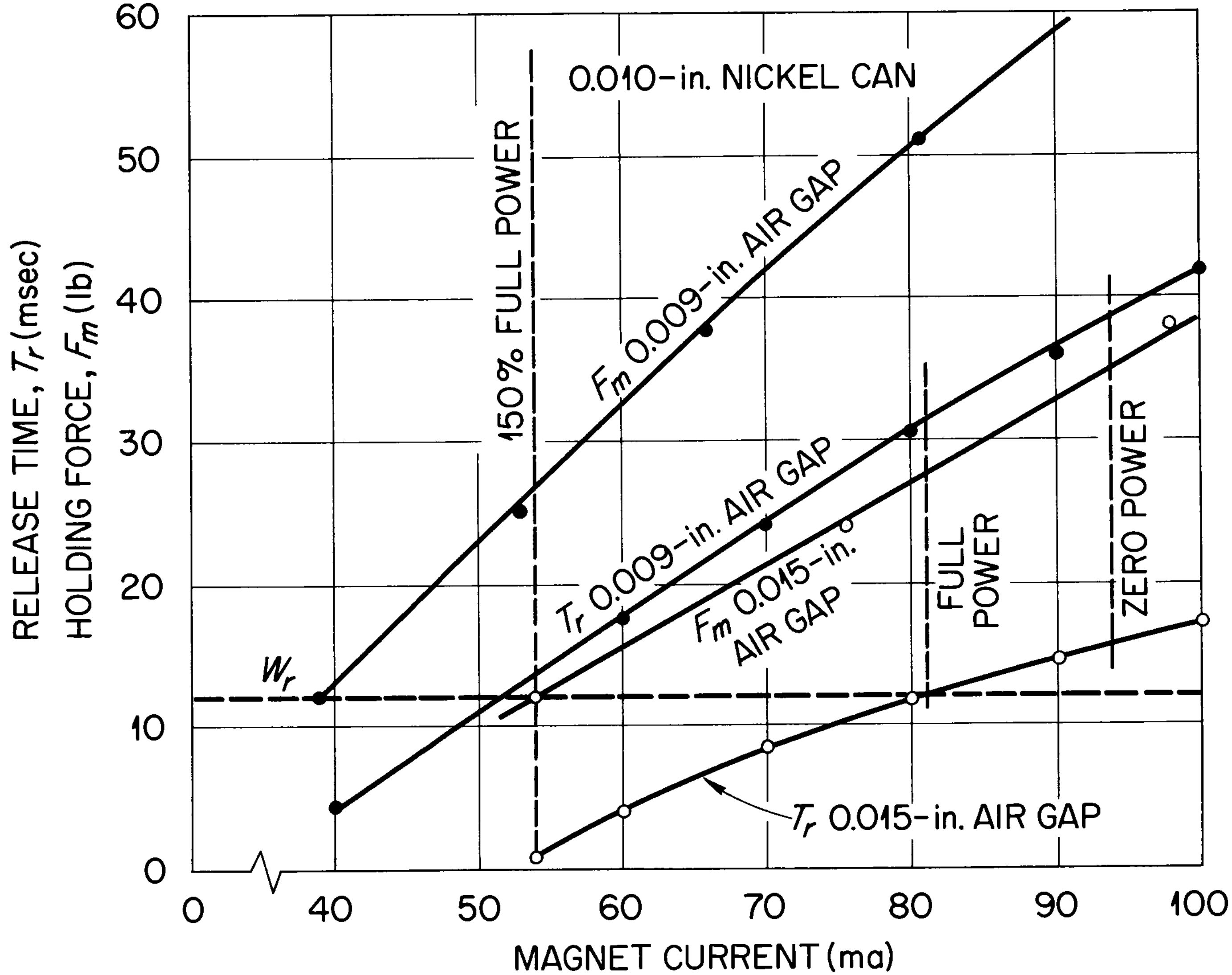

Fig. 16. BSF-Type Magnet with Large Air Gaps.

operators or maintenance people. In general, air gaps introduced by planned mechanical mismatch cannot be considered safe. They are subject to manufacturing error, or changes at some later date. For example, in many swimming pool type research reactors the magnet face is curved to a 26-in. radius and the magnet armature to a 24-in. radius. This gives a ball and socket type joint and a small fixed air gap. If the machining operations are done carefully and the magnet can fits perfectly, the air gap established by this joint is zero at the inside pole and about 0.004-in. at the outside pole. This gives an average air gap of about 0.002-in., and a total release time in the 100 millisecond region. At a later date the magnet armature may require refinishing due to rusting. During this process a change in the radius of curvature might easily go unnoticed. If the armature is machined to a 26-in. radius, the release time will go to infinity for high magnet currents as indicated in Figure 13.

An easily made air gap change such as this is beyond the control of the original designer and potentially dangerous. The permanent air gap can best be introduced in the form of a brass washer of appropriate thickness brazed to the inside pole of the magnet. The energy stored in this brass must be sufficient to demagnetize most of the iron (Part I).

Excess Holding Force

The holding forces shown in Figure 13 become very large, compared to the weight lifted, as the magnet current is increased. The excess holding force (total holding force less rod weight) produced by a given magnet is a function of the holding force and magnet amplifier characteristics, and the rod weight. For instance, at zero reactor power the magnet amplifier current is approximately 40 ma. above the magnet drop current, thus providing a very large excess holding force during rod withdrawal. As the reactor comes to full power the magnet amplifier current reduces to 27 ma. above the magnet drop current. This is sufficient to hold the rod provided vibrations and shocks are not large. The magnitude of holding force produced by the zero power and full power current is a function of the magnet holding force characteristics. Some shaping of these characteristics can be done to give larger excess holding forces. The release time follows the holding force characteristics as pointed out in Figure 10. If, in a given reactor, fast release is more important than large excess holding forces, it is necessary to either flatten the magnet holding force characteristics or adjust the operating characteristics of the magnet amplifier.

An important limitation in magnet design is the maximum magnet amplifier current. The desired maximum operating level is 100 ma. at zero power and 87 ma. at full power. This places an upper limit of 60 ma. on the magnet drop current. Since the magnet is supported at the end of a long lift tube which is subject to axial displacement or bending, it is necessary to make some allowance for an air gap length somewhat greater than the design value. In undertaking a magnet design this allowance is specified. If additional air gap appears, it is assumed corrective action will be taken. Once the magnet stroke (maximum air gap length) is specified, the magnet is designed to release the armature at 60 ma. with this air gap length. Since a temporary air gap may disappear on a given day, the magnet holding force can reach higher values as operation shifts to a steeper holding force curve. Magnets designed for large air gap variations can exert holding forces equal to many times the rod weight. The magnet amplifier is designed for constant current differences without regard to the excess holding forces produced.

Effect of Nickel Can

The stainless steel can encasing the magnet shown in Figure 1 is provided with a nickel face. Nickel is chosen because it is easy to fabricate into can bottoms, and represents a small magnetic air gap for a large physical thickness. The disadvantage of nickel is that it represents no permanent air gap at low flux densities. At medium flux densities nickel saturates more quickly than iron. In addition, it exhibits strong magnetic hysteresis[6] which requires additional demagnetizing energy during a flux decay. As a result, the nickel can appears as an air gap approaching its own physical thickness at high flux densities, but as an extension of the pole iron at low flux densities. In effect, the holding force available at the magnet face quickly saturates at higher flux densities.

The practical results of this effect are shown in Figure 17. This data was obtained for a BSF-Type magnet. Known air gaps were used with, and without, the addition of 0.010-in. nickel next to the magnet face to simulate the magnet can. At low magnet currents the effect of the nickel can is estimated to be less than 0.001-in. of air (contact irregularities included). At higher magnet currents it appears as 0.003-in. If this magnet were designed for high flux densities, the effect would become more pronounced. The release time curve follows the holding force curve in each case as is expected from its flux squared dependency. From a safety viewpoint, the nickel can is acceptable if sufficient permanent air gap is built into the magnet to protect against high coercive forces. From a practical viewpoint, the large variation in apparent air gap is undesirable.

Effect of Short-Circuits or Grounds

The effect of a high resistance short-circuit appearing across the magnet coil or a high resistance path to ground was investigated briefly. A BSF-Type magnet operating with a small air gap and heavy rod was used for this study. The results shown in Figure 18 indicate how the already long release situation is considerably aggravated. The resistors were added across the magnet coil. The carbon leakage path from a magnet lead wire to ground resulted from arcing during an experiment. An important point to make is that none of these shorts or grounds cause any noticeable alteration to the normal operating characteristics of the magnet amplifier. They can therefore exist undetected for long periods of time. Only during the rapid flux transient following magnet current interruption do they come into play. They appear across the infinite resistance of the pentode tube thus defeating its purpose. The increased time constant of the L/R magnet coil circuit becomes controlling, and the release time becomes resistance dependent.

One precaution which might be inferred from this experiment is to exercise care in locating terminal blocks in any damp area. Arcing across terminals can form a temporary low resistance path which will prolong the magnet release.

UNCLASSIFIED
ORNL–LR–DWG 21035

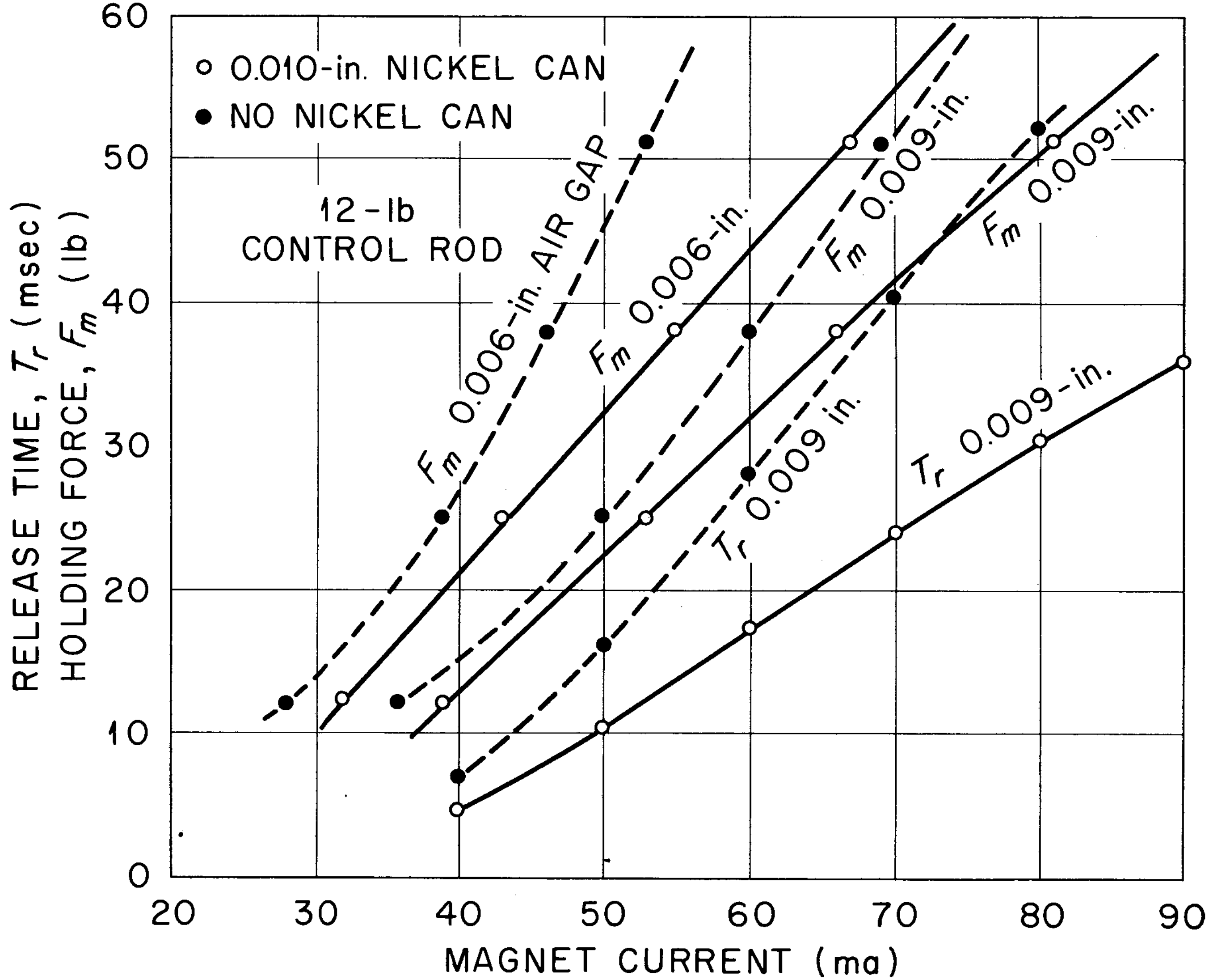

Fig. 17. Effect of Nickel Can on BSF-Type Magnet.

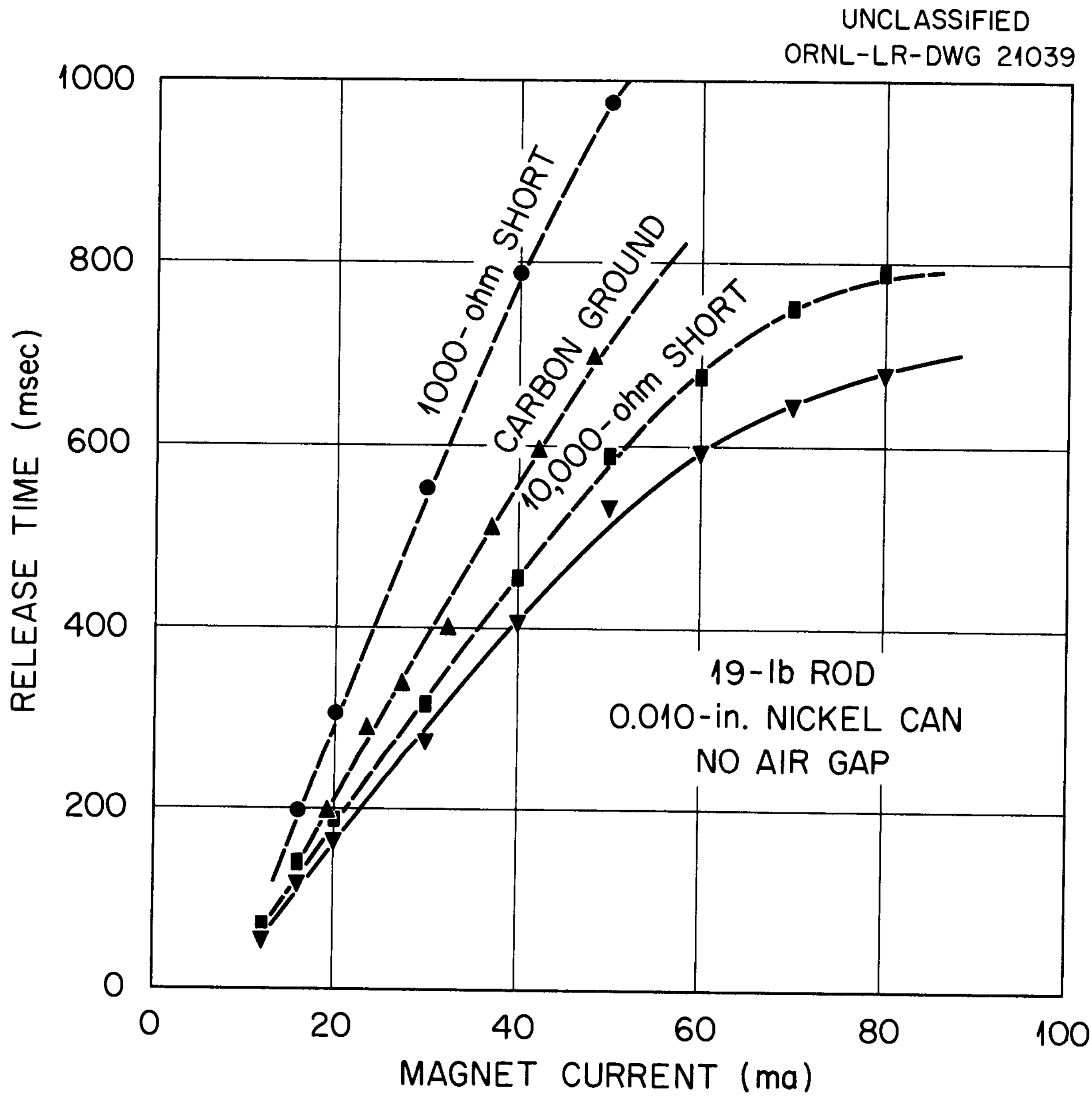

Fig. 18. BSF-Type Magnet with Shorts or Grounds.

BSF-Type Magnet Under Water

The release times shown thus far have been for out-of-water conditions. In the case of magnets designed to operate under water, the introduction of water adds a second possible variable -- that of vacuum breaking. As the magnet face and armature are brought together, water is excluded from the region between the face and armature. This exclusion of water creates the problem of void formation when the surfaces are separated again. A study of this effect for the BSF-Type magnet was made under water in the control rod test tank. The results of this study show that for the case where magnet armature and face are curved to match, the release time under water is considerably greater than in air.

In order to determine methods of alleviating this vacuum effect, a series of tests were conducted with known water gaps between the magnet face and armature. The results of these tests are shown in Figure 19. The air gap design is shown at the left. The cross-hatched region is a non-magnetic shim used to maintain a given magnetic separation between magnet face and armature. The blank area indicates the region occupied by water. The solid curves indicate the release time of a 12-lb. control rod with a dry air gap. The dashed curves are for under-water conditions. Since the weight of the rod supported under water is 10 pounds, it is necessary to correct for the resulting increase in release time. Release times for both a 10-lb. and 16-lb. under-water weight are shown. The release time for a 12-lb. under-water weight can be obtained by interpolation. It is seen from these curves that even for an 0.018-in. water gap, the vacuum holding effect is still appreciable. To alleviate this condition when it exists, an armature design must be chosen which provides low pressure drop paths for the water to quickly reach all void regions.

The magnet face and armature used for this study each had a 26-in. radius of curvature. This curvature formed a natural pocket to contain the void. The possibility that a flat face might reduce the vacuum breaking problem by allowing unrestricted movement of the void was not investigated.

UNCLASSIFIED
ORNL-LR-DWG 21036

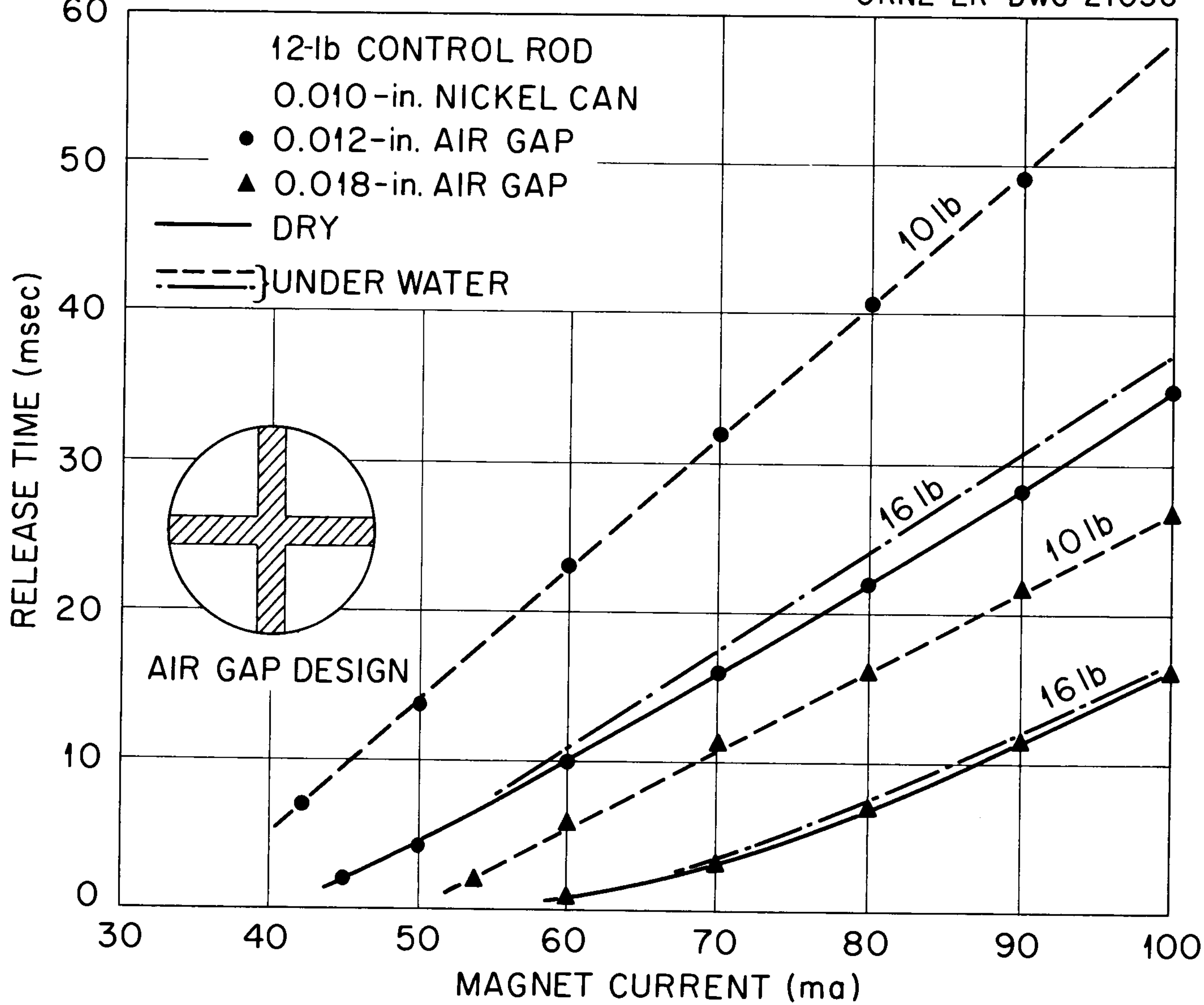

Fig. 19. BSF-Type Magnet Under Water.

References

1. H. E. Banta, S. H. Hanauer, Procedure for Testing Magnet Amplifiers, ORNL CF 56-5-30, Section C, 1954, Unclassified.

2. H. C. Roters, Electromagnetic Devices, John Wiley and Sons, Inc., New York, 1941.

3. L. C. Oakes, accompanying paper.

4. G. V. Mueller, Introduction to Electrical Engineering, McGraw-Hill Book Company, Inc., New York, 1948.

5. A. E. Knowlton, Standard Handbook for Electrical Engineers, McGraw-Hill Book Company, Inc., New York, 1949.

6. E. M. Wise, R. H. Schaffer, "The Properties of Pure Nickel", Metals and Alloys, September 1942.

ACCELERATION OF REACTOR CONTROL RODS

Arnold A. Sorensen

On loan from The Martin Company

ABSTRACT

This paper describes the results of tests on determination of entering velocities of a control rod of the BSF type. Tests were made changing the acceleration of the rod by means of varying the number of constant tension driving springs. Equations are fitted to the experimental data in an attempt to identify factors responsible for the effects noted.

Acceleration of Reactor Control Rods

Arnold A. Sorensen

Emergency shutdown of the ORNL Bulk Shielding Reactor is effected by the dropping of shim-safety rods into the reactor lattice. The reactor together with the rod and special fuel element into which it works, is described in the AEC publication "Research Reactors". This paper describes experiments performed to determine rod position during a drop and to measure the effect of additional acceleration over that provided by gravity.

In order to carry out the experiments, a tank equipped with plexiglass windows was constructed. Supports were provided in the tank for the special fuel element and the guide tube. Figure 1 shows a view of the tank with the components installed. The holding magnet, the armature and shock absorber, and rod are evident. The hoist to lift the magnet was located above the tank in the attic of the building and was controlled from the tank location.

A Fastex camera running at the rate of 2000 frames a second was used to photographically time the rod drop. Figure 2 shows a schematic diagram of the timing circuit arrangements. A timer provides a time delay allowing the camera to come up to speed before the rod drop signal occurs. One circuit is arranged to flash a small lamp when the timer contacts close which grounds the sigma bus and reduces the magnet current to zero. The other circuit causes the second lamp to flash when the magnet releases the armature. Twenty times rated voltage is applied to the lamps to reduce the flashing delay to less than a millisecond. Figure 3 shows a close-up of the timing equipment. A mirror places these lamps and a rotating 3600-rpm disc in the same field of view as that of the control rod. Thus, there is recorded in time sequence on the film the signal to drop the rod, the instant at which the drop begins, and its behavior during the drop. Figure 4 shows the camera and photographer in position.

The first test of the series was made with the control rod dropping under the influence of gravity as it does in the reactor. Figure 5 shows the results of this test. The results were somewhat surprising since it was expected that the rod would initially accelerate at nearly the value it does in air, and then the acceleration would be gradually reduced by the viscous action of the water. As can be seen, this was not the case. Rather, the acceleration of the rod was constant throughout almost all of the fall, with only a slight departure at the end of the drop.

Examination of the data shows that the equations

$$v = at$$

$$s = \frac{1}{2} at^2$$

can be fitted to the data. The observed acceleration is 20 ft/sec^2. Since

UNCLASSIFIED
PHOTO 40527

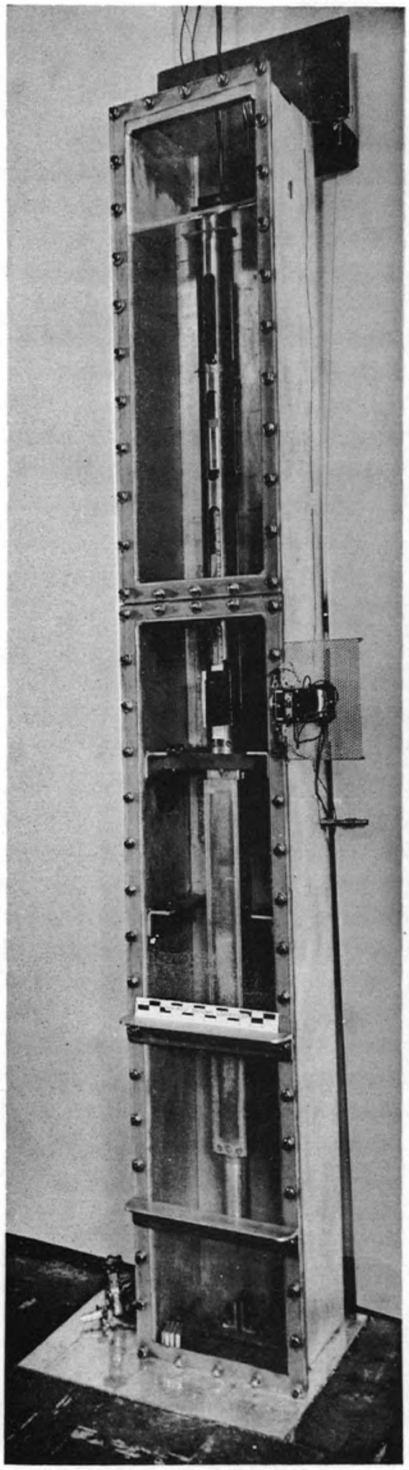

Fig. 1. Rod Drop Test Tank with Rod Assembly Installed.

UNCLASSIFIED
ORNL-LR-DWG 20978

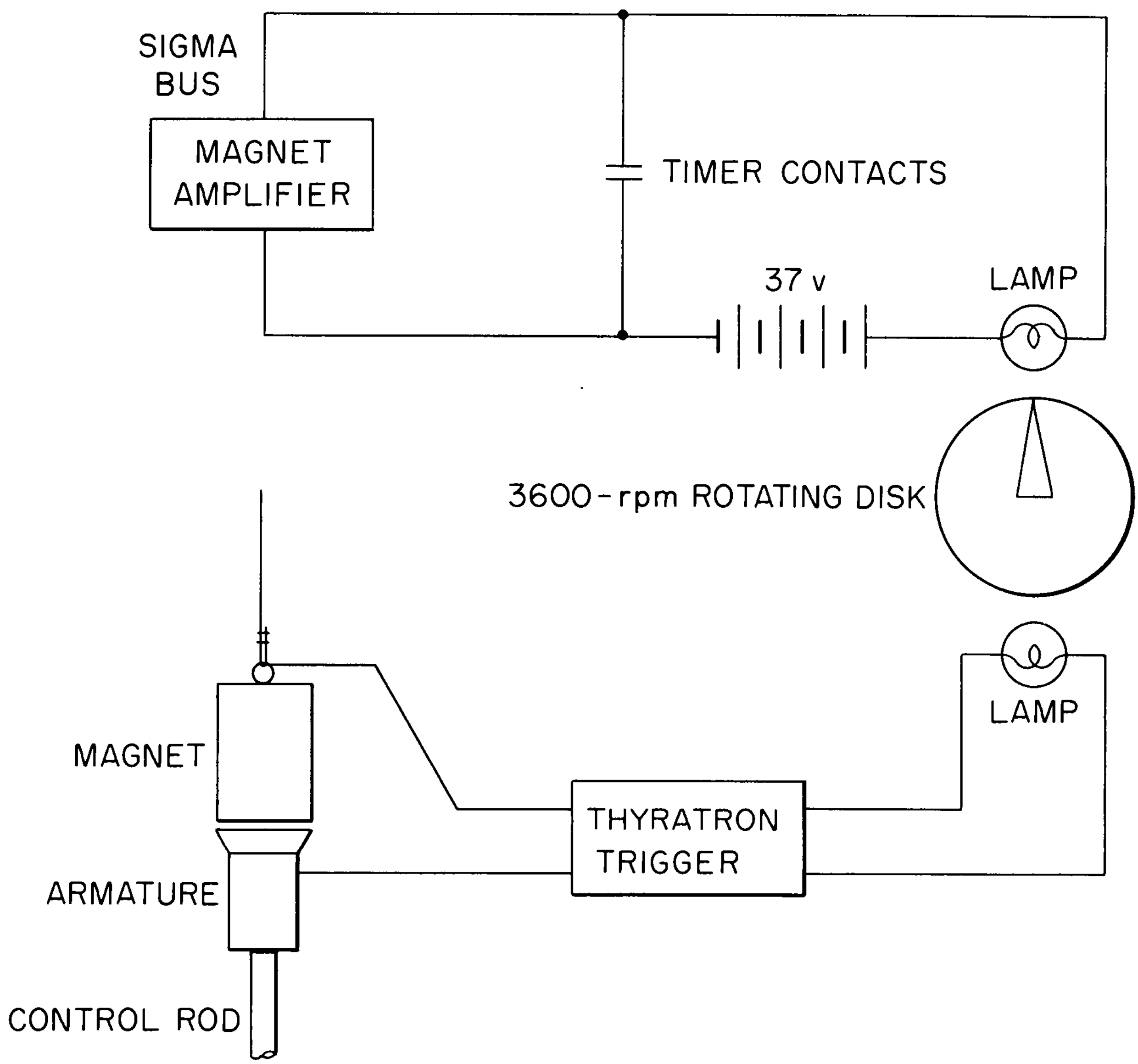

Fig. 2. Timing Arrangement.

UNCLASSIFIED
PHOTO 40524

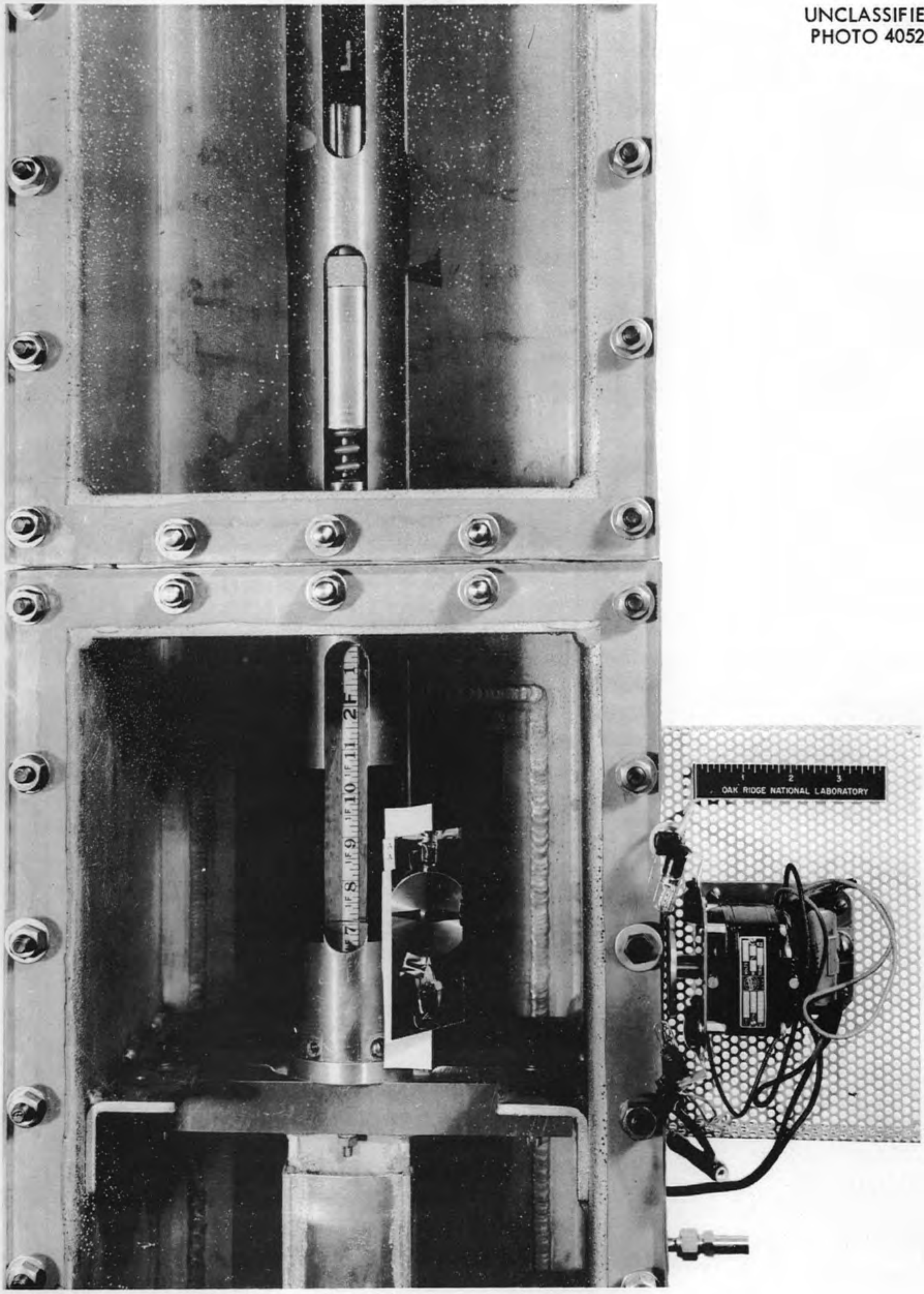

Fig. 3. Close-Up of Scale and Timing Equipment.

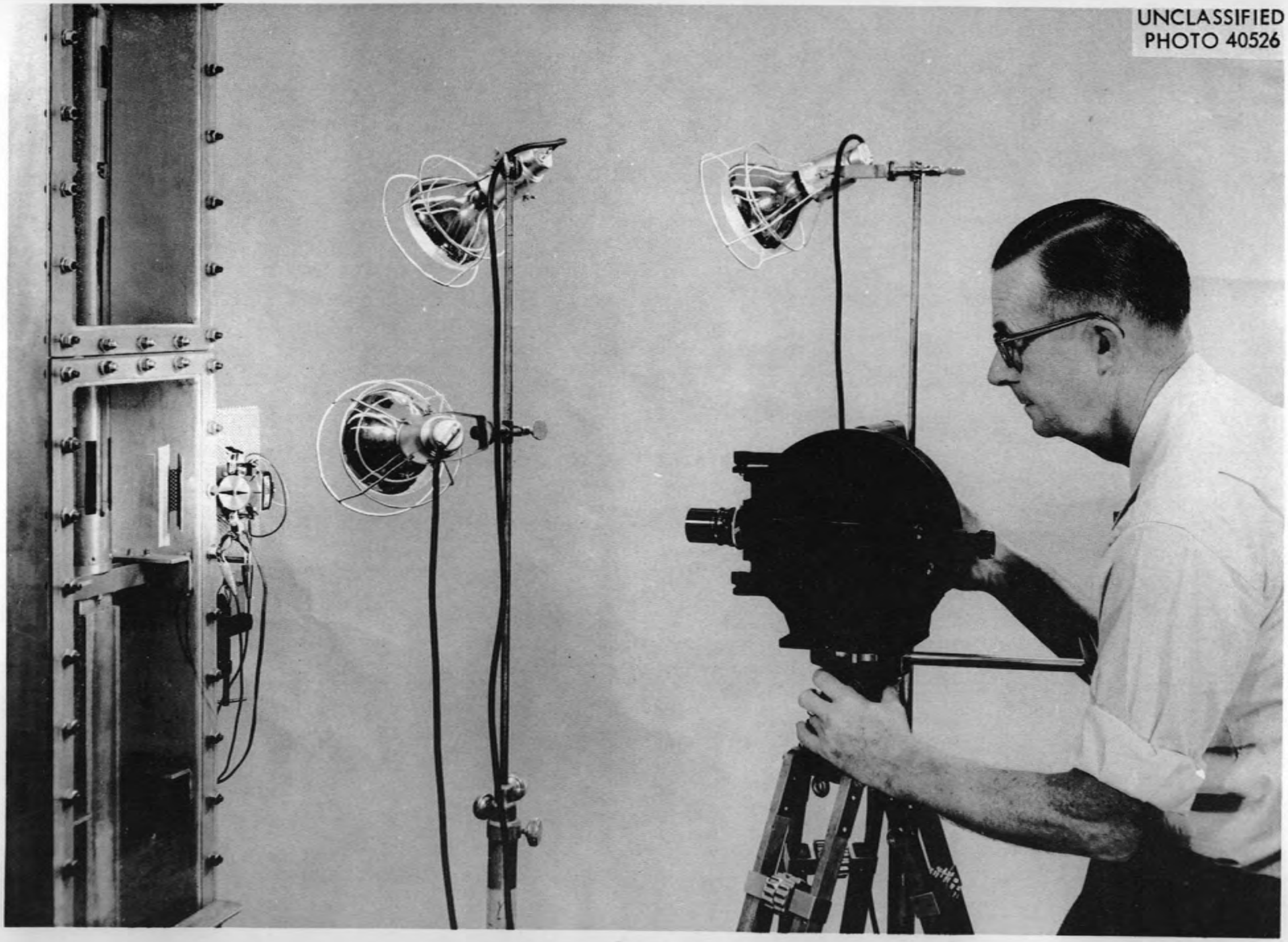

Fig. 4. High Speed Camera Positioned for Photographing Rod Drops.

UNCLASSIFIED
ORNL-LR-DWG 21213

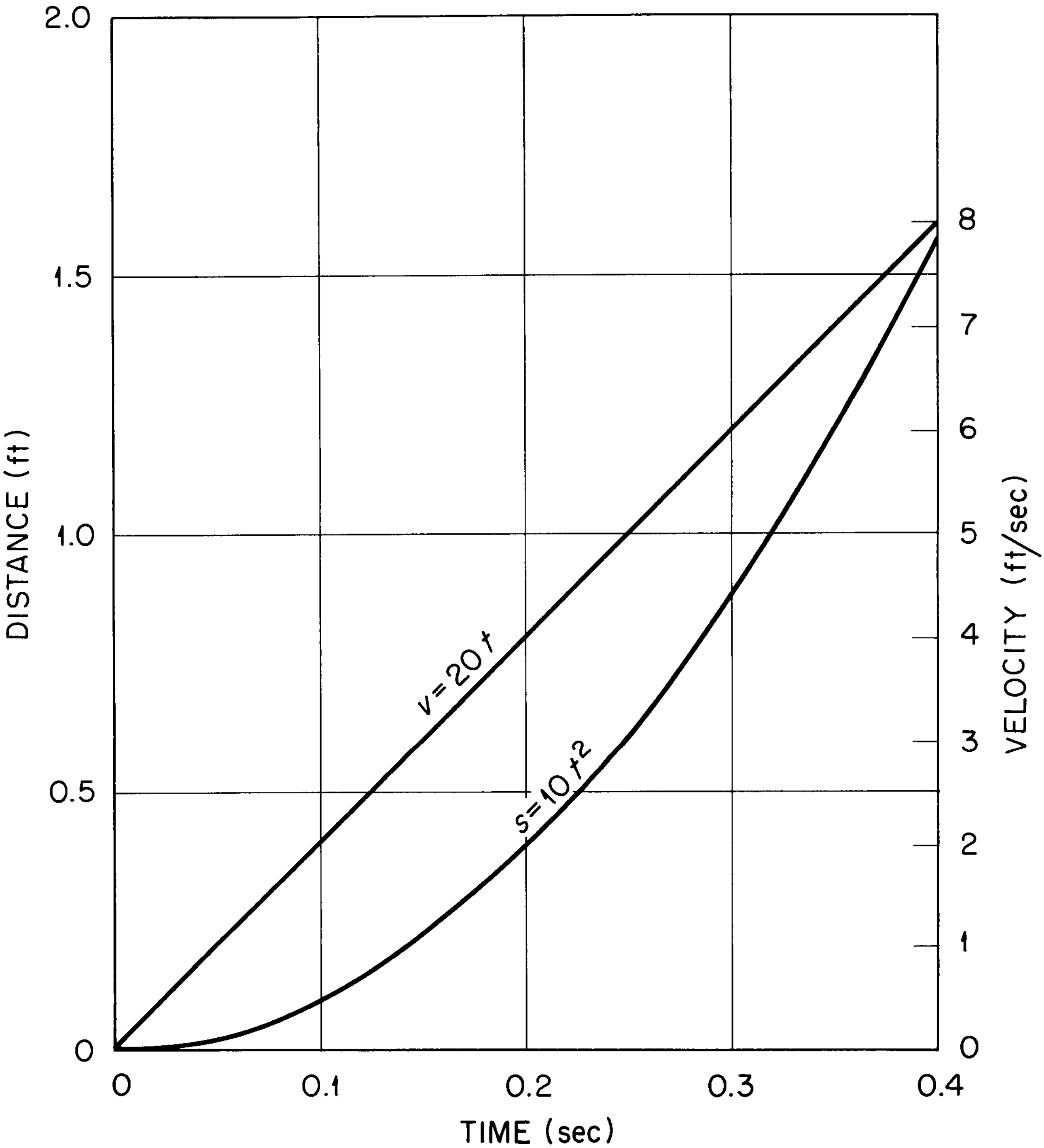

Fig. 5. BSF-Control Rod Drop Test. Free fall.

the rod weighs 11.85 pounds in air and 10.37 pounds in water, it provides an accelerating force of 10.37 pounds. Dividing this force by the observed acceleration gives 0.518 slugs as the total mass accelerated. This mass is equivalent to 16.7 pounds. Subtracting from this the weight of the control rod shows that 4.85 pounds of water are being moved with the rod.

Figure 6 gives the clearances around the control rod in the guide tube and in the special fuel element. This indicates that there is some basis for thinking of the rod as a piston pushing water along with it as it is dropping. The slots in the sides of the guide tube prevent this from being a simple case however.

Spring acceleration of control rods has been used in reactors and is of interest in current designs. The second set of tests was run to discover whether there was a change in the character of the rod drop as higher velocities were encountered.

The apparatus shown in Figure 7 was constructed in order to provide additional acceleration. This consisted of six "Negator" constant tension springs arranged to drive the cable drum. In this experiment, each spring produced a force which resulted in a rod acceleration approximately one-half that of gravity. By changing the number of springs attached to the driving shaft the pull may be varied. Figure 8 gives the spring motor calibration, each run number corresponding to the number of attached springs. Runs were started at the 9-inch position and pull was allowed to continue to the 30-3/4 inch position.

Figure 9 demonstrates how the motor was arranged to accelerate the rod for these tests. The cable is attached to the bottom of the rod and exerts a continuous pull on it. Figure 10 shows the results obtained from these tests with distance traversed plotted against time squared. It will be noted that the curves consist of three straight line segments. Comparing these with the spring calibration curves shows that part of this can be attributed to the irregularity in pull, since the springs had higher pull in the first two inches of their travel. The initial acceleration exists for such a short time that it was ignored in the following analysis, and the curves were assumed to be made up of two straight line segments.

From the tabulation of results, as shown in Figure 11, it will be noted that the total masses accelerated, m_t, as determined by dividing force, F, by acceleration, a, for the first straight line portion of the curve, are nearly equal. The procedure carried out for the second portion of the curve shows the mass accelerated is water, the equivalent mass of all of the mechanical parts, including rod, drum, spools, springs, is subtracted from the experimental values. This gives the amount of water accelerated, m_w, and is about 0.065 slugs or 4.8 pounds of water for the second half of the curve. Of course, it must be noted that these figures are the difference between two larger quantities, and therefore our equipment inaccuracies, friction differences, and effects neglected accumulate in these values.

UNCLASSIFIED
ORNL-LR-DWG 21211

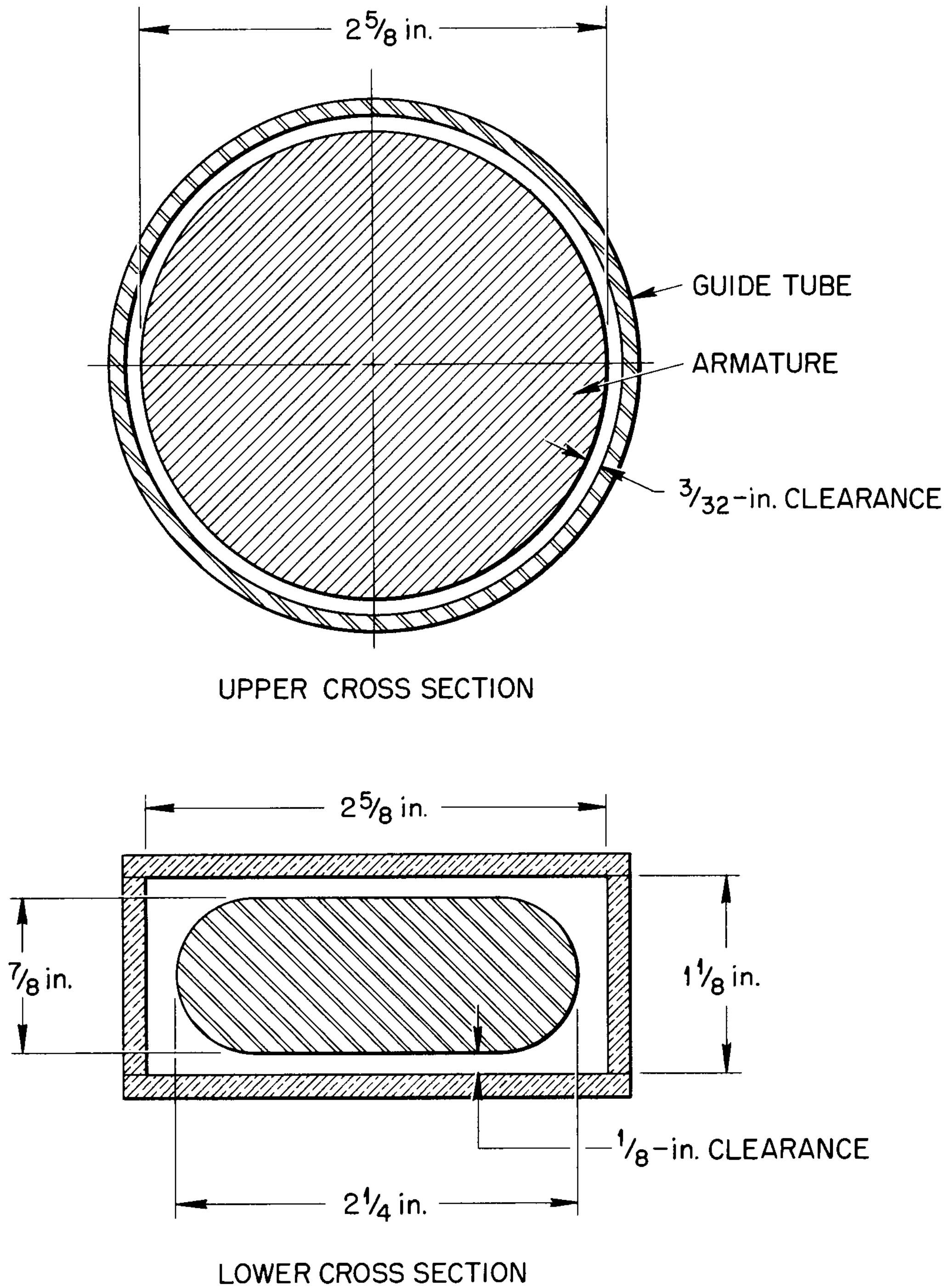

Fig. 6. BSF Control Rod.

UNCLASSIFIED
PHOTO 40525

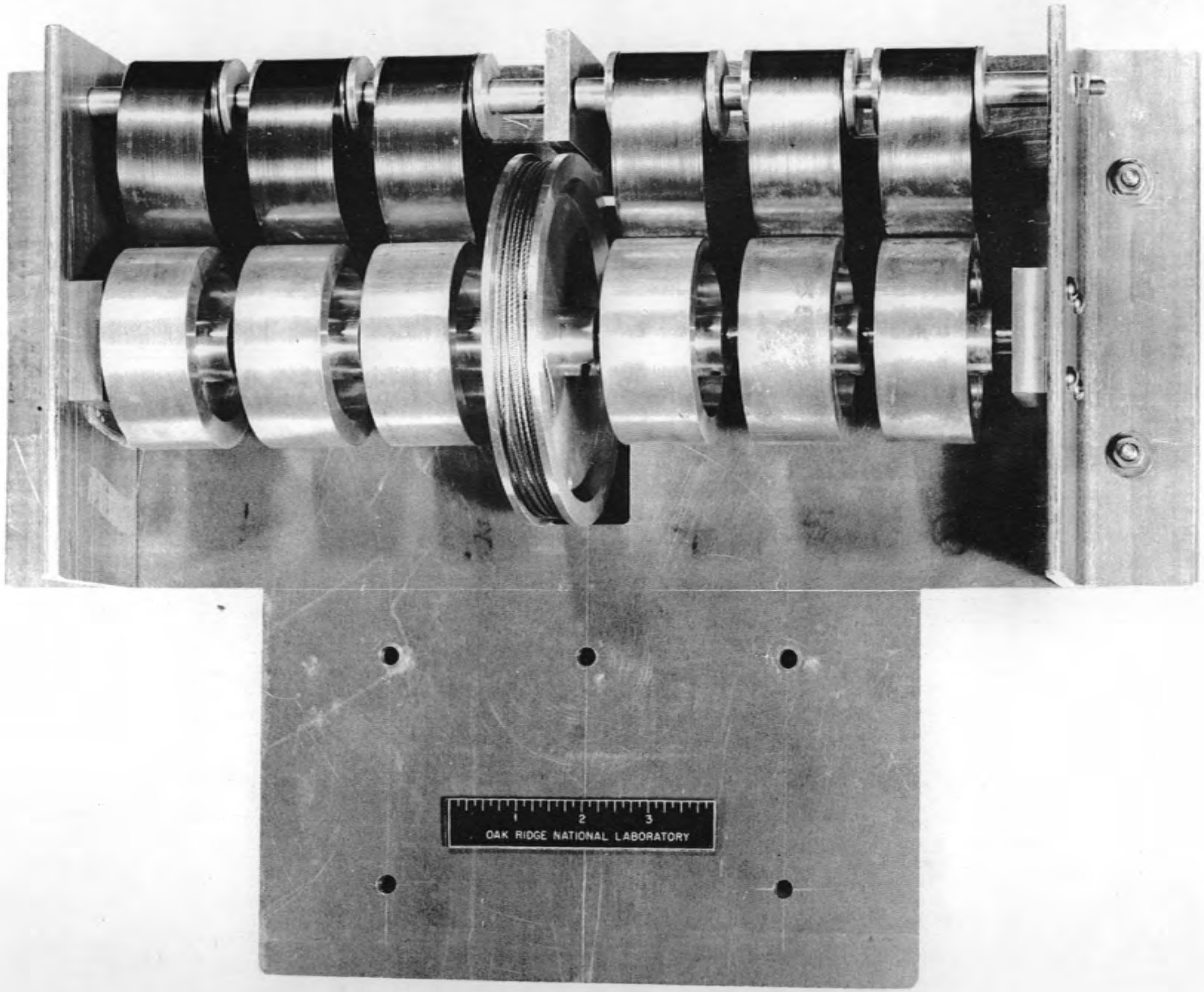

Fig. 7. "Negator" Rod Accelerating Assembly.

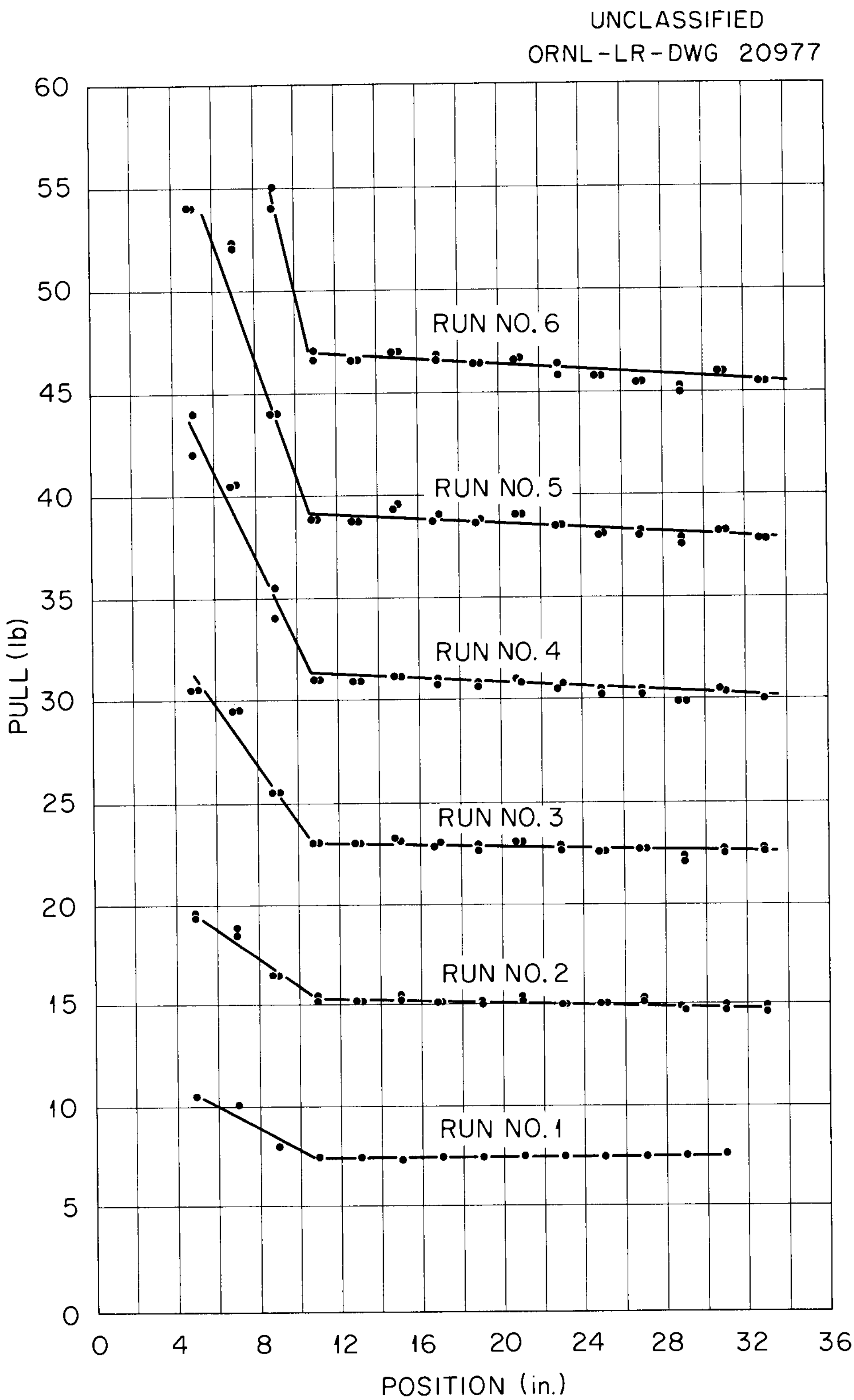

Fig. 8. Spring Motor Calibration.

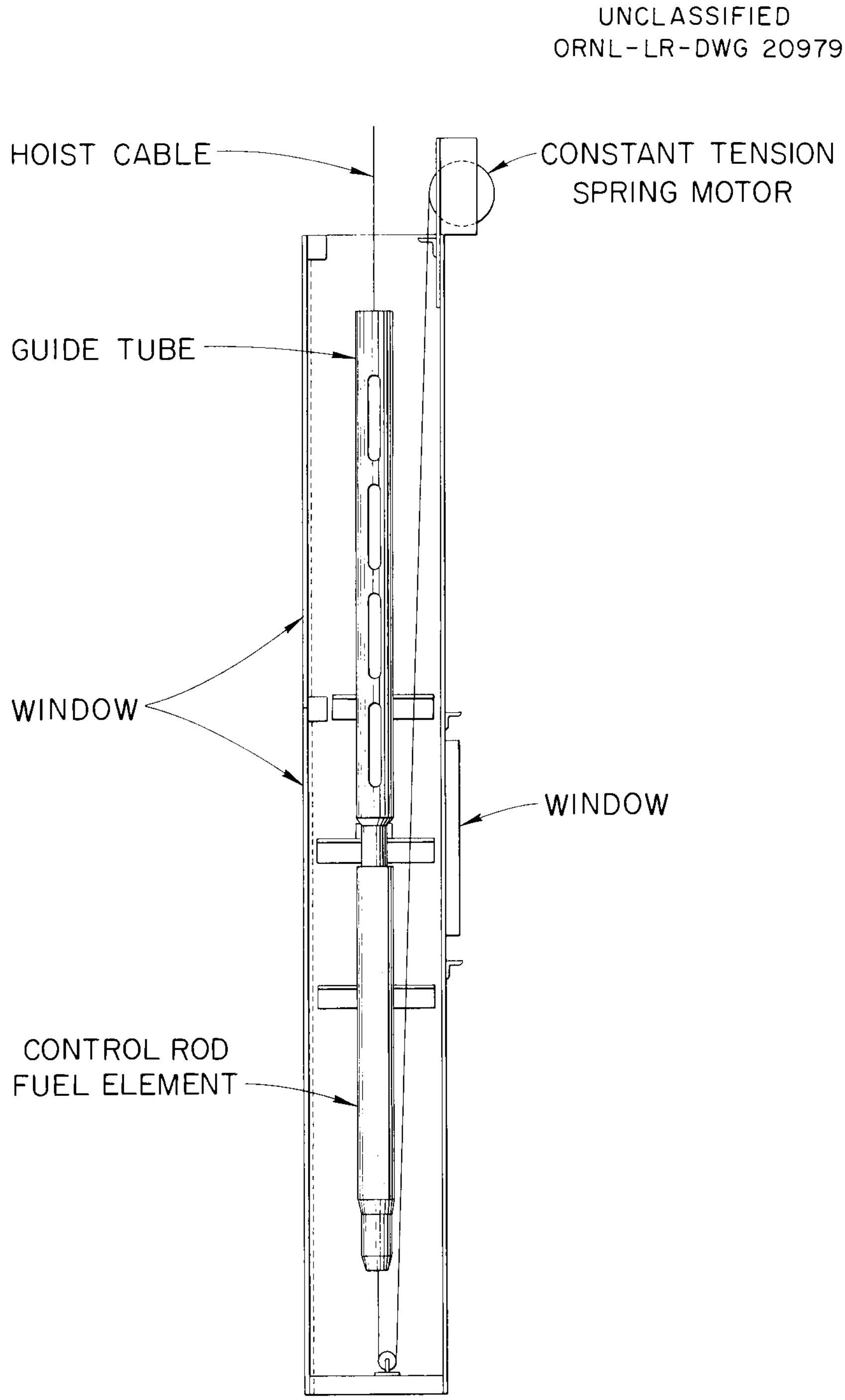

Fig. 9. Test Tank for Control Rod Acceleration.

UNCLASSIFIED
ORNL-LR-DWG 21212

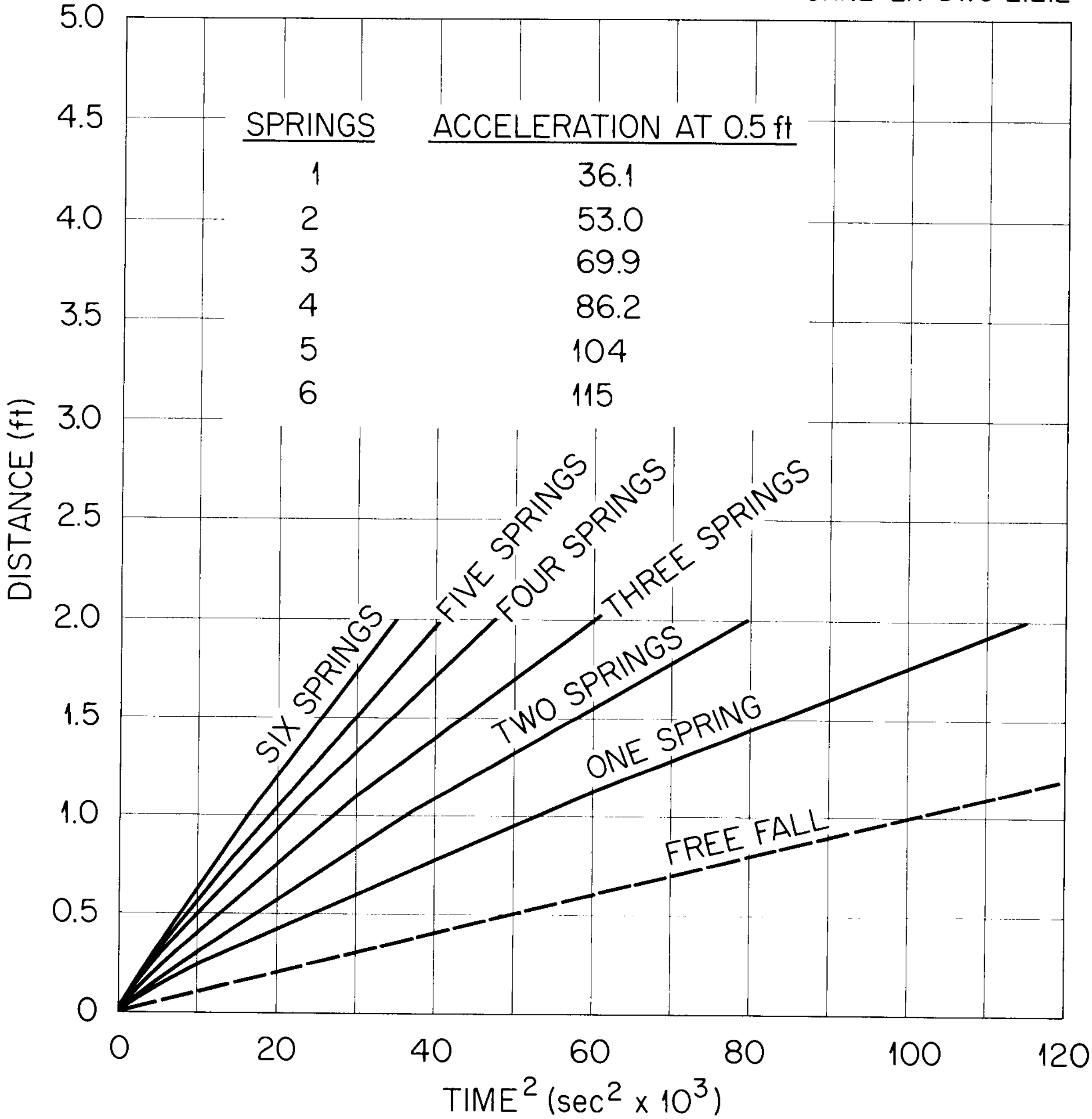

Fig. 10. BSF-Control Rod Drop Tests. Accelerated drops.

UNCLASSIFIED
ORNL-LR-DWG. 21304

Springs	m_s Slugs	First Straight Line Portion of Curve				Second Straight Line Portion of Curve			
		a ft/sec^2	F lb	m_t Slugs	m_w Slugs	a ft/sec^2	F lb	m_t Slugs	m_w Slugs
1	0.403	36.1	17.85	0.495	0.092	31.8	17.85	0.562	0.159
2	0.409	53.0	25.55	0.482	0.073	45.0	25.15	0.559	0.150
3	0.415	69.9	33.35	0.478	0.063	60.8	32.85	0.541	0.126
4	0.421	86.2	41.35	0.482	0.061	71.5	40.75	0.571	0.150
5	0.427	104.0	50.25	0.493	0.066	96.8	48.35	0.498	0.071
6	0.433	115.0	57.15	0.498	0.065	107.0	56.15	0.525	0.092

Fig. 11. Measured Acceleration of BSF Control Rod.

These values may be compared with the weight of water which could be contained within the envelope dimensions of the control rod assembly. This amounts to 75 cubic inches which is equivalent to 0.084 slugs of water. Additional experimentation is necessary to determine whether this correlation is affected by changes in slots of the guide tube or drilling holes in the sides of the special fuel element.

Another way to utilize the results of these tests is to devise a performance factor, consisting of the ratio of acceleration obtained during the drop to the acceleration that is computed if only the buoyancy of the water is considered. For the rod dropping under the influence of gravity, this factor is 0.7, computed as follows:

Net force on rod, considering only buoyancy = 10.37 lbs.

$$\text{Mass of rod} = \frac{11.85}{32.2} = 0.368 \text{ slugs}$$

$$\text{Computed acceleration, considering only buoyancy} = \frac{10.37}{0.368} = 28.2 \text{ ft/sec}^2$$

$$\text{Performance factor} = \frac{\text{measured acceleration}}{\text{computed acceleration}} = \frac{20}{28.2} = 0.7.$$

With any spring combination this factor is near 0.85 for the initial straight line portion of the curves shown. For the second portion it is 0.75 for the first four runs and 0.85 for the last two runs. Using these factors it is easy to estimate the performance of the rod under any new accelerating force within the limits tested.

It is concluded from these experiments with a control rod of the BSF type that:

a. Acceleration obtained is closely proportional to the accelerating force.

b. Displacement of water by piston action is the major factor affecting drop time.

ANALOGUE SIMULATION OF CORRECTIVE ACTION FOR A NUCLEAR EXCURSION

E. R. Mann and F. P. Green

ABSTRACT

Analysis of the corrective action provided by insertion of safety rods when a reactor is on a fast period has been made for a specific reactor. By means of analogue computing equipment the neutron flux and rod motion were simulated. The voltage corresponding to neutron flux was clamped in transient at a level of 0.1 volt and for a period 'τ'. Releasing the clamp without corrective action permitted the voltage to rise on a period 'τ' approaching the asymptotic period for three decades before the amplifiers saturated. By starting the safety rod action simultaneously with the release of the clamp, the voltage corresponding to neutron flux was reversed within the three decade range depending on the reactor period, the worth of the safety rods, their starting position and their acceleration.

The computer technique is applicable in analysis of safety systems of other reactors.

Analogue Simulation of Corrective Action for a Nuclear Excursion

E. R. Mann and F. P. Green

Limitations of Analogue Computers in Analyzing a Nuclear Excursion

The analysis of a nuclear excursion usually starts with a particular reactor and a particular set of initial conditions. The reactor is assumed to be in steady state when a positive perturbation in reactivity is introduced. The neutron flux is allowed to rise according to the kinetic equations of the reactor and any known equations of the safety system which provides corrective action.

The excursion can extend over a neutron flux range of several decades. The analogue computer could be used effectively in making such an analysis except for the limitation in range of the variables provided by such a device. The linear range of the analogue computer is about three orders of magnitude.

That portion of the analysis which deals with the time interval when corrective action is being taken can be made with certain restrictions by means of the analogue computer. In principle, one can prescribe the corrective action for a given excursion which limits the excursion to three decades. Or, one can describe the excursion for which the corrective action limits the neutron flux to a three decade range. This analysis determines the minimum reactor period for which a given safety rod limits the neutron flux excursion to three decades.

If a reactor is on a positive period, the pile period instrument will determine this fact in some interval of time. Likewise, if the flux level rises to an upper limit prescribed by the safety system some interval of time is required for an instrument to determine that the flux is at or above this limit. In either case, no corrective action is taken in the interval of time required by the sensors.

Once the sensing devices provide information for initiating corrective action, there is another interval of delay before this action becomes effective. For the particular reactor considered here, the magnets which hold the safety rods must release these rods so that they can move into the reactor lattice. Until this release is effected, the neutron flux continues to rise.

Starting with the instant when the safety rods are released, the system is taking corrective action. The analogue computer can be used to simulate just about any conceivable type of motion of the safety rods. The simulation can be carried out in real time or a time scale which is convenient for the computer. If the effective value of the rod is known in terms of reactivity as a function of the rod position, this value can be introduced into the analysis of the system in terms of reactivity as a function of time.

Simulation of a Specific Reactor

This analysis was carried out for a solid fuel water-moderated swimming pool type reactor with a mean neutron generation time of 5×10^{-5} sec. The total worth of the safety rod was 6% in reactivity.

The curve, Figure 1, shows the reactivity of the rod as a function of its position in the lattice. The stroke of the rod was taken as 22 inches. This reactivity function was set into the computer by a conventional diode function generator. The output of the function generator was reactivity as shown here on the vertical axis. The input was the simulated rod position[1].

Figure 2 shows the rod drop simulator. A constant current corresponding to constant acceleration is integrated once by integrator 1 to produce velocity. The output of integrator 1 is integrated a second time to give a voltage proportional to the square of the time. This voltage is proportional to the displacement of the rod and is the input to the function generator.

A limit switch on a recorder was used to initiate the rod drop at a particular value of the neutron flux during the excursion. The potentiometer 3 was used to establish the initial position of the safety rod, S_o, and potentiometer 5 was used to bias the initial function generator output to zero.

The computer time scale was taken as 100 times real time. This means that 10 milliseconds of real time was made equivalent to one second computer time.

Figure 3 shows the reactivity supplied by the rod insertion as a function of time for seven different values of acceleration[2], wherein $g = 32.2$ ft/sec^2. The 6% rod was withdrawn initially the full 22 inches at the instant of release. The rod non-linearity and relatively slow start combine to delay substantial corrective action.

Figure 4 shows the reactivity as a function of time for the same rod when released after having been withdrawn only 14 inches. It is to be noted that the worth of the remaining rod is only 4.5% and that the delay in corrective action is not as much as was the case for the rod starting from the 22 inch withdrawal position.

The computing equipment for simulating the kinetic equations of the reactor is shown in Figure 5.

The simulator circuit is essentially that used for solving the kinetic equations of a reactor[3] except that the time scale has been changed so that computer time is 100 times real time and the two longest life delayed neutron precursors were omitted. The multiplier used was a servo type. Provision for initiating the neutron flux excursion by means of the ganged switch F_2 allows the flux to be held "clamped" in transient at some low level until switch F_2 is closed.

Amplifiers 4 and 7 represent the prompt neutron loop. Amplifier 5 provides signal inversion and current load reduction on amplifier 4. Amplifier 6 and potentiometer 11 provide a vernier for accurate setting of the gain.

UNCLASSIFIED
ORNL-LR-DWG. 21378

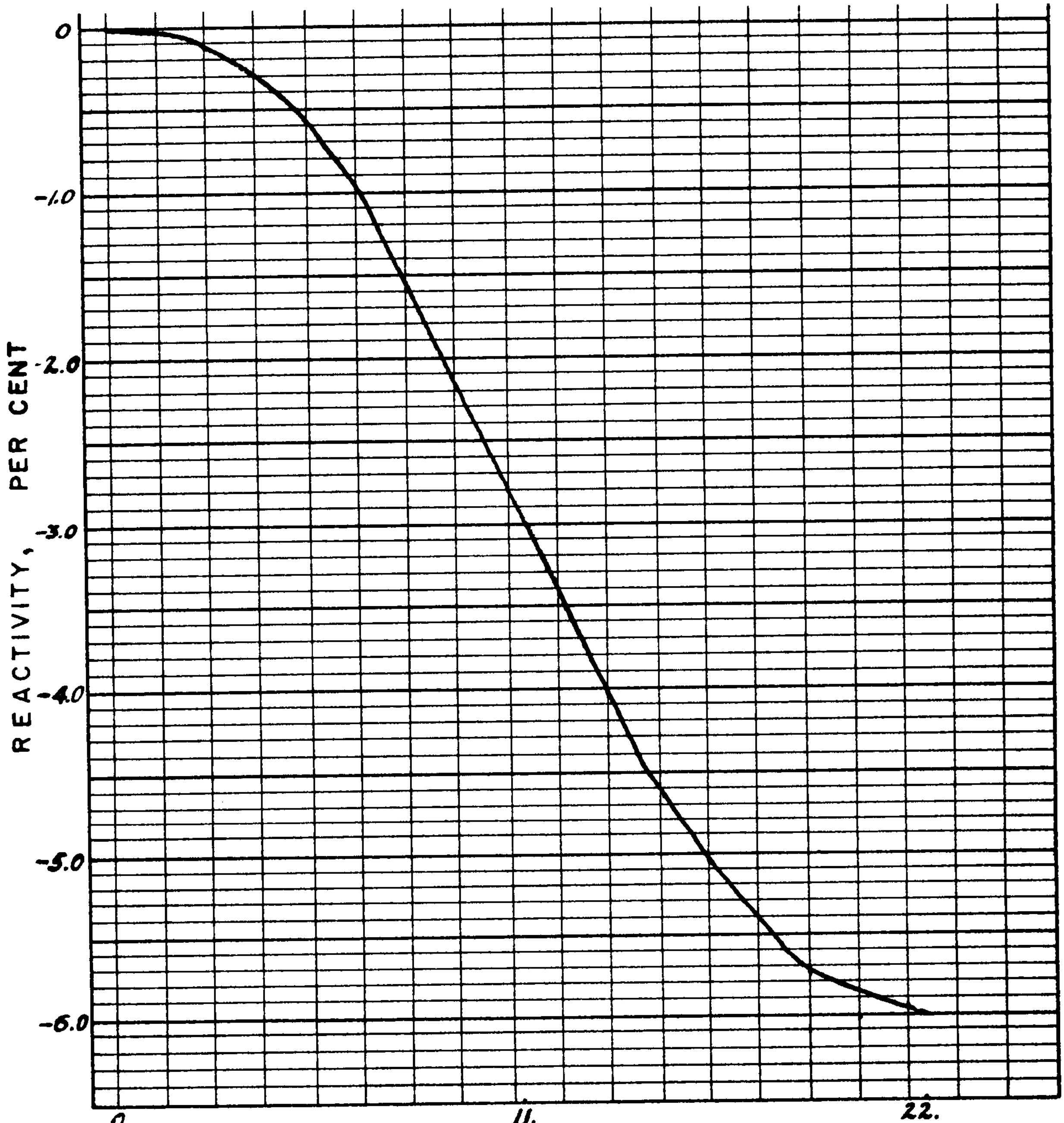

Fig. 1. Reactivity vs Rod Position.

UNCLASSIFIED
ORNL-LR-DWG. 21369

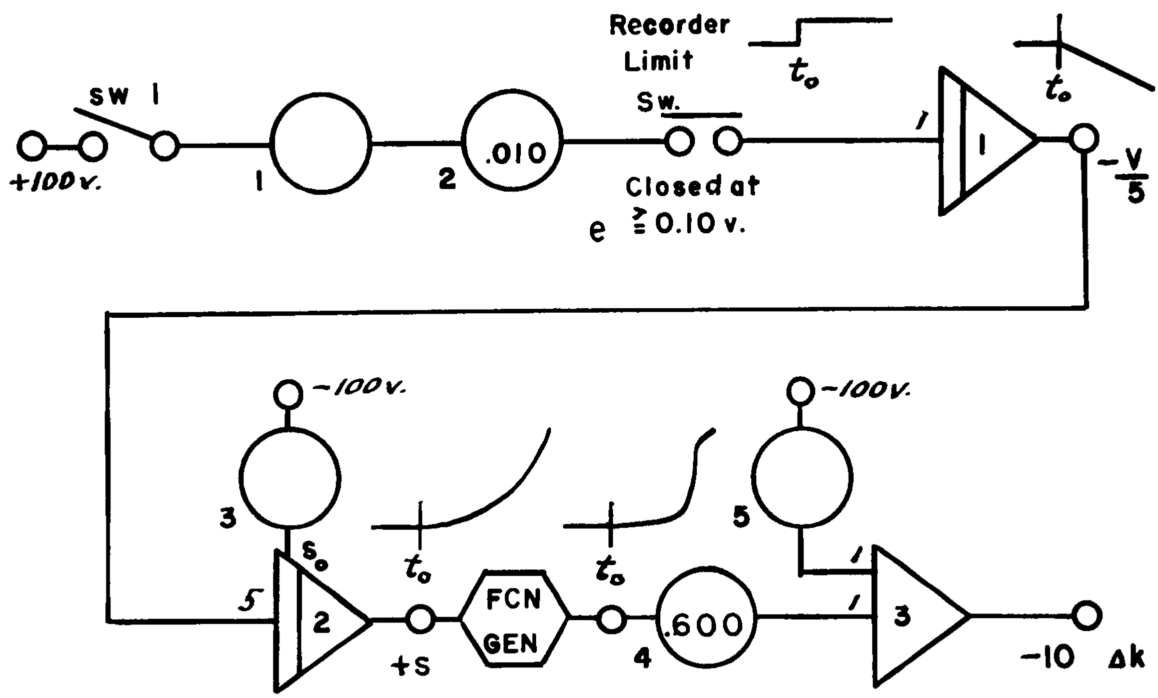

Fig. 2. Rod Drop Simulator Diagram.

UNCLASSIFIED
ORNL-LR-DWG. 21374

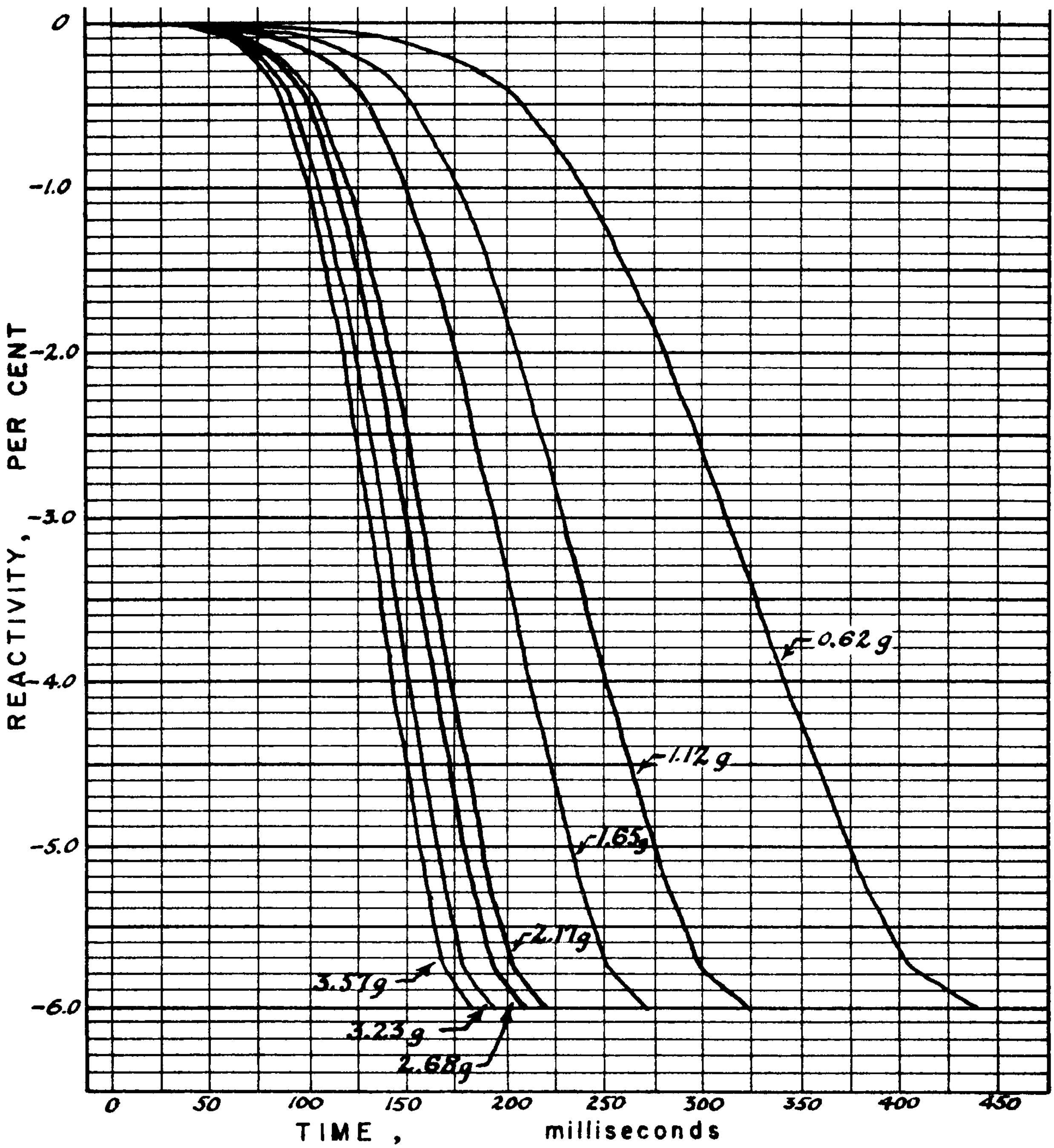

Fig. 3. Reactivity vs Time During Rod Insertion. Rod initially withdrawn 22 in.

UNCLASSIFIED
ORNL-LR-DWG. 21375

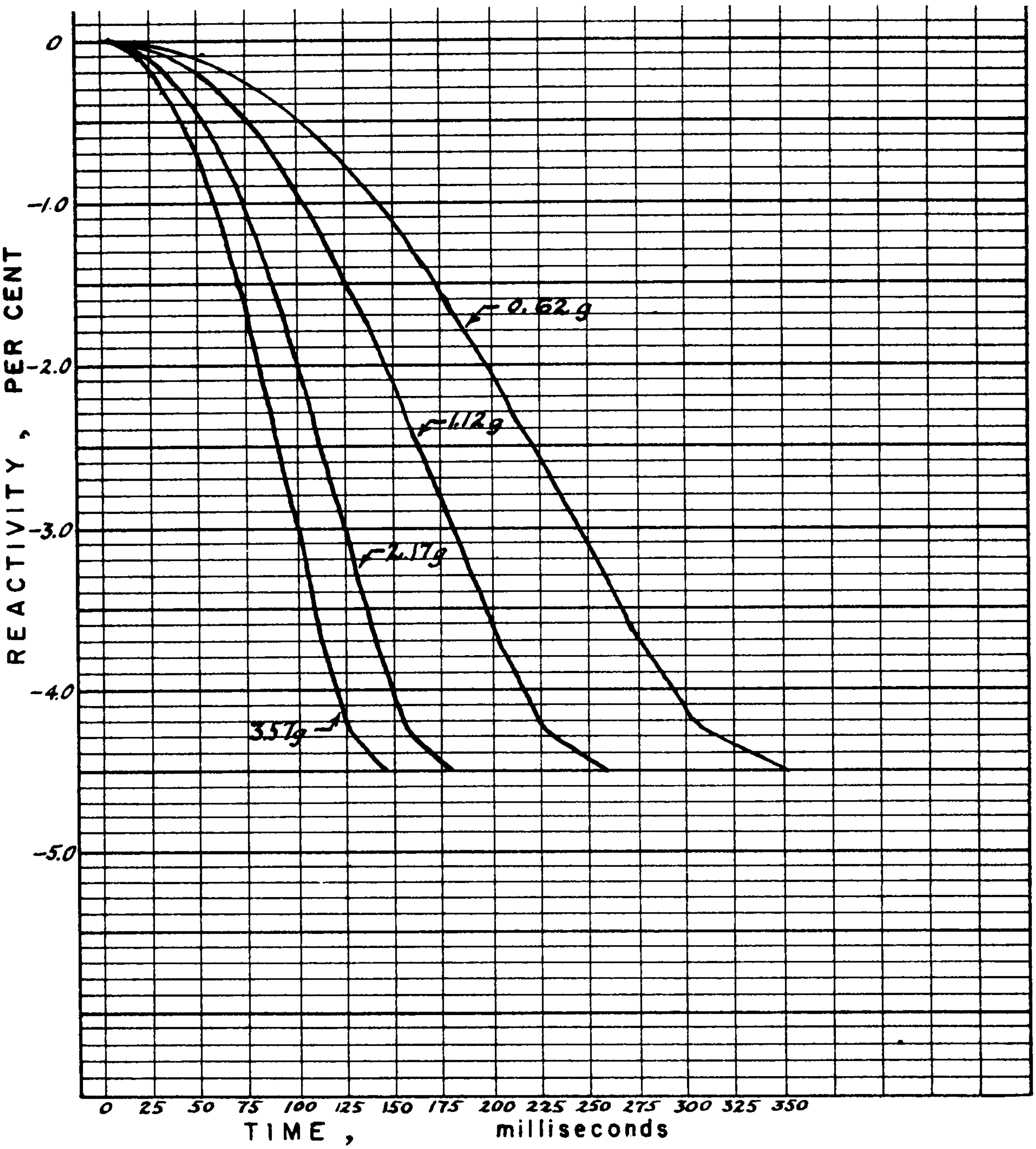

Fig. 4. Reactivity vs Time During Rod Insertion. Rod initially withdrawn 14 in.

UNCLASSIFIED
ORNL-LR-DWG 21368A

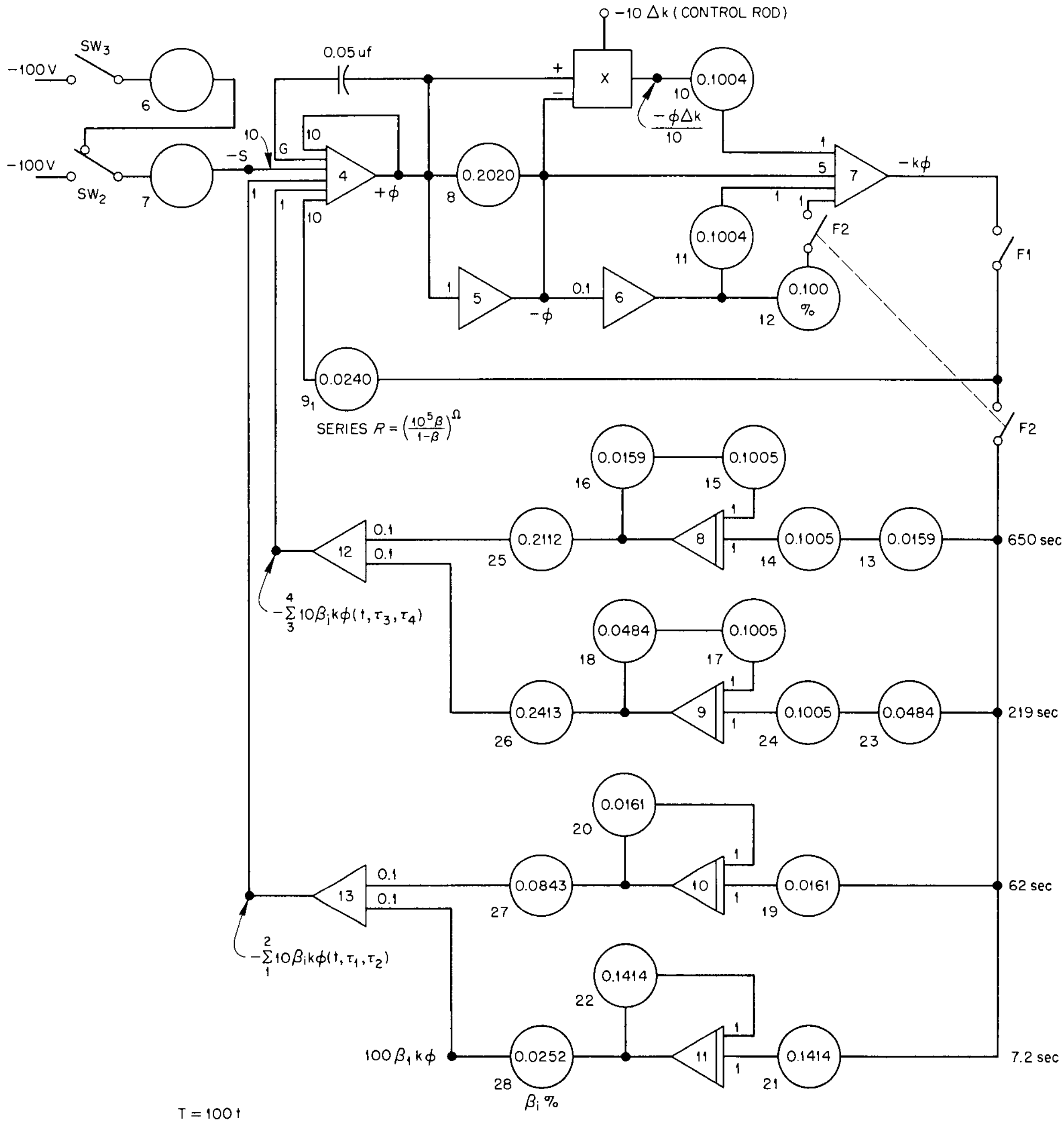

(30 K ohm POTENTIOMETER SETTINGS INCLUDE LOADING CORRECTIONS.)

Fig. 5. Reactor Simulator Diagram.

The open loop gain is set at unity by opening switches F1 and F2, setting potentiometer 10 at zero, and applying a nominal 100.0 volts with source potentiometer 7; potentiometer 8 is set as shown and potentiometer 11 is adjusted empirically for $-k\phi$ equal to 100.0 volts. With the source potentiometers set to provide 0.559 volts, i.e., the equivalent of $\sum_{i=1}^{4} \beta_i$ at a steady state of $-k\phi$ equal to 100.0 volts, and closing F1, a loop gain of unity can be set accurately by adjusting series resistor 9.

The value of ℓ^*, the mean neutron life time, was determined for the simulator by introducing a 0.559 volt step in the source voltage when the simulator was at a steady state with switch F2 open, switch F1 closed. This was done by closing switch 3, Figure 5. The curve, Figure 6, shows the rise in simulated relative neutron flux with time. The time required for a 63% rise was 8.5 milliseconds for the particular value of ℓ^* represented by this curve. The value of ℓ^* determined by stepping the source in this manner is equal to the time constant, 8.5 milliseconds determined here, multiplied by β which was taken as .00559, since two longest life groups of delayed neutron precursors were omitted. This gives 4.75×10^{-5} for the value of ℓ^*. The time scale shown in Figure 6 is real time although the original record was in computer time which was 100 times real time.

In order to get another check on the operation of the analogue equipment, both the period and the excess reactivity, determined experimentally as that required for a particular period, were recorded and the experimentally determined periods were plotted as a function of the excess reactivity needed. Since two delayed-neutron groups were deleted in the simulation, several test transients were run while potentiometer 12 was adjusted empirically for that excess $\Delta k/k$ required to limit the flux excursion to barely a factor of 10^3 following initiation of corrective action. At the proper setting, a final transient was recorded with no corrective action to obtain the actual stable period produced. Figure 7 shows the empirical relation between period and excess reactivity. For comparison the stable period is plotted as a function of the excess reactivity as determined from the in-hour equation.

The voltage corresponding to neutron flux was clamped in transient at 0.1 volt and the voltages corresponding to the delayed neutron precursors were clamped at ground potential. This was permissible since the neutron flux from the decay of precursors is insignificantly small when the total flux is represented by 0.1 volt.

Releasing the clamp on the simulator allowed the flux voltage to rise on a period determined by the excess reactivity previously set in the computer. The flux was recorded and the period was determined from the recorder chart as the time required for the voltage to rise from 100/e to 100 volts. The 100 to 1 ratio of machine time to real time made possible accurate recording of excursions with 2.5 millisecond periods.

When the clamp was released, the recorder limit switch in the rod drop simulator, Figure 2, initiated the rod release as the voltage corresponding to the neutron flux passed through the 0.1 volt level.

UNCLASSIFIED
ORNL-LR-DWG. 21377

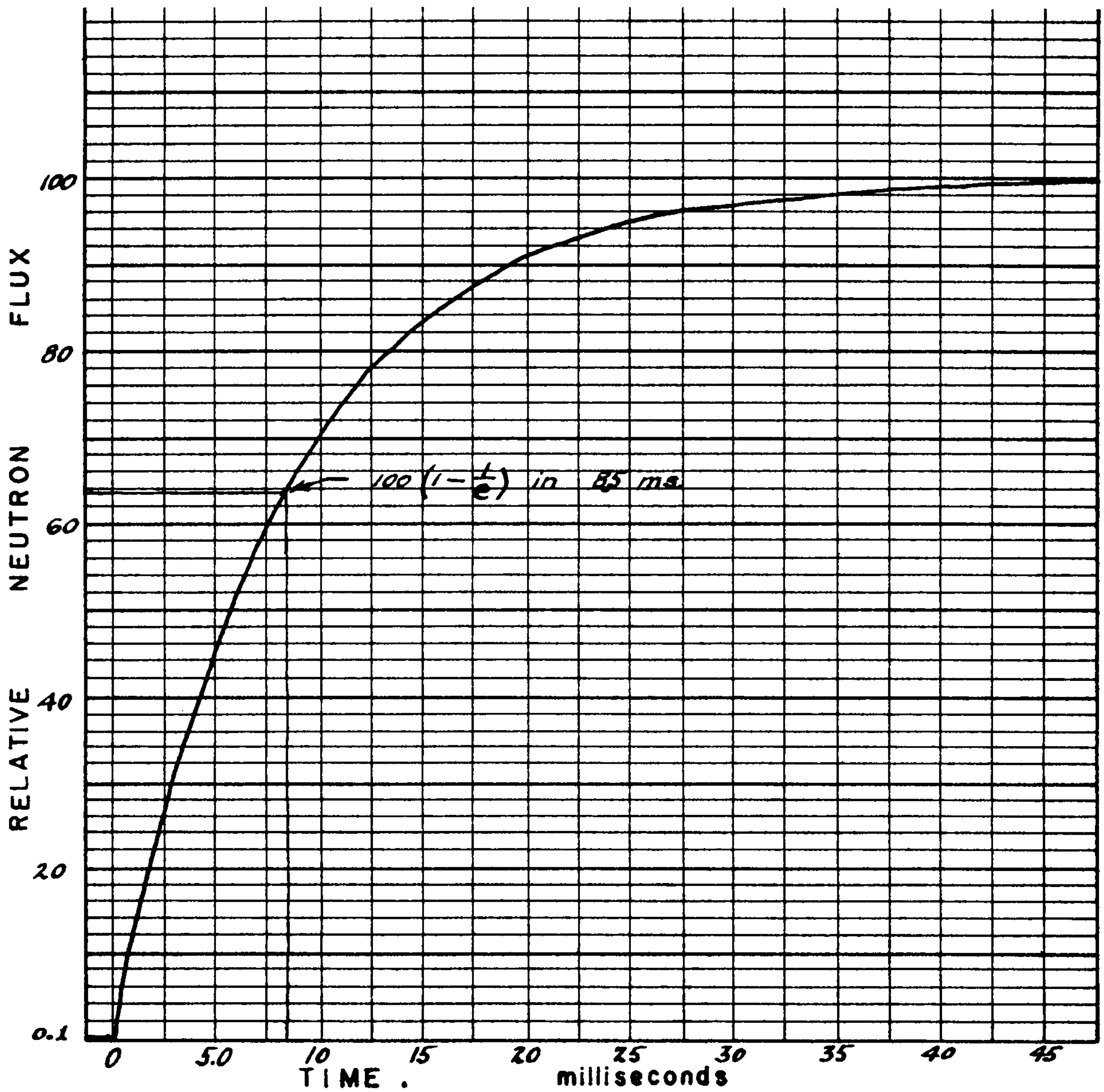

Fig. 6. Response of Neutron Flux to a Step in Source.

UNCLASSIFIED
ORNL-LR-DWG. 21373

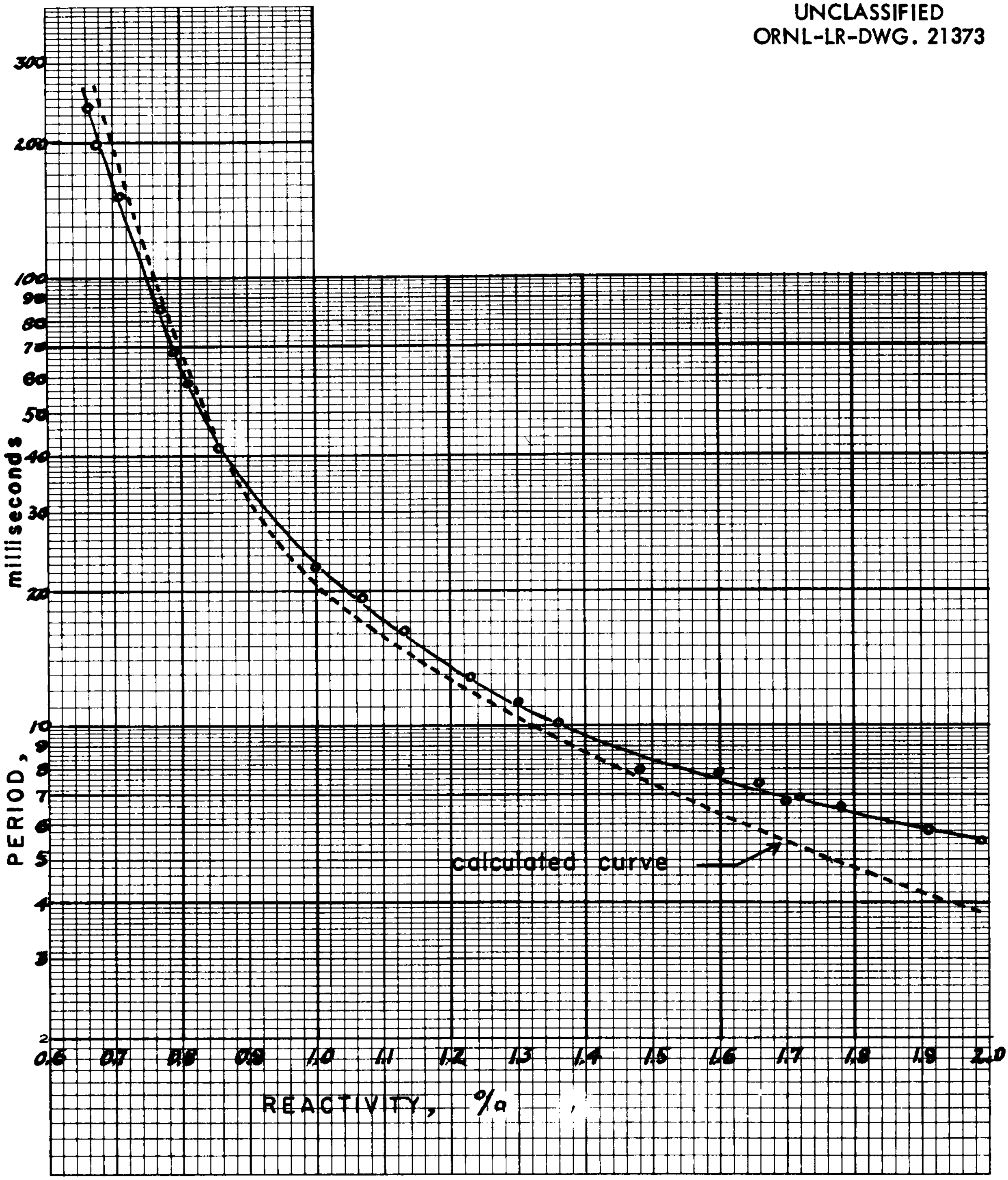

Fig. 7. Stable Period, τ vs Reactivity Determined Experimentally on the Computer ($L^* = 5 \times 10^{-5}$ sec).

Essentially, then, the corrective action started with the release of the clamp. The neutron flux rose and the rod action decreased the reactivity until the excursion was turned back. Shorter and shorter periods were selected until the shortest period was found for which the corrective action limited the excursion to three decades rise. To obtain the total flux excursion, this rise could then be added to the calculated rise which took place while the sensor and magnet release mechanism were operating and during which times no corrective action was taken.

Figure 8 shows on linear scale the relative neutron flux as a function of time for an excursion which, without corrective action, was on a 23 millisecond period. The seven curves where corrective action was taken represent the six percent rod initially withdrawn 22 inches and accelerated with seven different accelerations. The lowest acceleration limits the excursion to three decades.

Figure 9 shows the same excursion with a 23 millisecond period but with a single step in reactivity as corrective action. A step of -0.20% is not enough to turn back the excursion. The step of -0.25% is enough to turn it back temporarily. And the step of -0.22% is precisely enough to flatten it temporarily. This negative reactivity of -0.22% is exactly that needed to reduce the prompt multiplication to unity. The growth of delayed neutrons cause the flux to rise again after this short interval of zero rate of change. It follows that to turn back the excursion, the rod must introduce enough negative reactivity to reduce the prompt multiplication to unity. If then, the rod is in motion at a substantial velocity and has enough remaining negative reactivity it will shut the reactor down.

Figure 10 shows the minimum period for which the corrective action supplied by this rod can limit the excursion to three decades. The minimum period is shown as a function of rod acceleration. The top curve is for the initial rod position of 22 inches withdrawal, and shows minimum periods extending from 23 milliseconds for an acceleration of 0.62 g to 10 milliseconds for an acceleration of 3.57 g.

The middle curve shows these periods as a function of rod accelerations for the initial rod position of 18 inches withdrawal. The range in values of the minimum period for this case is from a 14 millisecond period to one of about 6.7 milliseconds.

The bottom curve is for the initial rod withdrawal of 14 inches and shows a range in values of period from 10 milliseconds to 5 milliseconds.

These three curves show the effects of increasing the rod acceleration on the minimum period for which corrective action limits the excursion to three decades. They also show the effect of having the rod in a favorable position when an excursion occurs.

Figure 11 illustrates the factors which enter into evaluation of the safety system of a nuclear reactor of the type analyzed here. These are not all of the factors. However, an analysis such as this shows what items of the system may need improvement as well as those which are adequate when compared to the rest of the system.

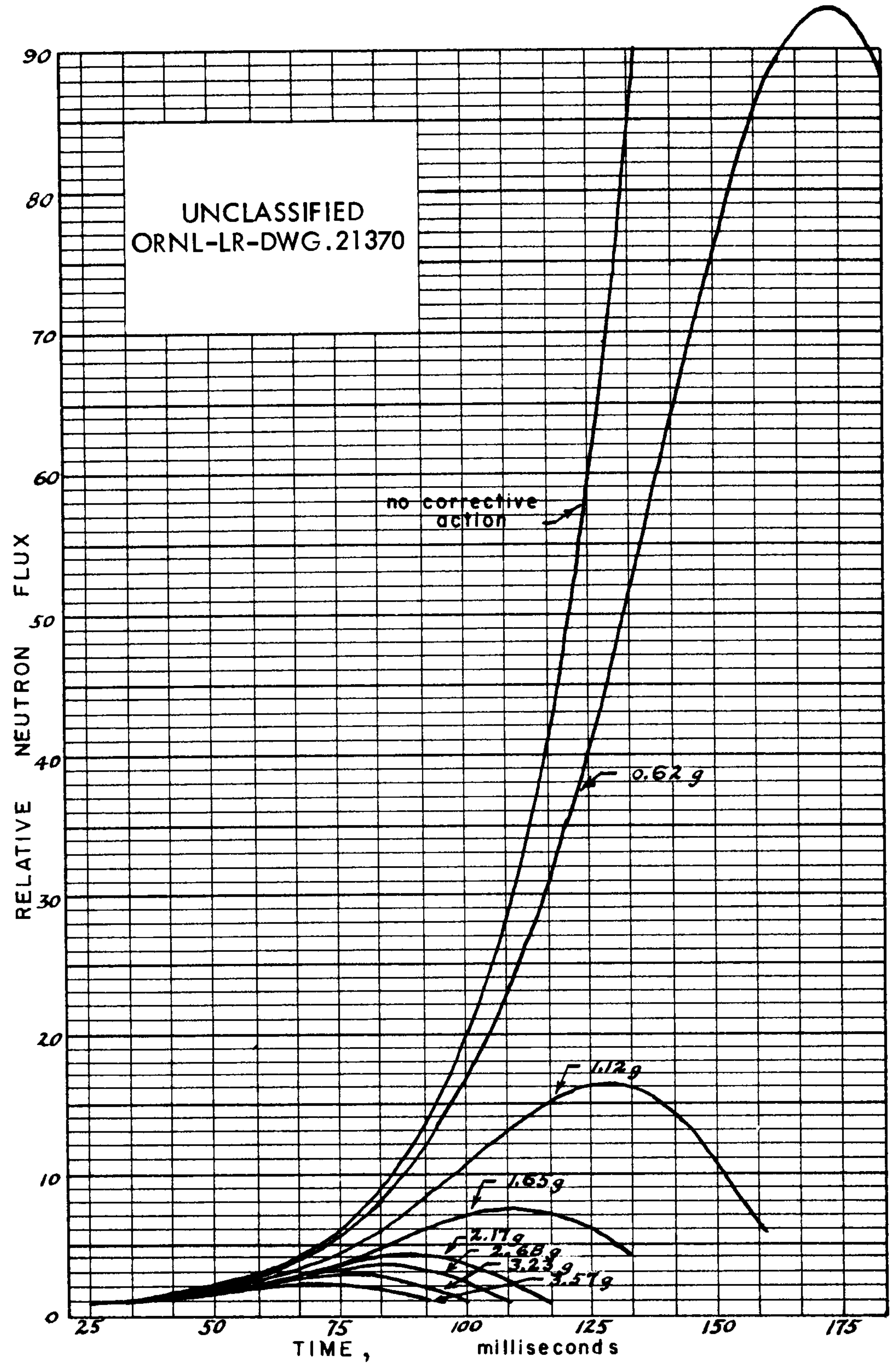

Fig. 8. Neutron Flux Excursion (τ = 23 ms) for Specific Rod Accelerations.

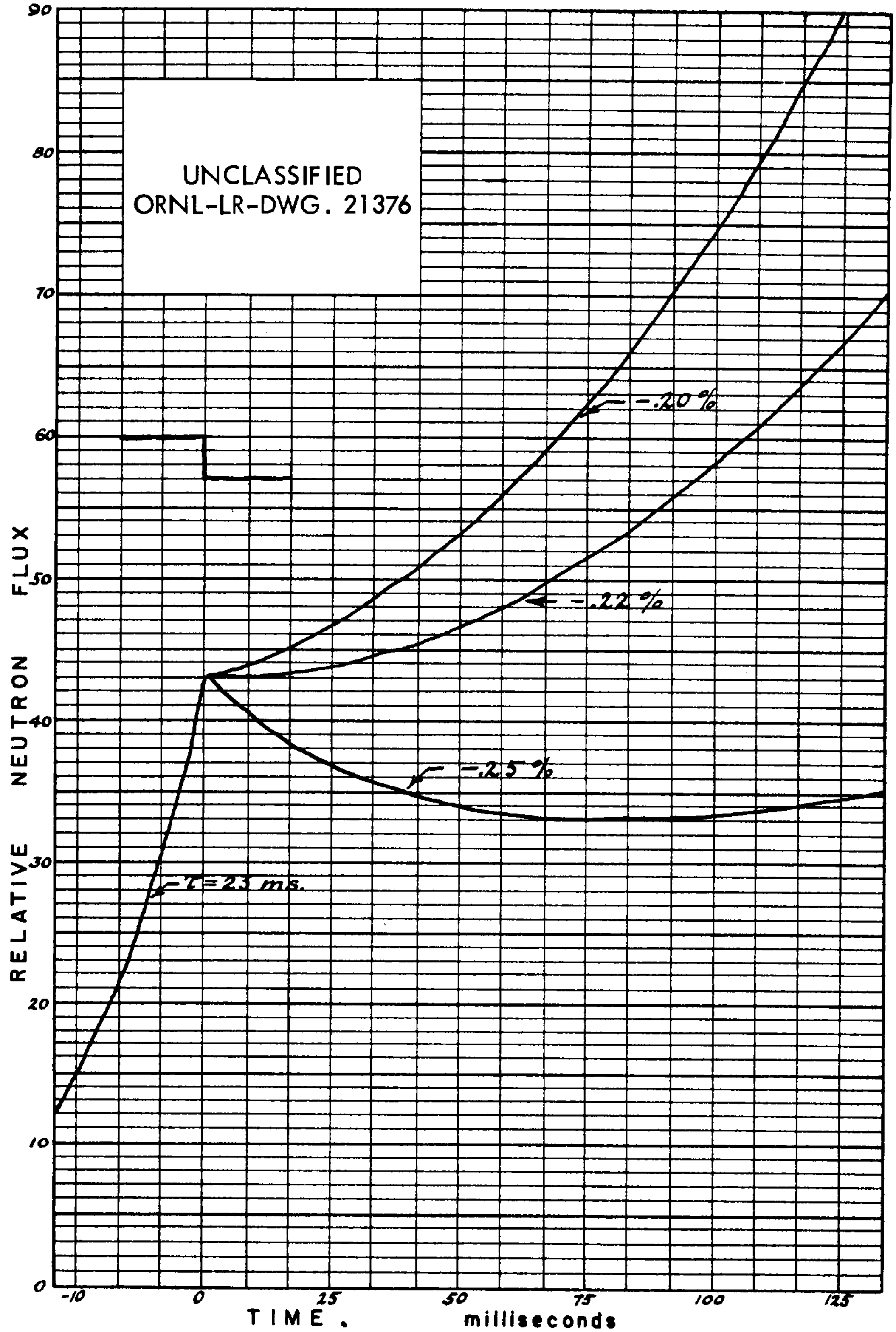

Fig. 9. Flux Response for a Single Step in Reactivity as Corrective Action.

UNCLASSIFIED
ORNL-LR-DWG. 21372

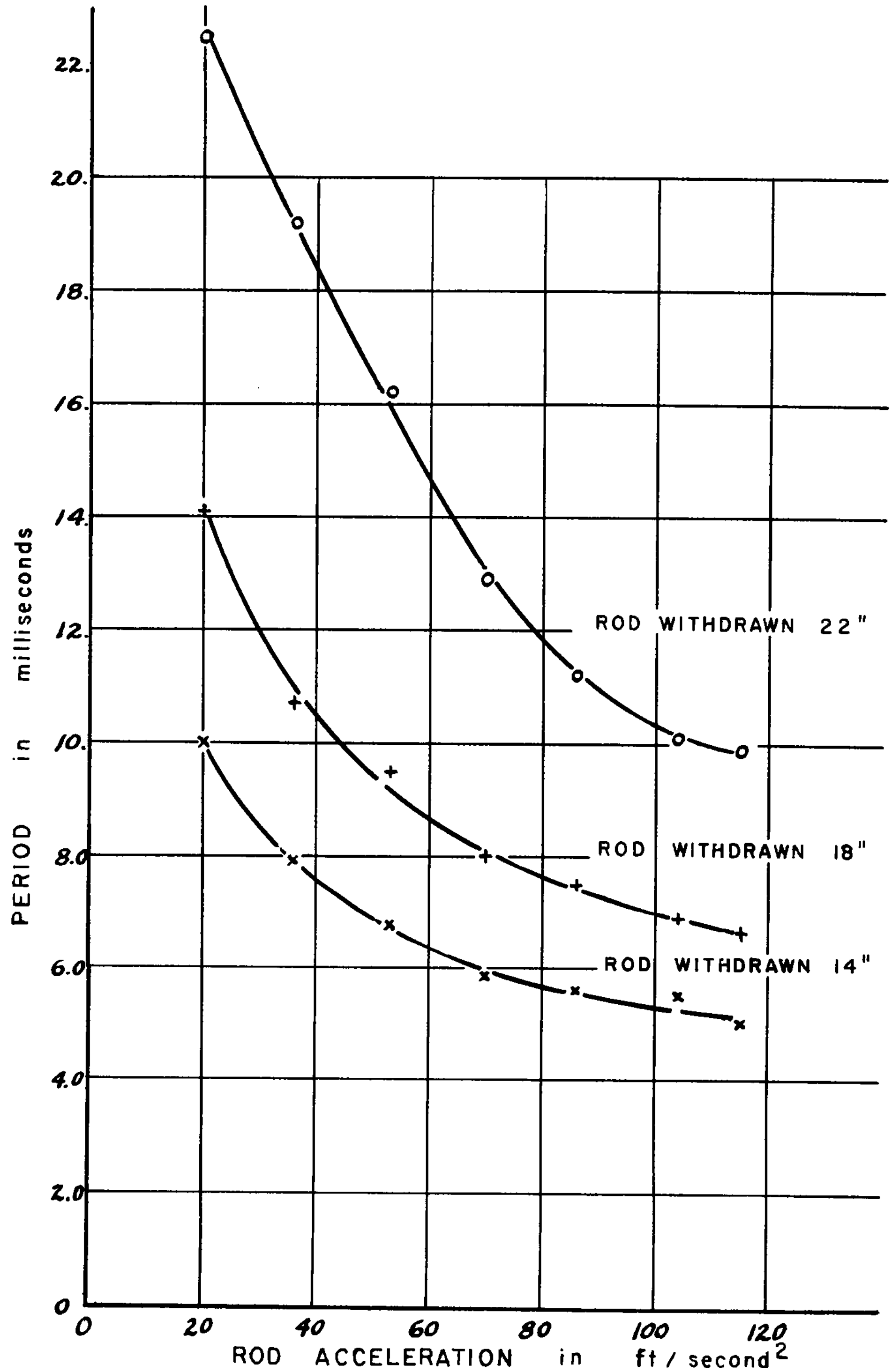

Fig. 10. Stable Period for Which the Rod Action Limits Flux Excursion to Three Decades vs Rod Acceleration.

ORNL-LR-DWG. 21371
UNCLASSIFIED

τ = 23 milliseconds

MAGNET RELEASE TIME	FLUX RISE			
	SENSOR	MAGNET RELEASE	CORRECTIVE ACTION	TOTAL
50 ms.	$< e$	8.9	10^3	$< 8.9 \times 10^3 e$
40	"	5.7	"	$< 5.7 \times 10^3 e$
30	"	3.7	"	$< 3.7 \times 10^3 e$
20	"	2.4	"	$< 2.4 \times 10^3 e$
10	"	1.6	"	$< 1.6 \times 10^3 e$
5	"	1.3	"	$< 1.3 \times 10^3 e$

τ = 5 milliseconds

50 ms.	$< e$	2.2×10^4	10^3	$< 2.2 \times 10^7 e$
40	"	3.0×10^3	"	$< 3.0 \times 10^6 e$
30	"	410	"	$< 4.1 \times 10^5 e$
20	"	53	"	$< 5.3 \times 10^4 e$
10	"	7.4	"	$< 7.4 \times 10^3 e$
5	"	2.7	"	$< 2.7 \times 10^3 e$

Fig. 11. Neutron Flux Rise During an Excursion.

For an excursion where the neutron flux is on a 23 millisecond period, a 50 millisecond release time and rod acceleration of 0.62 g will limit the rise to about four decades. On the other hand, for an excursion where the flux is on a 5 millisecond period the magnet release time must be decreased about an order of magnitude and the rod must have a large acceleration and be operating over its linear range when the excursion is initiated if the excursion is to be limited to four decades.

Sensor response to a short-period neutron flux excursion was assumed to occur in a time equivalent to less than an 'e'-fold increase in flux level.

This analysis could have been extended to determine total energy released during the excursion. Rod motions other than those with constant acceleration could have been investigated. This analysis was limited to the situation where known data for a particular reactor were available.

Conclusions

This method of analysis of a part of a nuclear excursion shows that the analogue computer can be very useful even though these excursions would normally extend over a range which far exceeds that of the computer. The analysis has emphasized a few items pertaining to the safety system which previously had not been obvious. In the first place, for short periods, the safety system has only to decrease the reactivity enough to reduce the prompt multiplication to unity in order to turn back the excursion. This fact has been determined experimentally by Schroeder, et. al.[4] Likewise, the importance of spring loading the rod and of its position in the lattice when the excursion starts have been clarified.

The importance of magnet release time has been shown in that if this time is not kept small no amount of spring loading can prevent a large excursion for short periods.

Bibliography

1. Data given in private communication by S. H. Hanauer of the ORNL Reactor Controls Department.

2. "Acceleration of Reactor Control Rods" by A. A. Sorensen.

3. "Electronic Analog Devices for Design of Reactor Controls" by E. R. Mann, IRE-Transactions-Nuclear Science, Vol. NS-3, No. 2, pp. 12-17, March, 1956.

4. "Experimental Study of Transient Behavior in a Subcooled, Water-Moderated Reactor", F. Schroeder, S. G. Forbes, W. E. Nyer, F. L. Bentzen, and G. O. Bright, Nuclear Science and Engineering, Vol. 2, No. 1, pp. 96-115, February 1957.